Energy Systems in Electrical Engineering

Behrooz Vahidi
Ramezan Ali Naghizadeh

Principles and Modeling of the Power Transformers

Springer

Energy Systems in Electrical Engineering

Series Editor

Muhammad H. Rashid, Florida Polytechnic University, Lakeland, USA

Energy Systems in Electrical Engineering is a unique series that aims to capture advances in electrical energy technology as well as advances electronic devices and systems used to control and capture other sources of energy. Electric power generated from alternate energy sources is getting increasing attention and supports for new initiatives and developments in order to meet the increased energy demands around the world. The availability of computer–based advanced control techniques along with the advancement in the high-power processing capabilities is opening new doors of opportunity for the development, applications and management of energy and electric power. This series aims to serve as a conduit for dissemination of knowledge based on advances in theory, techniques, and applications in electric energy systems. The Series accepts research monographs, introductory and advanced textbooks, professional books, reference works, and select conference proceedings. Areas of interest include, electrical and electronic aspects, applications, and needs of the following key areas:

- Biomass and Wastes Energy
- Carbon Management
- Costs and Marketing
- Diagnostics and Protections
- Distributed Energy Systems
- Distribution System Control and Communication
- Electric Vehicles and Tractions Applications
- Electromechanical Energy Conversion
- Energy Conversion Systems
- Energy Costs and Monitoring
- Energy Economics
- Energy Efficiency
- Energy and Environment
- Energy Management, and Monitoring
- Energy Policy
- Energy Security
- Energy Storage and Transportation
- Energy Sustainability
- Fuel Cells
- Geothermal Energy
- Hydrogen, Methanol and Ethanol Energy
- Hydropower and Technology
- Intelligent Control of Power and Energy Systems
- Nuclear Energy and Technology
- Ocean Energy
- Power and Energy Conversions and Processing
- Power Electronics and Power Systems
- Renewable Energy Technologies
- Simulation and Modeling for Energy Systems
- Superconducting for Energy Applications
- Tidal Energy
- Transport Energy

The books of this series are reviewed in a single blind peer review process by the main editor and/or the advisory board.

Behrooz Vahidi · Ramezan Ali Naghizadeh

Principles and Modeling of the Power Transformers

Springer

Behrooz Vahidi
Department of Electrical Engineering
Amirkabir University of Technology
Tehran, Iran

Ramezan Ali Naghizadeh
Department of Electrical Engineering
Hamedan University of Technology
Hamedan, Iran

ISSN 2199-8582 ISSN 2199-8590 (electronic)
Energy Systems in Electrical Engineering
ISBN 978-981-99-5795-8 ISBN 978-981-99-5796-5 (eBook)
https://doi.org/10.1007/978-981-99-5796-5

Preface

The transformer is a very important part of the power system network and transformer modeling is an earliest science within the field of power system engineering. This means that changes can happen in this field for changes we need to know the previous studies fully.

In this book, an in-depth survey of the transformer modeling is presented which can be used in power system study. This book offers different models for power transformers in the range of different frequencies (low frequency, medium frequency, and high frequency). Those models are collected from different sources.

Therefore, to whom is this book directed? It will truly be of use to postgraduate students and power system engineers.

This book is divided into six chapters. Chapter 1 provides an introduction to power transformers. Chapter 2 deals with power transformer construction. Chapter 3 discusses different types of transformers, connections, protections, and remaining life. Chapter 4 is about power transformer core modeling Chapter 5 is concerned with the low-frequency and mid-frequency modeling of the transformers. Chapter 6 discusses high-frequency modeling of transformer.

The goal of this book is to educate postgraduate students and engineers about principles and modeling of the transformers.

The authors' special thanks go to all readers in advance who will give us a feedback on the book.

Tehran, Iran
June 2023

Behrooz Vahidi
Ramezan Ali Naghizadeh

Acknowledgments The authors wish to acknowledge the assistance provided by Dr. Ashkan Teymouri for providing the last typesetting of the book.

Contents

Chapter 1
Power Transformers

1.1 Introduction

Power transformers were first invented in the ninetieth century. Power transformers are an essential part of transmission and distribution networks.

Through their primary terminals, transformers take electrical power at a specific voltage that yields a certain current and delivers it to their secondary terminals with change voltage and current levels [1–3]. Concerning electrical motors and generators, transformers have higher efficiency.

In the secondary of transformer voltage level increased and thus current level reducing, the transmission lines of power system network losses considerably [4, 5]. Transformers' active part (winding + core) also produces loss dissipated as heat. The transformer heat is removed by a cooling system (natural or forced cooling system) so that the winding temperature is not exceeding more than the standard limitations [6–8]. Transformers are also subjected to high voltage stresses, and their insulation should survive when these stresses are below specific values, which are mentioned in standards [9–12].

At the first stage of transformers' manufacturing in the ninetieth century, the designer of transformers used insulation oil to cool and insulate the transformers. Still, new insulation and cooling techniques are used [2, 3]. Early transformers used oil and insulating paper in their construction, which now is improved, and other kinds of insulations are used.

Oil insulation properties of the transformer can be used for condition monitoring of the transformer. A large amount of knowledge about the transformer condition can be inferred by analyzing specific properties of the insulating liquid [5].

The power transformers' field of study is vast and diverse, which can be attractive to any power engineer.

B. Vahidi and R. A. Naghizadeh, *Principles and Modeling of the Power Transformers*, Energy Systems in Electrical Engineering,
https://doi.org/10.1007/978-981-99-5796-5_1

1.2 Transformer Theory

1.2.1 Ideal and Real Transformer

Power transformers are an essential part of the electrical network. Different types of power transformers exist, such as shell and core types. The core types are widely used [3].

The transformer changes the voltage and current to another level through electromagnetic coupling between the primary and secondary winding.

For a winding with N turns in the magnetic field, we can obtain the induced voltage as follow:

$$v(t) = N\frac{d\phi}{dt} \tag{1.1}$$

where:

ϕ is magnetic flux

t is time.

For sinusoidal varying flux:

$$\phi = \phi_m \cos(2\pi ft) \tag{1.2}$$

ϕ_m is flux amplitude

f is frequency.

Then,

$$v(t) = 2\pi Nf\phi_m \sin(2\pi ft) = \sqrt{2}V \sin(2\pi ft) \tag{1.3}$$

V is the practical value of voltage and can obtain from the following equation.

$$\left(\frac{V}{N}\right) = \sqrt{2}\pi f\phi_m = 4.44fB_mA \tag{1.4}$$

where:

B_m is maximum flux density (Tesla)

A is the core cross-section area (m^2).

An ideal transformer consists of two winding (primary and secondary). These windings are only linked to mutual flux in the core, no need for magnetizing current, and no loss in the windings. Therefore, input and output power are equal and can write $V_1I_1 = V_2I_2$. Figure 1.1 shows the diagram of a single-phase transformer.

From Eq. (1.4) can write:

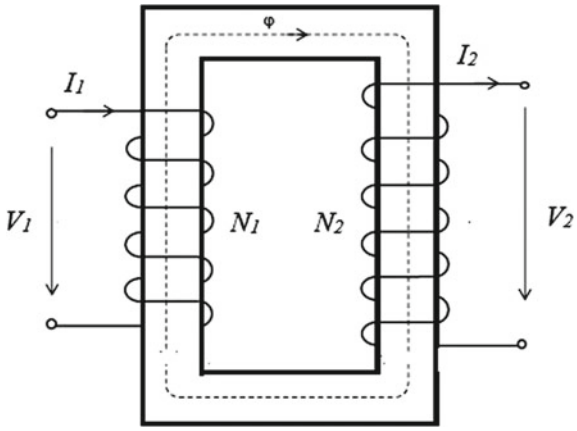

Fig. 1.1 A schematic diagram of a single-phase transformer

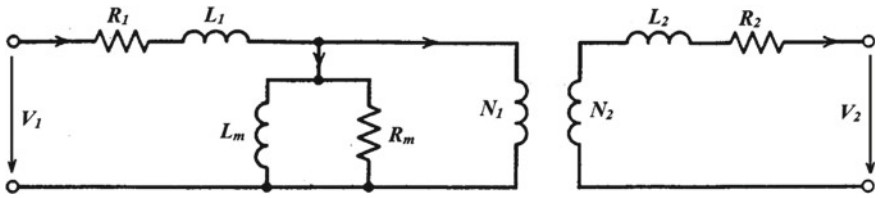

Fig. 1.2 Equivalent circuit of a real single-phase transformer

$$\frac{V_1}{V_2} = \frac{N_1}{N_2} \qquad \frac{I_1}{I_2} = \frac{N_2}{N_1} \tag{1.5}$$

In a real transformer, flux is not restricted to the core. It is also outside the core, and the transformer has different losses, such as windings loss, core, and other metallic part losses. Resistors show these losses in the equivalent circuit of the actual transformer. Figure 1.2 shows the equivalent circuit of a real single-phase transformer.

1.2.2 Impedance

The impedance of a transformer is:

$$Z\% = \sqrt{(R\%)^2 + (X\%)^2} \tag{1.6}$$

This is the positive or the negative sequence short circuit impedance. Load loss presents resistance behavior, and leakage flux presents reactance behavior [3]. *R* can

be computed from load loss by measurement or from the following equation [3]:

$$I^2R = \frac{J^2\rho \times 10^9}{d_{cu}} \tag{1.7}$$

where:

ρ is conductor resistivity at 20 °C

J is the current density of conductor (A/mm^2) at 75 °C

d_{cu} is conductor density.
For copper:

$\rho = 1.724 \times 10.^8$ Ω.m

$d_{cu} = 8.89$ kg/dcm^3
Therefore:

$$I^2R = 2.36\,J^2\,(\mathrm{W/kg}) \tag{1.8}$$

X (reactance) can be computed from Eq. (1.9) [3]:

$$X\% = 0.124 \times \frac{(kV/\phi)}{h_{wdg}(V/N)^2} \times \frac{f}{50} \times \Sigma Da \times R_g \tag{1.9}$$

Parameters of Eq. (1.9) can be computed as follows in Fig. 1.3.
where:

kVA/ϕ is per phase power rating of the transformer

V/N is voltage per turn

h_{wdg} is the average magnetic height of windings (mm)

f is the frequency (Hz)

$\Sigma Da = (d_1 \times a_1)/3 + (d_{12} \times a_{12}) + (d_2 \times a_2)/3$, dimensions are according to Fig. 1.3.

R_g is the Rogowski correction factor and can be computed from Eq. (1.10)

$$R_g = 1 - \frac{(a_1 + a_{12} + a_2)}{\pi \cdot h_{wdg}}\left(1 - e^{\frac{-\pi h_{wdg}}{(a_1 + a_{12} + a_2)}}\right) \tag{1.10}$$

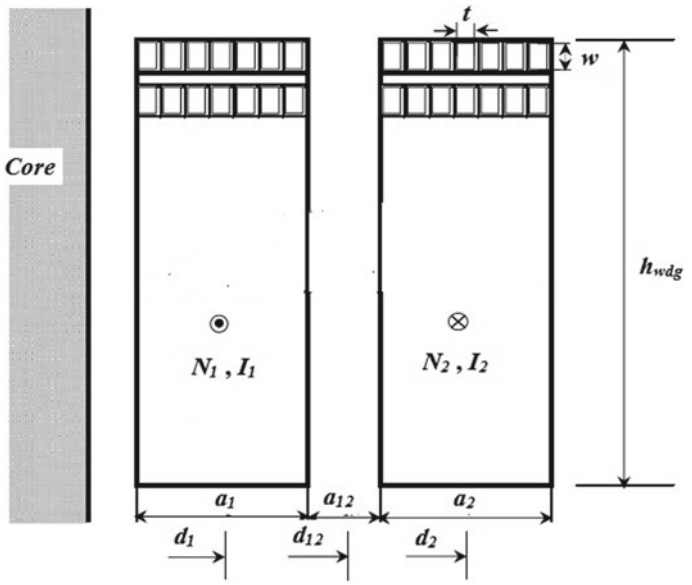

Fig. 1.3 Dimensions of two windings of a transformer

1.3 Power Transformer Steady State Modeling

In most studies of power systems such as load fellow, short circuit, harmonics, random outage, and…., a simple model for transformer is used [13, 14]. Figure 1.4 shows this simple model for two winding transformers.

In many applications, the parallel branch can be neglected. Also, the transformer has a zero-sequence equivalent model as well. The transformer's zero-sequence model depends on windings connections and the method of grounding. Figure 1.5 shows zero-sequence models for different transformer connections. Sometimes the core loss is included in the series branch, and Fig. 1.4 changes to Fig. 1.6.

The positive sequence of three winding transformers is as Fig. 1.7.

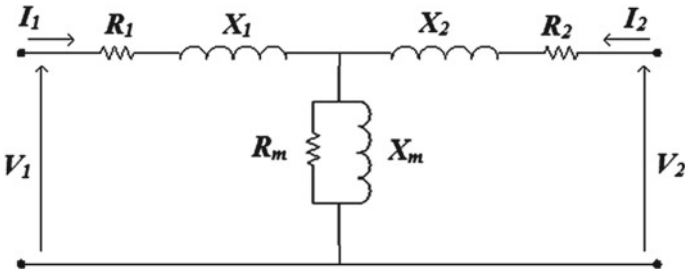

Fig. 1.4 A simple model of two winding transformers (T model)

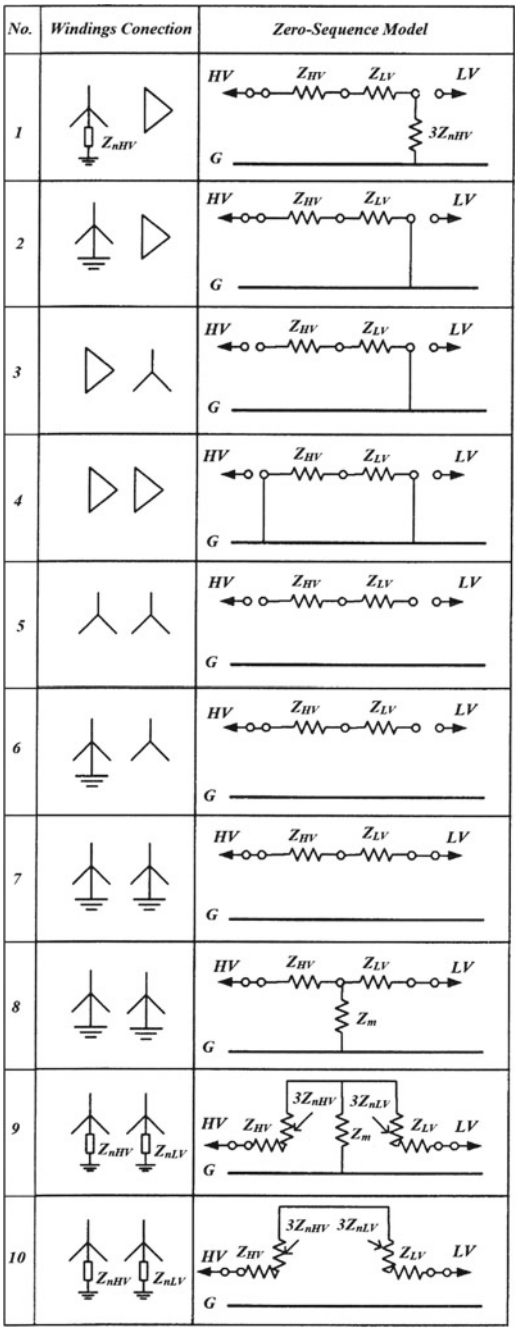

Fig. 1.5 Zero-sequence models for different transformer connections

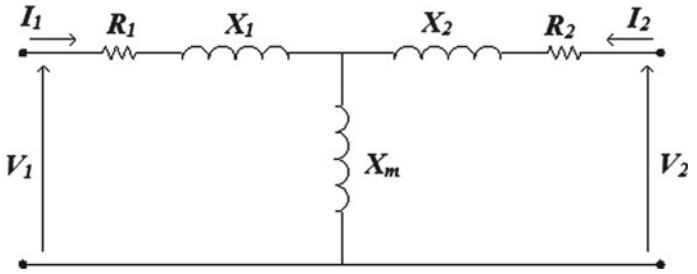

Fig. 1.6 A simple model of two winding transformers without R_m (T model)

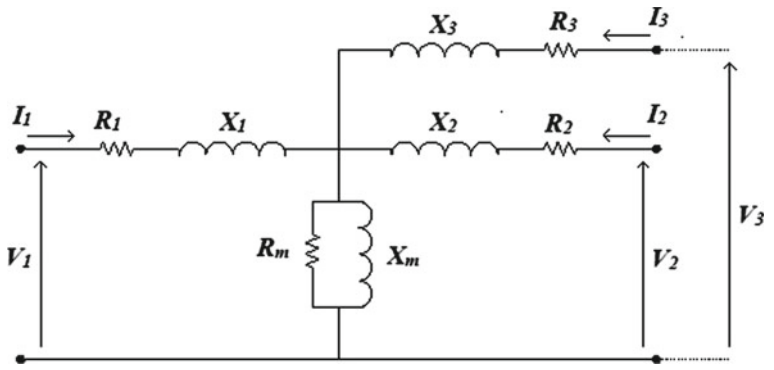

Fig. 1.7 Positive-sequence model for three winding transformers

1.3.1 Experiments that Can Be Used to Extract a Power Transformer Steady State Model

According to standards, manufacturers must conduct no-load test, load loss test, and…. on the transformer before leaving the factory [6, 8]. Although the primary purpose of these tests is not to extract the transformer model, these tests can be used for extracting the transformer model. To extract the component of Figs. 1.4 and 1.6 following experiments are required:

- No-load test: From the results of this test, resistance and reactance of parallel branches (R_m and X_m) can be extracted.
- Load loss and impedance voltage test: From this test's results, the model's series components (R_1, R_2, X_1, X_2) can be extracted.
- Experimental tests of components of the zero-sequence model: from the results of these tests, components of the zero-sequence model can be extracted. Although with good approximation, the components of the zero-sequence model can be obtained from components of the positive-sequence model.

- Experimental tests of windings resistance: this test is not used directly for computing components of the model but can be used for determining the load loss at a working temperature [15].

1.3.2 No-Load Test and Parallel Impedance Modeling

For the no-load test, a no-load transformer will be connected to a source such as a Fig. 1.8.

The manufacturer tests the transformer according to one of the standards [6, 7] and records the results on the test report. The measurements are done by wattmeter, voltage, and current transformer. To reduce the laboratory's equipment cost, the test can be conducted on low voltage winding.

For example, tests are conducted on the low voltage side in a three-winding transformer (230 kV/63 kV/20 kV).

Assume that the results of the no-load test on a transformer are as follows:

- The nominal feeding voltage in the no-load test is V_n (kV)
- Nominal feeding power in the no-load test S_n (MVA)
- Nominal power of windings (MVA):

$$S_{\max} = \text{Max}\{S_{HV}, S_{MV}, S_{LV}\}$$

- The test is conducted at α percent of nominal voltage at a nominal tap
- The total corrected three-phase loss power is $P_{loss(corrected)}$ (kW)
- Measured currents (A) are i_a, $i_{b,}$ and i_c

Power is measured at test temperature and should be transferred to 75 °C temperature, the highest working temperature mentioned in the standard [16]. The power loss at 75 °C is used in the computation.

The component of the model can be extracted from the following equations:

The no-load current of the transformer is the average value of the three phase's currents:

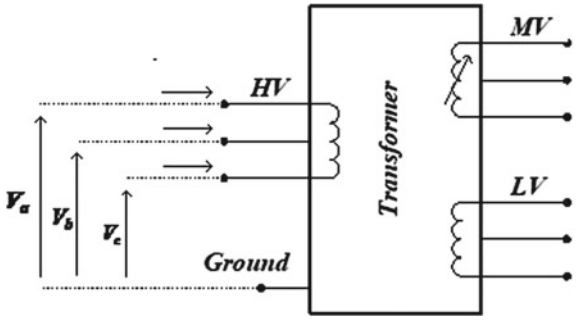

Fig. 1.8 A transformer under no-load test

$$i_{no-load} = \frac{i_a + i_b + i_c}{3} \tag{1.11}$$

Per unit no-load current at measuring side (i_0) is:

$$I_{n(test)} = \frac{1000 S_n}{\sqrt{3} V_n} \tag{1.12}$$

$$i_0 = \frac{i_{no-load}}{I_{n(test)}} \times 100 \tag{1.13}$$

where:

$I_{n(test)}$ is nominal current of feeding side.

Practically the low voltage winding is the feeding side, and in three winding transformers power of the low voltage side is less than the power of other windings; therefore, i_0, which is obtained from Eq. (1.13), is unrealistic high, then it should be corrected as follow:

$$i_{0(S_{\max})} = i_0 \times \frac{S_n}{S_{\max}} \tag{1.14}$$

The per-unit value of the no-load loss is:

$$P_{loss(perunit)} = \frac{P_{loss(corrected)}}{1000 S_{\max}} \tag{1.15}$$

$P_{loss(corrected)}$ is a three-phase power loss at 75 °C.

Components of the parallel branch in per-unit are as follows (all parameters in equations are in per-unit):

$$Z_m = \frac{1}{i_{0(S_{\max})}} \tag{1.16}$$

$$R_m = \frac{1}{P_{loss(pu)}} \times \left(\frac{\alpha}{100}\right) \tag{1.17}$$

$$Z_m = \frac{R_m \cdot X_m}{\sqrt{R_m^2 + X_m^2}} \tag{1.18}$$

$$X_m = \frac{Z_m \cdot R_m}{\sqrt{R_m^2 - Z_m^2}} = \frac{1}{\sqrt{i_{0(S_{\max})}^2 - P_{loss(pu)}^2}} \tag{1.19}$$

If Fig. 1.6 is used, then:

$$X_m = \frac{1}{i_{0(S_{\max})}} \tag{1.20}$$

Example 1.1 A no-load test is conducted on a three-winding transformer (400 kV Y/230 kV Y/20 kVΔ) at f = 50 Hz. The power of each star winding is 200 MVA, and the power of delta winding is 40 MVA. Measurements are done at 20 kV side in the range of 70–110% of nominal voltage, and the results are as Table 1.1.

Solution:

If voltage is the nominal value ($\alpha = 1$), then the average value of three-phase currents is:

$$i_{no-load} = \frac{1}{3}(4.09 + 5.12 + 4.19) = 4.47\,\text{A}$$

The nominal current at the 20 kV side is:

$$i_{n(test)} = \frac{1000 \times 40}{\sqrt{3} \times 20} = 1155\,\text{A}$$

Therefore no-load current is:

$$i_0 = 100 \times \frac{4.47}{1155} = 0.386\%$$

In 200 MVA base, the no-load current from Eq. (1.14) is:

$$i_{0(S_{\max})} = 0.386 \times \frac{40}{200} = 0.077\%$$

The manufacturer indicated the total no-load loss at 75 °C; therefore, the per-unit value of the no-load loss on the 200 MVA base is:

$$P_{loss} = \frac{56.93}{1000 \times 200} = 0.000285\,pu = 0.0285\%$$

From Eq. (1.16), the per-unit value of impedance on the 200 MVA base is:

Table 1.1 Results of the no-load test

Test voltage (kV)	i_a (A)	i_b (A)	i_c (A)	$P_{total} = P_a + P_b + P_c$ (75 °C) (kW)
110% = 22	3.86	5.45	4.97	80.39
100% = 20	4.09	5.12	4.19	56.93
90% = 18	3.97	4.80	3.98	44.32

$$Z_m = \frac{1}{0.00077} = 1298.7\,pu$$

$$R_m = \frac{1}{0.000285} \times (1)^2 = 3513.1\,pu$$

From Eq. (1.19), the per-unit value of reactance is:

$$X_m = \frac{1298.7 \times 3513.1}{\sqrt{3513.1^2 - 1298.7^2}} = 1397.7\,pu$$

Or

$$X_m = \frac{1}{\sqrt{0.00077^2 - 0.000285^2}} = 1397.7\,pu$$

1.3.3 Load Loss Test and Impedance Voltage

With the aid of this test, the R_1, R_2, X_1, *and* X_2 can be computed. Different configurations of load tests on a three-winding transformer are shown in Figs. 1.9, 1.10, and 1.11. For this test following points have to be considered:

- The test is conducted at environment temperature, and measuring loss will transfer to 75 °C; therefore, the environment temperature should be indicated in the test report.

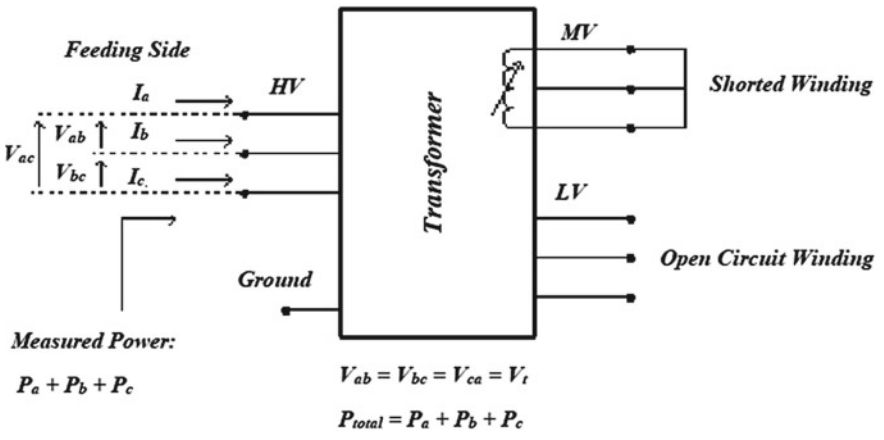

Fig. 1.9 A transformer under load test (MV winding shorted and HV winding fed)

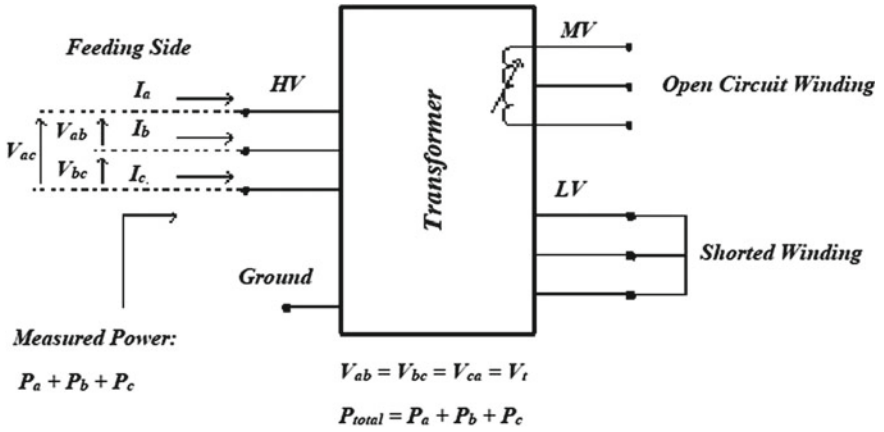

Fig. 1.10 A transformer under load test (LV winding shorted and HV winding fed)

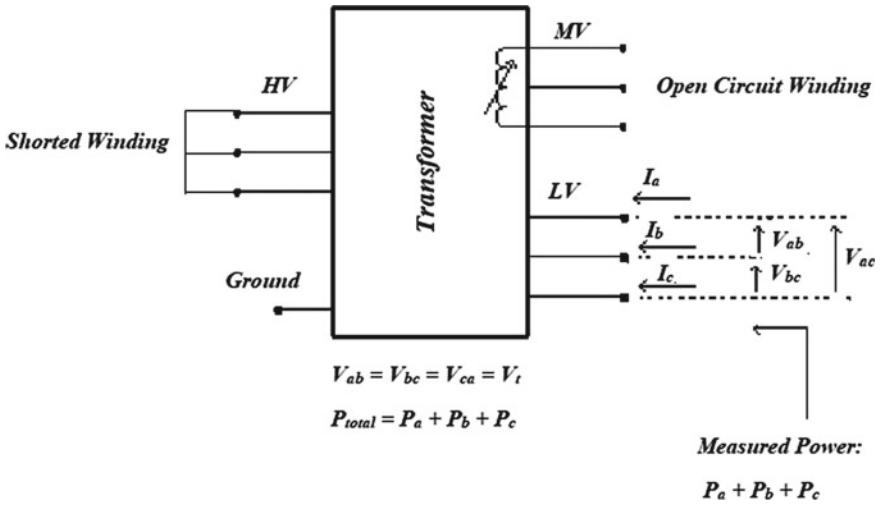

Fig. 1.11 A transformer under load test (HV winding shorted and LV winding fed)

- Currents of three phases are measured, and the final current of the transformer is the average value of these currents.
- Usually, the low voltage side is the feeding side.
- In power transformer cooling system (Oil natural, Air natural (ONAN)—Oil natural, Air forced 1 (ONAF 1)—Oil natural, Air forced 2 (ONAF 2), or Oil forced, air forced (OFAF), and during load changing the cooling method may change; therefore test should be repeated for these different conditions.
- In the tests that winding with tap is sorted or fed, this test should be repeated for nominal, minimum, and maximum voltages.

In transformer modeling, the results of the tests on the nominal tap are the closest case for extracting model components, but if the transformer is working on other taps, the results of tests on the other taps can be used [1, 17].

Assume the load and impedance test is conducted on the transformer in Fig. 1.8. The feeding and shorted windings are shown in Figs. 1.9, 1.10 and 1.11. Assume [18]:

S_{ns} (MVA) is the smallest power among powers of feeding and shorted windings.

V_{ns} (kV) is the nominal voltage of feeding winding.

I_{ns} (A) is the nominal current at feeding winding.

V_t (kV) is the voltage that produces a nominal current in the winding with the lowest power.

I_a, I_b, and I_c (A) are the effective value of three phases of currents.

$P_{loss75\,C}$ (kW) is the three-phase loss at 75 °C

$$I_t = \frac{1}{3}(I_a + I_b + I_c) \tag{1.21}$$

$$I_{ns} = \frac{1000 \times S_{ns}}{\sqrt{3}V_{ns}} \tag{1.22}$$

To compute the impedance in per-unit or impedance voltage in a percent:

$$Z_{pu} = \frac{Z_{actual}}{Z_{base}} = \frac{V_t/\sqrt{3}I_t}{V_{ns}/\sqrt{3}I_{ns}} = \frac{V_t}{V_{ns}} \cdot \frac{I_{ns}}{I_t} \tag{1.23}$$

$$U_k\% = 100 \times Z_{pu} \tag{1.24}$$

To compute the resistance in per-unit or ohmic part of impedance voltage in a percent:

$$\begin{aligned} R_{pu} &= \frac{R_{actual}}{Z_{base}} = \frac{1000P_{loss75\,C}/3I_t^2}{V_{ns}^2/S_{ns}} \\ &= \frac{P_{loss75\,C}}{1000S_{ns}} \cdot \left(\frac{S_{ns}}{\sqrt{3}V_{ns}}\right) \cdot \frac{1}{I_t^2} = \frac{P_{loss75\,C}}{1000S_{ns}} \cdot \left(\frac{I_{ns}}{I_t}\right)^2 \end{aligned} \tag{1.25}$$

$$U_R\% = 100 \times R_{pu} \tag{1.26}$$

During the test, the responsible engineer tries to keep the I_t as close as possible to the I_n. Therefore, the Eqs. (1.23) and (1.25) can be written as:

$$Z_{pu} = \frac{V_t}{V_{ns}} \tag{1.27}$$

$$R_{pu} = \frac{P_{loss75\,C}}{1000 S_{ns}} \tag{1.28}$$

In the practical case, I_t is not the same as I_n; therefore, it is better to use Eqs. (1.23) and (1.25).

Example 1.2 Assume that the load and impedance voltage test on the transformer of Example 1.1 is done at 23.5 °C. The test results are shown in Tables 1.2, 1.3 and 1.4. This transformer got 18 tap steps on the 230 kV side, and the test results are at the minimum, nominal, and maximum tap. Table 1.2 shows the test results for the ONAF2 condition that the transformer is at its full load (200 MVA). How much is the impedance per unit?

Solution:

The example is solved for the nominal tap condition.

i. Finding $U_{k(1.2)}\%$ and $U_{r(1.2)}\%$

The average value of current is obtained from Eq. (1.21):

$$I_t = \frac{1}{3}(284.3 + 283.4 + 283.7) = 283.8\ \text{A}$$

Table 1.2 Results of load test; 230 kV side shorted and measurement is done at 400 kV side at 200 MVA

Tap number	I_a (A)	I_b (A)	I_c (A)	V_t (kV)	$P_{3\varphi}$(W) (75 °C)
1	254.7	253.8	254.1	39.27	349,670
10	284.3	283.4	283.7	39.22	377,924
19	278.5	277.8	278	39.52	543,654

Table 1.3 Results of load test; 20 kV side shorted and measurement is done at 400 kV side at 40 MVA

Tap number	I_a (A)	I_b (A)	I_c (A)	V_t (kV)	$P_{3\varphi}$(W) (75 °C)
–	36.8	36.8	36.7	38.89	77,180

Table 1.4 Results of load test; 20 kV side shorted and measurement is done at 230 kV side at 40 MVA

Tap number	I_a (A)	I_b (A)	I_c (A)	V_t (kV)	$P_{3\varphi}$(W) (75 °C)
1	85.4	85.4	85.5	27.61	70,053
10	86.5	86.5	86.5	24.68	77,305
19	95.8	95.8	95.8	24.03	92,995

As the 230 kV side is shorted and measurement is done on the 400 kV side, data from Table 1.2 is used.

From Eq. (1.22):

$$I_{ns} = \frac{1000 \times 200\,\text{MVA}}{\sqrt{3} \times 400\,\text{kV}} = 289\,\text{A}$$

From Eq. (1.23):

$$Z_{1-2(pu)} = \frac{39.22\,\text{kV}}{400\,\text{kV}} \cdot \frac{289\,\text{A}}{283.8\,\text{A}} = 0.0998\,pu$$

From Eq. (1.24):

$$U_{k(1-2)}\% = 100 \times 0.0998 = 9.98\%$$

From Eqs. (1.25) and (1.26):

$$R_{(1-2)pu} = \frac{377.924\,\text{kW}}{200000\,\text{kVA}} \cdot \left(\frac{289\,\text{A}}{283.8\,\text{A}}\right) = 0.0019\,pu$$

$$U_{r(1-2)}\% = 100 \times 0.0019 = 0.19\%$$

The above values are computed on a 200 MVA base.

ii. Finding $U_{k(1.3)}\%$ and $U_{r(1.3)}\%$

The average value of current is obtained from Eq. (1.21):

$$I_t = \frac{1}{3}(36.8 + 36.8 + 36.7) = 36.79\,\text{A}$$

As the 20 kV side is shorted and measurement is done on the 400 kV side, data from Table 1.3 is used.

From Eq. (1.22):

$$I_{ns} = \frac{1000 \times 40\,\text{MVA}}{\sqrt{3} \times 400\,\text{kV}} = 57.8\,\text{A}$$

From Eq. (1.23):

$$Z_{1-3(pu)} = \frac{38.89\,\text{kV}}{400\,\text{kV}} \cdot \frac{57.8\,\text{A}}{36.79\,\text{A}} = 0.1528\,pu$$

From Eq. (1.24):

$$U_{k(1-3)}\% = 100 \times 0.1528 = 15.28\%$$

From Eqs. (1.25) and (1.26):

$$R_{(1-3)pu} = \frac{77.180\,\text{kW}}{40000\,\text{kVA}} \cdot \left(\frac{57.8\,\text{A}}{36.79\,\text{A}}\right) = 0.0047\,pu$$

$$U_{r(1-3)}\% = 100 \times 0.0047 = 0.47\%$$

The above values are computed on a 40 MVA base.

iii. Finding $U_{k(2.3)}\%$ and $U_{r(2.3)}\%$

The average value of current is obtained from Eq. (1.21):

$$I_t = \frac{1}{3}(86.5 + 86.5 + 86.5) = 86.5\,\text{A}$$

As the 20 kV side is shorted and measurement is done on the 230 kV side, data from Table 1.4 is used.

From Eq. (1.22):

$$I_{ns} = \frac{1000 \times 40\,\text{MVA}}{\sqrt{3} \times 230\,\text{kV}} = 100.4\,\text{A}$$

From Eq. (1.23):

$$Z_{2-3(pu)} = \frac{24.68\,\text{kV}}{230\,\text{kV}} \cdot \frac{100.4\,\text{A}}{86.5\,\text{A}} = 0.1245\,pu$$

From Eq. (1.24):

$$U_{k(2-3)}\% = 100 \times 0.1245 = 12.45\%$$

From Eqs. (1.25) and (1.26):

$$R_{(2-3)pu} = \frac{77.305\,\text{kW}}{40000\,\text{kVA}} \cdot \left(\frac{100.4\,\text{A}}{86.5\,\text{A}}\right) = 0.0026\,pu$$

$$U_{r(2-3)}\% = 100 \times 0.0026 = 0.26\%$$

The above values are computed on a 40 MVA base.

1.3.4 Computation of Transformer Load Loss at 75 °C

If the load loss is not given at 75 °C, it should be transferred to this temperature. In the load test, two kinds of loss are produced [17, 19]:

i. Resistive loss is due to passing a current through primary and secondary resistance.
ii. Extra losses (stray loss) due to passing flux through the tank, oil, eddy currents, and …

The total load loss and testing room temperature can be computed as:

$$P_{total\ loss} = (P_a + P_b + P_c) \tag{1.29}$$

where:

P_a, P_b, and P_c are loss of a-phase, b-phase, and c-phase.

Extra loss (ii) can't be calculated directly; therefore, at first resistive losses should be computed; therefore, by extracting it from total load loss (Eq. 1.29), the result is extra loss. The resistance of windings and tern ratios are obtained from the test.

If the resistances referred to feeding side of the test are r_a, r_b, and r_c then the total resistance of windings is:

$$r_{total} = r_a + r_b + r_c \tag{1.30}$$

For computing, the resistances referred to feeding side Eq. (1.31) can be used.

$$r_i = r_{1i} + \left(\frac{V_{n(meas)}}{V_{n(shorted)}}\right)^2 r_{2i},\ i = a,\ b,\ c \tag{1.31}$$

where:

r_i has referred to the resistance of the a, b, and c phases.

r_{1i} is the resistance of each phase of the feeding side.

r_{2i} is the resistance of each phase of shorted side.

$V_{n(meas)}$ is the nominal voltage of the feeding (measuring) side.

$V_{n(shorted)}$ is the nominal voltage of shorted side.

Resistances are measured at the temperature of test time (T_{RM}) to have the value of resistance at the temperature of load loss measuring test (T_{LM}); the Eq. (1.32) can be used [19].

$$r_{total(T_{LM})} = \frac{T + T_{LM}}{T + T_{RM}} \times r_{total(T_{RM})} \tag{1.32}$$

For copper: $T = 234.5$
For Aluminium, $T = 228$
Resistive loss $\left(P_{R_{total(T_{LM})}}\right)$ at T_{LM} is:

$$P_{R_{total(T_{LM})}} = r_{total(T_{LM})} \times I_{ns}^2 \tag{1.33}$$

Extra losses (stray loss $P_{stray_{(T_{LM})}}$) can be computed from Eq. (1.34).

$$P_{stray_{(T_{LM})}} = P_{total_{(T_{LM})}} - P_{R_{total(T_{LM})}} \tag{1.34}$$

These losses should be transferred to 75 °C by using the following equation.

$$P_{stray(75)} = \frac{T + T_{LM}}{T + 75} \times P_{stray(T_{LM})} \tag{1.35}$$

$$P_{Rtotal(75)} = \frac{T + 75}{T + T_{LM}} \times P_{R(T_{LM})} \tag{1.36}$$

$$P_{total(75)} = P_{R_{total(75)}} + P_{stray(75)} \tag{1.37}$$

Example 1.3 Assume impedance voltage test is done on the transformer of Examples 1.1 and 1.2 at the nominal tap. The 230 kV side is shorted, and measurements are done at the 400 kV side (feeding side); and results of this test are mentioned in Table 1.2. Losses are not at 75 °C; the loss at the nominal tap at 23.3 °C is 337442 W. DC resistances of primary and secondary sides at 20 °C are mentioned in Table 1.5. What is the value of the loss at 75 °C?

Solution:

Measurement is done at the HV side. Therefore, the resistance of each phase is computed regarding the HV side. By using Eq. (1.31):

$$r_a = 0.5007 + \left(\frac{400}{230}\right) \times 0.1782 = 1.0397\,\Omega$$

$$r_b = 0.5011 + \left(\frac{400}{230}\right) \times 0.1798 = 1.0449\,\Omega$$

$$r_c = 0.5015 + \left(\frac{400}{230}\right) \times 0.1758 = 1.0332\,\Omega$$

$$r_{total} = r_a + r_b + r_c = 1.0397 + 1.0449 + 1.0332\,\Omega$$

This resistance is at 20 °C and should be referred to the test temperature (23.5 °C) (Eq. 1.32).

Table 1.5 The resistances of 400 kV side (HV) and 230 kV side (LV) at 20 °C in ohms

HV: r_a	HV: r_b	HV: r_c	LV: r_a	LV: r_b	LV: r_c
0.5007	0.5011	0.5015	0.1782	0.1798	0.1758

$$r_{total(23.5\,^{\circ}\mathrm{C})} = \frac{234.5 + 23.5}{234.5 + 20} \times 3.1178 = 3.1607\,\Omega$$

Resistive loss at 23.5 °C $\left(P_{R_{total(23.5)}}\right)$ is computed using Eq. 1.33.

$$P_{R_{total(23.5\,^{\circ}\mathrm{C})}} = 31.1607 \times 189^2 = 263984\,\mathrm{W}$$

$P_{stray_{(23.5^{\circ}\mathrm{C})}}$ can be computed from Eq. 1.34.

$$P_{stray_{(23.5\,^{\circ}\mathrm{C})}} = 337442 - 263984 = 73458\,\mathrm{W}$$

$P_{stray(75)}$ and $P_{Rtotal(75)}$ can be computed from Eqs. 1.35 and 1.36.

$$P_{stray(75)} = \frac{234.5 + 23.5}{234.5 + 75} \times 73458 = 61234\,\mathrm{W}$$

$$P_{Rtotal(75)} = \frac{234.5 + 75}{234.5 + 23.5} \times 263984 = 316678\,\mathrm{W}$$

Total loss at 75 °C $\left(P_{total(75)}\right)$ can be computed from Eq. 1.37.

$$P_{total(75)} = 316678 + 61235 = 377913\,\mathrm{W}$$

1.3.5 Computation of Components of Transformer Model

Figure 1.4 is a T model for two winding transformers. The model's components can be computed according to the equations mentioned above. The two winding transformer model can also be shown in Fig. 1.12 [20].

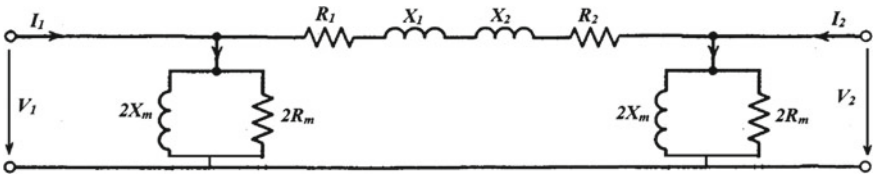

Fig. 1.12 A simple model of two winding transformers (π model)

References

1. M.J. Heathcote, *The J & P Transformer Book*, 13th edn. (Elsevier, 2007)
2. J.H. Harlow, *Electric Power Transformer Engineering* (CRC Press, 2004)
3. F. Zhu, B. Yang, *Power Transformer Design Practices* (CRC Press, 2021)
4. S.D. Myers, J.J. Kelly, R.H. Parrish, A guide to transformer maintenance, in *Transformer Maintenance Institute Division*, 2nd edn (S. D. Myers Inc., Ohio, USA, 1988)
5. A. Abi-Siada, *Power Transformer Condition Monitoring and Diagnosis Power Transformer Condition Monitoring and Diagnosis* (The Institution of Engineering and Technology, 2018)
6. IEC 60076-1, Power Transformers–Part 1: General (2000)
7. IEC 60076-2, Power Transformers–Part 2: Temperature rise (1993)
8. C57.12.00, IEEE standard General requirements for liquid-Immersed distribution, power, and regulating transformer (2000)
9. IEC 60076-3, Power transformers–Part 3: insulation levels, dielectric test and external clearances (2000)
10. C57.98 Guide of impulse testing techniques, interpretation of oscillograms and failure detection criteria (1993)
11. R. Feinberg, *Mdern Power Transformer Practice* (The Macmillan Press Ltd., 1979)
12. R.M. Del Vecchio, B. Poulin, P.T. Feghali, D.M. Shah, R. Ahuj, *Transformer Design Principles* (CRC, 2002)
13. ABB Power Technology Management Ltd., *Transformer Handbook* (ABB, Switzerland, 2004)
14. K. Karsai, D. Kerenyi, L. Kiss, *Large Power Transformers* (Elsevier Publication, Amsterdam, Netherland, 1987)
15. *Westinghouse Electric Transmission and Distribution Handbook*, 4th edn. (Westinghouse Electric Co., East Pittsburgh, PA, 1964)
16. L.F. Blume, A. Boyajian, G. Camili, T.C. Lennox, S. Minneci, V.M. Monstinger, *Transformer Engineering* (Wiley, New York, and Chapman and Hall, London, 1951)
17. M. Waters, *The Short Circuit Strength of Power Transformers* (Macdonald, London, 1966)
18. B. Vahidi, M.R. Banktavakoli, *Modeling of Power System Equipment; Generator, Transformer, Transmission Line, Arrester, and Circuit Breaker* (in Persian) (Kerman Regional Power Company, Kerman, Iran, 2008)
19. ANSI/IEEE C57.12.90, Part II: Guide for short circuit testing of distribution and power transformers (1993)
20. K. Shaarbafi, *Transformer Modeling Guide* (Teshmont Consultants LP, Alberta, 2014)

Chapter 2
Power Transformers Construction

2.1 Introduction

Generally, the construction of power transformers for transformers rated a few kVA up to several hundred MVA is according to similar principles [1]. Also, manufacturing the larger size transformers need much experience and sophistication [1–6]; therefore, most manufacturers divide the production into two categories i. distribution transformers (up to 2500 kVA) and large size transformer (>2500 kVA). Large-size transformers may also divide into medium power and large power transformers. Facilities for large power transformer manufacturing are more expensive than those facilities for medium power or distribution size transformers.

The essential components of a transformer are:

1. Laminated core
2. Windings
3. Insulating materials
4. Transformer oil
5. Tap changer
6. Oil conservator
7. Breather
8. Cooling tubes
9. Buchholz relay
10. Explosion vent.

One of the most critical challenges in design and manufacturing power transformers is to use the most suitable design and manufacturing both technically and economically. Due to the design complexity and requested performance guarantees, a satisfactory result may not be obtained simply by solving several equations. The calculation should repeat with different parameters to find the most suitable design. Several parameters, such as conductor current density, can be adjusted during the design process, which affects winding loss and cooling.

B. Vahidi and R. A. Naghizadeh, *Principles and Modeling of the Power Transformers*, Energy Systems in Electrical Engineering,
https://doi.org/10.1007/978-981-99-5796-5_2

Maximum current density is one of these parameters, which varies for different sizes of the transformers because it is related to the cooling method of the transformer.

The current densities of 3.2 A/mm^2 to 5.5 A/mm^2 are used for distribution transformers and larger with force cooling for class A insulated transformers [7–9]. For large non-forced cooling transformers current density is 4 A/mm^2. For compact transformers, the current density is about 7 to 7.3 A/mm^2 for 75 to 95 °C rises for class H insulation. Another critical parameter in transformer design is flux density in the transformer's core, which is generally selected as 1.7 T.

The winding insulation should be arranged not only to establish sufficient electric strength against breakdown under different conditions that will be met in service but also to allow adequate circulation of the cooling medium so that no part of the winding gets excessively hot [5].

2.2 Different Types of Winding

Windings are subjected to a shrinking and seasoning process, so no further shrinkage occurs during service. Adjustable devices are provided for taking up possible shrinkage in service. Coils are supported at different intervals by using wedge-type insulation spacers that are permanently secured in place and provide the proper oil circulation. Before use for permanent tightness of winding assembly, the insulation spacers must be dried and compressed under high pressure [10]. A sharp bend on the windings should not be because it may damage the insulation or produce high dielectric stresses. "Materials used in the insulation and assembly of the windings shall be insoluble, non-catalytic, and chemically inactive in the hot transformer oil. They shall not be softened unless otherwise affected under the operating conditions [10]". There are different types of windings of transformers, such as:

2.2.1 Layer Winding

In a layer winding, the conductors are wound in the axial direction in helix form. In this type of winding, there is no radial spacer between turn-to-turn insulation; therefore, heat dissipation from winding is poor compared to other winding types.

Figure 2.1 shows a schematic diagram of the layer winding—the actual layer winding on a power distribution transformer in Fig. 2.2.

The winding thickness (winding outer radius–winding inner radius) is not high. Therefore mechanical strength of winding under short circuit conditions is not high. This type of winding is used for low voltage and current transformers [3].

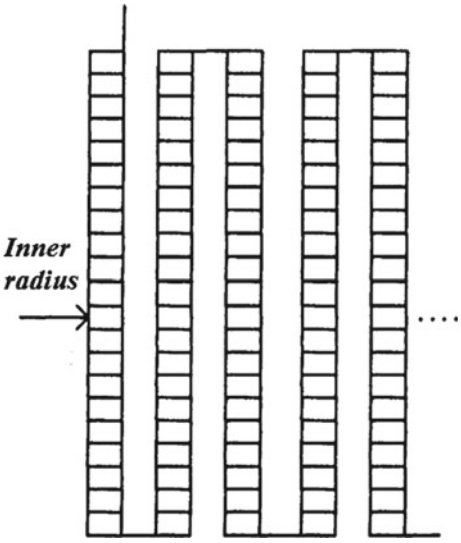

Fig. 2.1 A schematic diagram of layer-type winding

Fig. 2.2 A power distribution transformer with layer-type winding

2.2.2 Multi-start Winding

Multi-start winding is essentially several helical windings that are wrapped together. This type of winding is used as tap winding, and the advantage of this type is that each

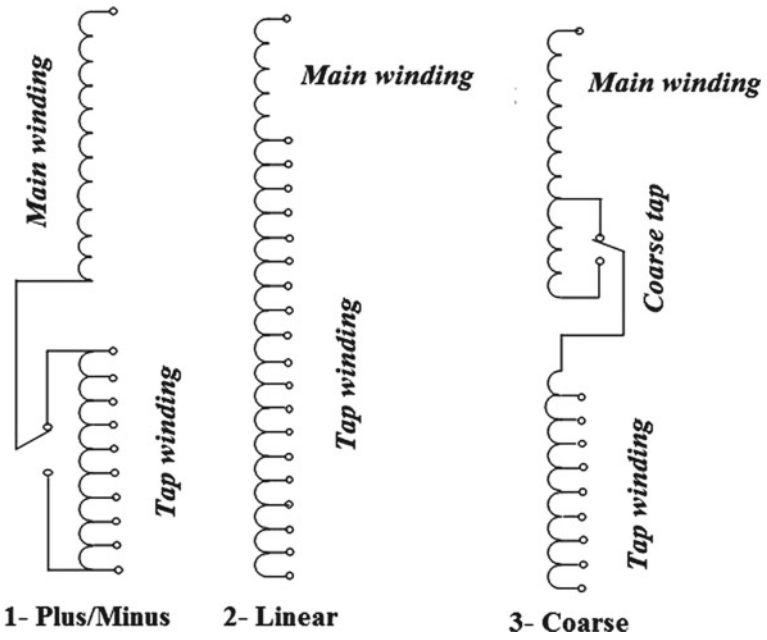

Fig. 2.3 A schematic diagram of the tap-type winding

tap has its turns distributed uniformly along the whole length; therefore, ampere-turn and magnetic balances can be achieved [3]. Figure 2.3 shows tap windings.

2.2.3 Helical Winding

In helical winding type, turns are wrapped in a helix form on a cylinder shape pressboard. This type of winding is used for high current and low voltage winding, and each turn can consist of several conductors. Figure 2.4 shows the schematic diagram of a helical winding.

2.2.4 Disc Winding

Disc type winding is used for medium current and high voltage winding. Several discs are connected and placed in an axial direction to make the winding. Each disc consists of several turns, and each turn may consist of several conductors. Figure 2.5 shows the disc windings.

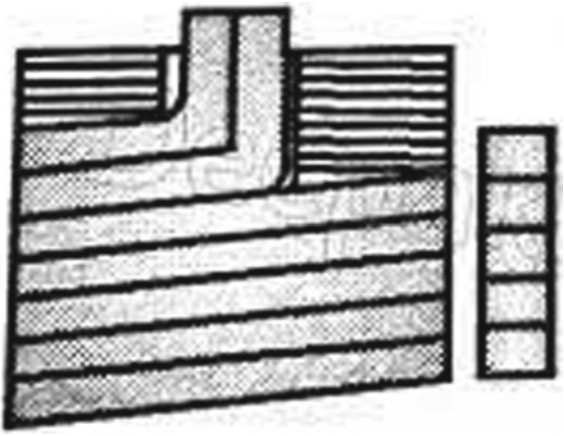

Fig. 2.4 Schematic diagram of a helical winding

Fig. 2.5 Disc windings

2.2.5 Transposition

By loading a transformer, current passes through LV and HV windings producing a magnetic field, and the leakage flux, which, unlike the core flux, exists outside the core. This leakage flux induces a voltage in windings. Due to the non-uniform

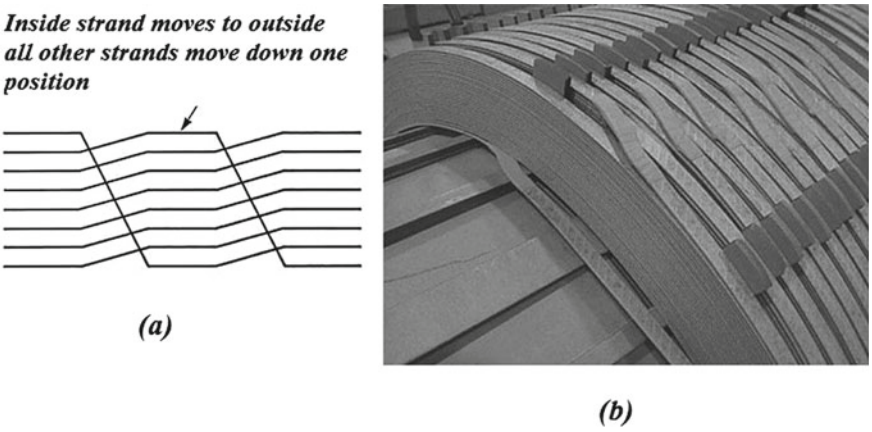

Fig. 2.6 **a** Movement of strands **b** transposed winding

distribution of the leakage flux, the induced voltage in the conductor is dependent on the conductor's location.

The result of this phenomenon is producing circulating current losses. In some large transformers misdesigned, the circulating currents are so high that they cause higher-than-expected load losses, overheat the conductor insulation papers, and eventually bring failures.

It is possible to reduce this circulating current by reducing the induced voltage by transposing the conductors. The transpositions give each conductor the exact spatial location to get the same induced voltage. The sum of induced voltage and circulating current in a loop reduces as much as possible. Figure 2.6 shows the transposition of winding conductors.

2.2.6 Half-Turn Effect

If the winding leads are taken out from the different sides of the core, the half-turn effect is present. In this case, an additional half-turn in one of the core windows in a single-phase transformer can produce over-fluxing of the core, which yields excessive losses and temperature rises [11]. Figure 2.7 shows a schematic representation of the half-turn case.

2.2.7 Split Windings

Some transformers have a set of LV and HV windings. The two set windings can sometimes be stacked one on top of another, called axial split winding. Another

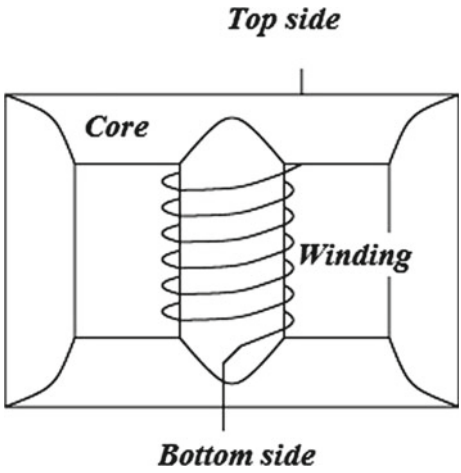

Fig. 2.7 Schematic diagram of half-turn

method is to separate them radially, called radial split winding design. Figure 2.8 shows a schematic diagram of split winding.

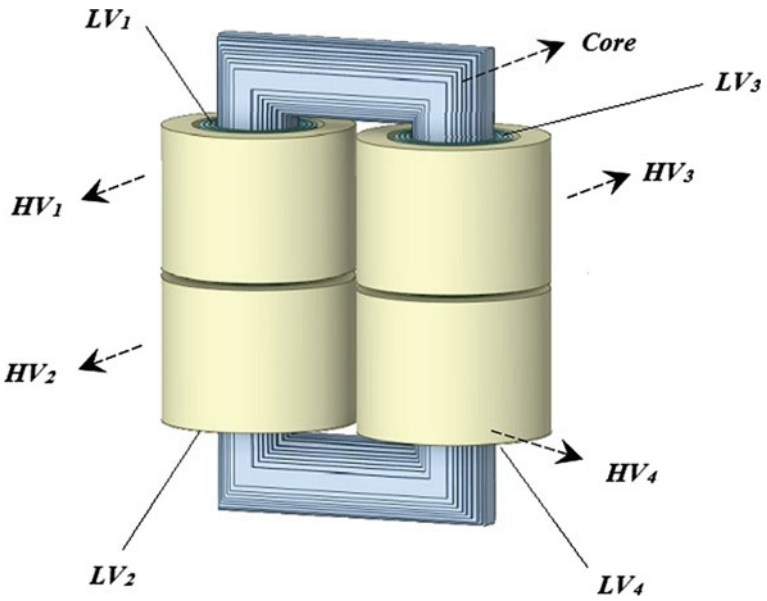

Fig. 2.8 Schematic diagram of split winding

2.2.8 Cables Used in Winding

Different types of wire cables are used in windings, such as single-strand, twin-strand, or triple-strand cables. When the winding's current is low, these strand types are used simply without transposition (Fig. 2.9)., but for windings with high current, the continuously transposed cables are transposed (Fig. 2.10). This dramatically reduces the eddy current losses in windings and improves the space factor.

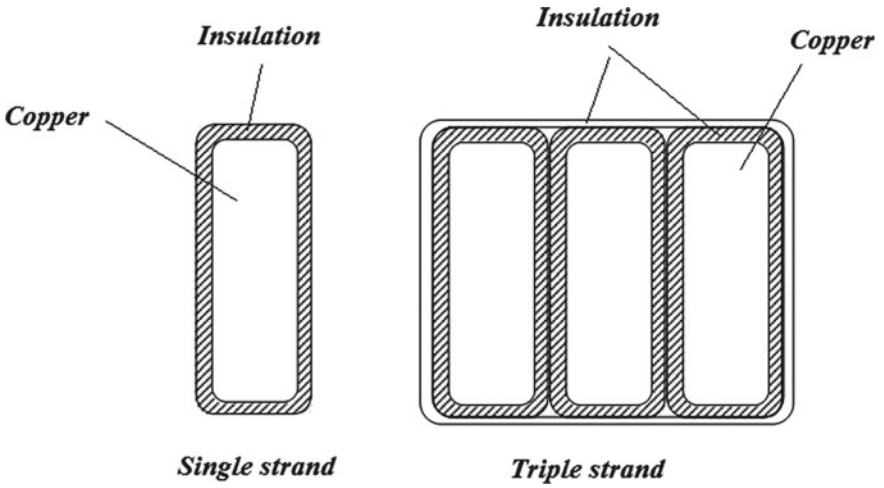

Fig. 2.9 Stranded wire cable without transposition

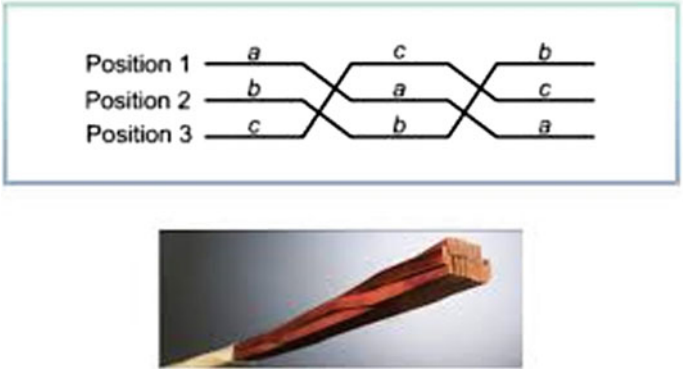

Fig. 2.10 Stranded wire cable with transposition

2.3 Transformer Core

The duty of the transformer core has to provide a low reluctance path for passing magnetic flux by linking the primary and secondary windings [1]. Due to this flux, hysteresis and eddy currents losses in the core produce heat. The alternating flux generates noise which can be high in high-power transformers. In a high-power transformer core, losses can be considerable. Some 5 percent of all electric power generated is estimated to be dissipated as iron losses in electrical equipment [1]. Figure 2.11 shows a transformer core.

The hysteresis loss can be computed from Eq. (2.1)

$$W_h = k_1 f B_m^n \ \text{(W/kg)} \tag{2.1}$$

The eddy current loss can be computed from Eq. (2.2)

$$W_e = k_2 f^2 t^2 \frac{B_{eff}^2}{\rho} \ \text{(W/kg)} \tag{2.2}$$

where;

Constant k_1 and constant k_2 depend on the core material.

Frequency (Hz) is f.

The thickness of material in millimeters is t.

The maximum flux density in Tesla is B_m.

B_{eff} in Tesla is the flux density due to the application of R.M.S. of voltage.

The 'Steinmetz exponent' is n that, dependent on the material's essence, and is chosen as 1.6. However, in the cases of materials with higher values of flux densities, n can be chosen between 1.6 to 2.5 and higher [1].

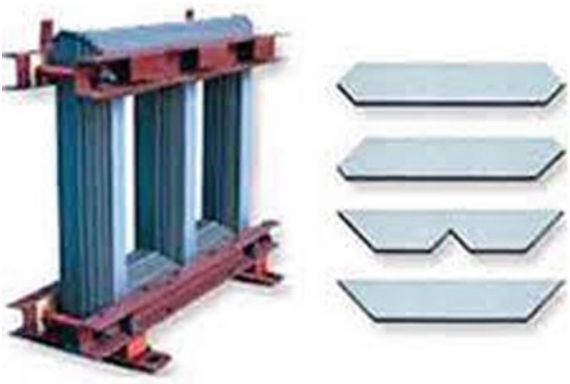

Fig. 2.11 A transformer core

Fig. 2.12 A three-leg core

2.3.1 Core Types

For three-phase transformers, two core types are used:

i. Three-leg core
ii. Five-leg core.

2.3.1.1 Three-Leg Core

The three-leg core transformer has a particular configuration because there is not a return path for the flux of upper and lower yokes, and for positive or negative sequence fluxes which are produced by applied balanced voltages, the sum of three legs fluxes is zero because fluxes have the same magnitude and are 120° apart from each other [1, 3]. For residual zero-sequence flux, which is produced by the unbalanced applied voltage; this flux leaves one yoke and returns to another yoke through insulation oil. The high reluctance of this path impresses the flux and reduces the voltage impedance. Therefore the three-leg core acts as a closed circuit for positive and negative sequence flux but acts as an open circuit for zero-sequence flux [1, 3]. Figure 2.12 shows a three-leg core.

2.3.1.2 Five-Leg Core

The three-leg core may cause more shipping height than bridges and tunnel limits for large unit three-phase transformers. In these cases, the five-leg core is used to reduce yoke height. Therefore the height of the core and the height of the transformer are reduced. Also, the cooling of yokes is greatly improved [1, 3]. The five-leg core acts as a closed circuit for zero-sequence flux and both positive/negative sequence fluxes

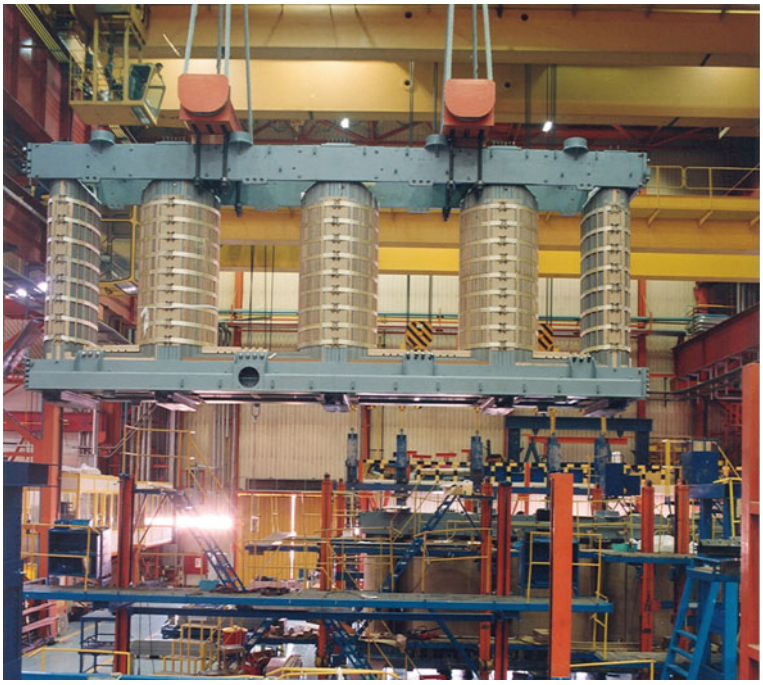

Fig. 2.13 A five-leg core

because the unwounded legs for zero-sequence flux act the same as a low reluctance path as the wound legs to positive/negative sequence fluxes.

Figure 2.13 shows a five-leg core.

2.4 Transformer Assembling

2.4.1 Core Building

A leg is made from core laminations and has a nearly circular cross-section for optimal use of the cylindrical space inside the windings. The approximate cross-section area of the core to circular shape depends on how many strips with different widths are used. The strips fill approximately 93% to over 95% of the core circle [3]. Figure 2.14 shows strips of core laminations, and Fig. 2.15 shows how technicians build a core from strips.

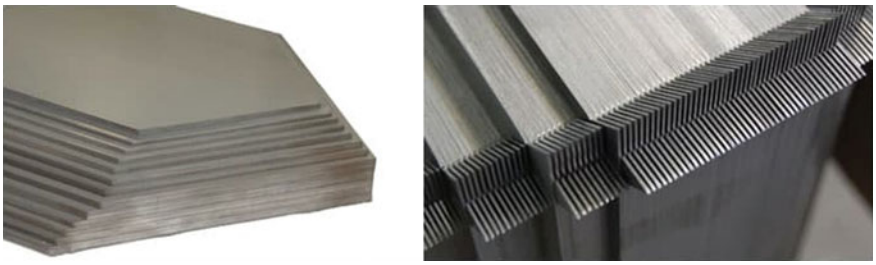

Fig. 2.14 Strips of core laminations

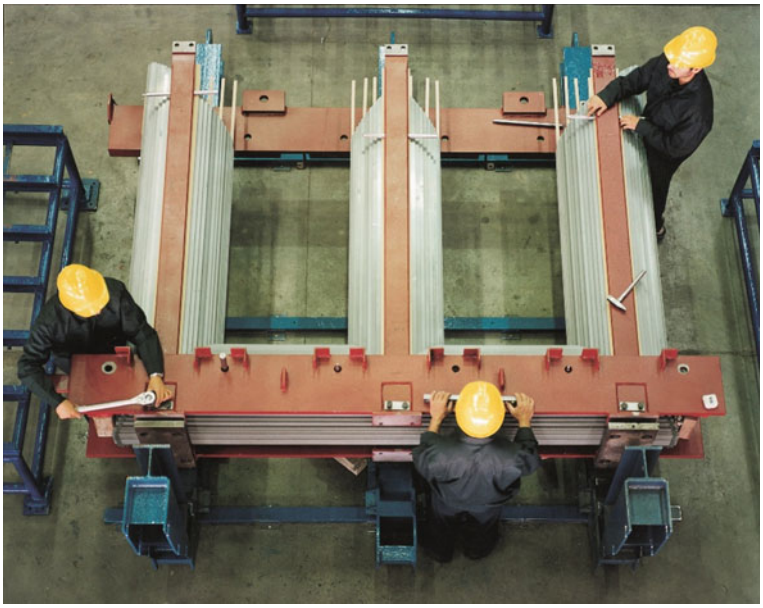

Fig. 2.15 Technicians are building a core

2.4.2 Core Insulation and Grounding

The core and other metallic parts are insulated, but the core is grounded at one point at the upper yoke. Several grounding points may cause a circulating current and could produce local heating. The core sheets are insulated from each other by an insulating layer on both sides of the sheet. Suitable insulating materials must be used for this job because a low thermal rating material could shorten the service life of the core. It should be noted that circulating current in the core or other metallic parts should be restricted to control local heating. Also, in high power transformers, stray 50 Hz and third harmonic fluxes due to unbalanced voltage can leave the core and flow in the space inside the transformer.

Fig. 2.16 A transformer tank

This flux can produce a circulating current inside the metal parts of the transformer, and local heating is the result. The five-leg core can solve the problem by preparing paths with low reluctance around the three core legs between the upper and lower yokes.

2.4.3 Transformer Tank

The transformer tank acts as a container for the active part and insulating oil and is under force during the transportation of the transformer [1, 3].

Generally, transformer tanks are constructed of steel sheets. To have access, the active part tank must have a removable cover bolted around the tank. Figure 2.16 show a tank of transformer.

Gaskets are used to connect the main cove and the tank to prevent oil leakage.

2.4.4 Transformer Bushing

Bushings are an essential component in power system networks. Their prominent role is to carry current at high voltage through the grounded parts. The bushing of the transformer is installed on the top or side of the tank for connection to the external circuit.

Different types of bushing are:

1. Bushings are made by porcelain insulators and used for up to 11 kV transformers.

Fig. 2.17 Transformer bushings

2. Bushings are filled with oil and consist of a hollow porcelain cylinder of a particular shape and are used for voltages above 33 kV.
3. Capacitor-type bushings are covered by porcelain rain shed and used for voltages above 33 kV.

Figure 2.17 shows transformer bushings.

2.4.5 Transformer Tapchanger

Tap changers adjust the output voltage of transformers at the proper level. Adjusting the voltage can do on-load, as on-load tap changers do this for many large transformers. Off-load tap changers are used for distribution transformers (rated voltage kV and rated power 2500 kVA) [1]. Figure 2.18 shows on-load tap changers (*a*) and off-load tap changers (*b*).

Tap changers adjust the output voltage by plus tap winding to the primary winding or minus it from the main winding by shorting the tap winding [1]. Off-load tap changers typically have three (±5%) or five tap steps ($2 \times \pm 2.5\%$), but on-load tap changers have more tap steps. The middle tap is for rated voltage.

Users of transformers need tapping for reasons such as the following:

- For compensating the variation in the voltage on the large systems.
- For compensating the regulation within the transformer for keeping the output voltage at a constant value.
- To control VAR flows of the system.
- For compensating the factors unclear at the planning time or allowing the future change of power system conditions and keeping the voltage in the proper range.

Fig. 2.18 On-load tap changers (**a**) and off-load tap changers (**b**)

2.4.6 Transformer Conservator Tank

The transformer's conservator tank is one of its most critical operation parts. Its essential duty is not only to circulate and keep the oil level in the transformer but also has an essential role in the earth faults protection of the transformer, heating, and maintaining the insulation of the windings. It is installed on the top of the transformer tank and based on the rating of the transformer, and it can have different capacities. Generally, it is installed between the main transformer tank and the outlet breather, which maintains the healthiness of the transformer oil. Its first duty is to maintain the transformer oil in the main tank within the standard levels. Figure 2.19 show a transformer conservator tank.

2.4.7 Buchholz Relay in Transformers

A Buchholz relay is mounted as a protection device on some oil-filled transformers with conservators. Buchholz relay is sensitive to the effects of dielectric failure that can happen inside the transformer, which they are protected, and is a kind of gas detection relay. Buchholz relay has two main floating parts, each with a mercury switch. The upper one operates when the oil level falls under the standard value. The

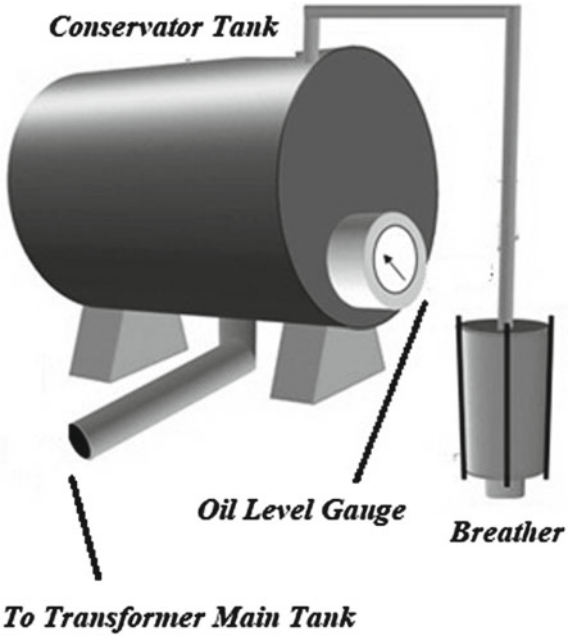

Fig. 2.19 A transformer conservator tank

lower one operates when oil enters the relay from that inlet at high pressure due to gas production in transformer oil. In addition to these main elements, a Buchholz relay has gas-release pockets on top.

The electrical leads from both mercury switches are taken out through a molded terminal block. Figure 2.20 shows the Buchholz relay.

2.4.8 Transformer Oil Temperature Indicators

Thermometers for measuring transformer oil temperature are essential for transformers with oil insulation to measure accurate oil temperature.

Direct Mount Transformer Thermometer: This thermometer is installed directly on the transformer tank. It is typically installed on the top or side wall of the transformer. "The design is such that the temperature probe is inserted into a pocket (well) on the tank wall at the mounting point. A direct mount thermometer is fairly easy to identify, as it has a probe straight out the back of the device, with the temperature gauge on the front." [12].

Fig. 2.20 The Buchholz relay

2.4.8.1 Remote Mount Type Thermometer of Transformer

In this type of thermometer, the probe is located in a pocket on the transformer, and the probe is connected to the visual indicator by a capillary tube.

In remote mount type of thermometers, you can display winding temperature, or you can show the oil temperature [12].

Figure 2.21 shows different types of thermometers.

2.5 Transformer Cooling System and Methods

The losses in transformers produce heat which should be dissipated out of transformers. If the dissipation of produced heat is not done correctly, the transformer temperature increases continually and can destroy the transformer's insulation. Therefore control of temperature in the permissible range is essential so that the transformer can have a long life by reducing the damage due to thermal degradation

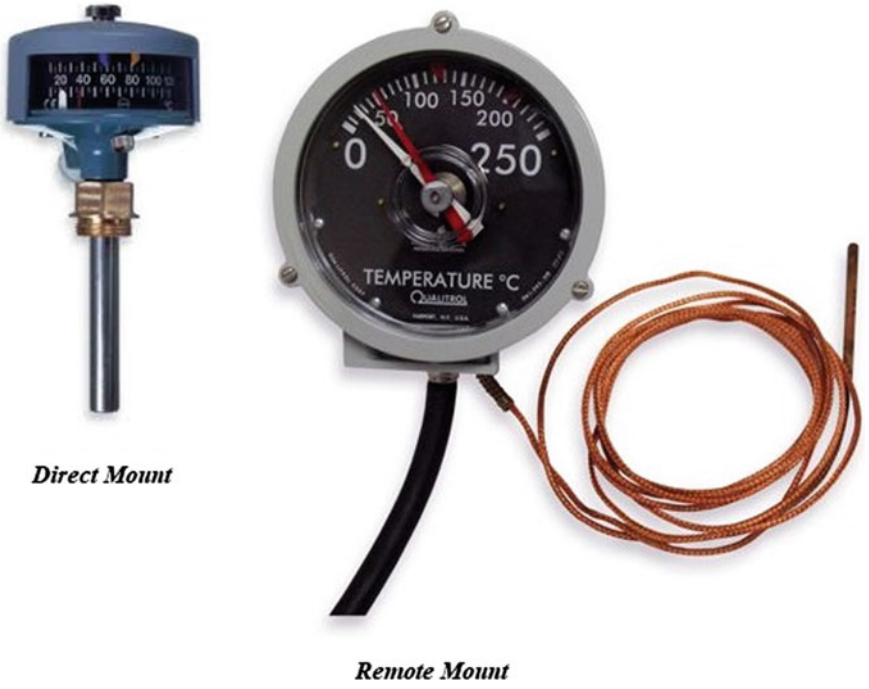

Fig. 2.21 Different types of thermometers

of transformer insulation. External cooling in a large transformer accelerates the transformer's heat dissipation rate. Types of cooling in transformers are different. Different methods are used to accelerate the cooling of transformers, which depend on the size and ratings of transformers [13].

2.5.1 ONAN Cooling of Transformer

This method is a straightforward method for cooling transformers. The ONAN is the abbreviation for "Oil Natural Air Natural." In the ONAN method, natural oil flow is responsible for heat dissipation.

In the ONAN method, the hot oil and cold oil change their position in the upper and lower portions of the tank of the transformer. By natural conduction, convection, and radiation in the air, the hot oil on the upper side of the tank can transfer the heat to the environment, and its temperature falls. Therefore transformer oil in the tank continually circulates during the transformer loading [13].

2.5.2 ONAF Cooling of Transformer

Increasing the dissipation surface increases the dissipated heat, but for faster heat dissipation, using fans on the surface of the transformer tank is necessary. ONAF is the abbreviation for "Oil Natural Air Forced."

2.5.3 OFAF Cooling of Transformer

In the oil forced air natural cooling system of the transformer, the heat dissipation is accelerated by using forced air on the dissipating surface; however, the hot oil circulation in the transformer tank is a natural convectional flow. The heat dissipation rate can still be increased if this oil circulation is accelerated by applying some force [13]. In the OFAF cooling system, the oil is forced to circulate within the closed loop of the transformer tank using oil pumps. OFAF means "Oil Forced Air Forced."

2.5.4 OFWF Cooling of Transformer

In the exact weather condition, the ambient temperature of the air is higher than water. Therefore water can use as a better heat transfer media concerning air. In the OFWF cooling method, the hot oil of the transformer is sent to the exchanger system by the pump, and cold water is cooling the exchanger pipes. OFWF is the abbreviation for "Oil Forced Water Forced" cooling in transformers [13].

2.5.5 ODAF Cooling of Transformer

ODAF, the abbreviation for "oil directed air forced" cooling of the transformer, is an improved version of OFAF.

In this method, the oil is forced to circulate and flow through predetermined paths inside the winding of the transformer.

The cool oil from the cooler system passes inside the winding through ducts inside the insulation of the winding to take the heat from the winding and give it to the cooling system. Generally, the ODAF cooling method is used in very high-power transformers [13].

2.5.6 ODWF Cooling of Transformer

ODWF or oil-directed water forced cooling of transformer is just like ODAF. The only difference is that the hot oil is cooled in a cooler using forced water instead of air. These transformer cooling methods are called forced directed oil cooling of the transformer [13].

References

1. M.J. Heathcote, *The J & P Transformer Book*, 13th edn (Elsevier, 2007)
2. J.H. Harlow, *Electric Power Transformer Engineering* (CRC Press, 2004)
3. F. Zhu, B. Yang, *Power Transformer Design Practices* (CRC Press, 2021)
4. S.D. Myers, J.J. Kelly, R.H. Parrish, A guide to transformer maintenance, in *Transformer Maintenance Institute Division*, 2nd edn (S. D. Myers Inc., Ohio, USA, 1988)
5. R. Feinberg, *Mdern Power Transformer Practice* (The Macmillan Press Ltd, 1979)
6. R.M. Del Vecchio, B. Poulin, P.T. Feghali D.M. Shah, R. Ahuj, *Transformer Design Principles* (CRC, 2002)
7. K. Karsai, D. Kerenyi, L. Kiss, *Large Power Transformers* (Elsevier Publication, Amsterdam, Netherland, 1987)
8. *Westinghouse Electric Transmission and Distribution Handbook*, 4th edn (Westinghouse Electric Co., East Pittsburgh, PA, 1964)
9. L.F. Blume, A. Boyajian, G. Camili, T.C. Lennox, S. Minneci, V.M. Monstinger, *Transformer Engineering* (John Wiley and Sons, New York, and Chapman and Hall, London, 1951)
10. General specifications/requirements for oil immersed power transformer (Energy efficient-level 3), https://etenders.dpsdae.gov.in ›b2_785_pt_Spec
11. G.B. Kumbhar, S.V. Kulkarni, V. S. Joshi, Analysis of half-turn effect in power transformers using nonlinear-transient FE formulation. IEEE Trans. Power Deliv. **22**(1) (2007)
12. How to choose the right transformer oil temperature indicator (thermometer), https://insulect.com/energy-blog/how-to-choose-the-right-transformer-oil-temperature-indicator-thermometer
13. Electrical 4U, Transformer cooling system and methods, https://www.electrical4u.com/transformer-cooling-system-and-methods/, Last updated: 26 Oct. 2020

Chapter 3
Different Types of Transformers and Connections, Protections and Remaining Life

3.1 Introduction

Transformers are constructed in different sizes and types for proposed applications [1, 2].

Different types of transformers are:

1. Power transformers
2. Distribution transformers
3. Phase shifting transformers
4. Rectifier transformers
5. Dry-type transformers
6. Instrument transformers
7. Step-voltage regulators
8. Constant-voltage transformers
9. Autotransformers.

3.2 Power Transformers

Power transformer type selection is based on the kind of application and size of the transformer. Large power transformers are used as step-up transformers on the generator side of the system and are known as generator step-up transformers (sometimes as machine transformers). Also, power transformers are used as step-down transformers for feeding distribution systems. High power transformers are constructed as single-phase or three-phase; for outdoor application, the liquid immersed transformer is used, but liquid immersed and dry type are used for indoor application [1–3].

B. Vahidi and R. A. Naghizadeh, *Principles and Modeling of the Power Transformers*, Energy Systems in Electrical Engineering,
https://doi.org/10.1007/978-981-99-5796-5_3

Fig. 3.1 Three sizes of power transformers

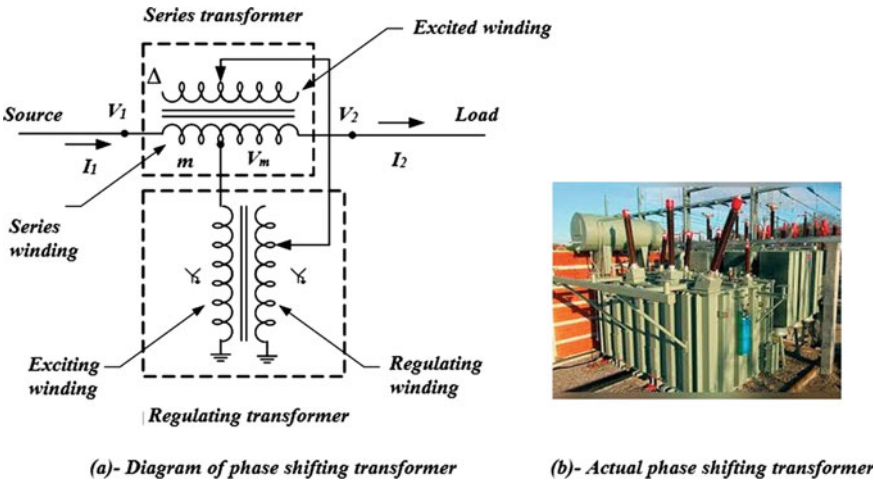

Fig. 3.2 Phase shifting transformer

Power transformers are divided into three groups based on their power.

1. Small power transformers up to 2500 kVA
2. Medium power transformers from 2500 kVA to 100 MVA
3. Large power transformers above 100 MVA.

Figure 3.1 show these three sizes of transformers.

3.3 Distribution Transformers

Those transformers that take voltage from a primary distribution circuit and "step down" or reduce it to a secondary distribution circuit or a consumer's service circuit are distribution transformers. Distribution transformers' power is 5 to 2500 kVA. The distribution transformers are a kind of small power transformers [1, 4].

3.4 Phase Shifting Transformers

To transfer power between two points of an electrical system, a difference between the voltage of the source and the voltage of load in quantity or phase angle is necessary. Due to the inductive behavior of the power system, the active power flow from source to load should be accomplished with a phase lag between the terminals. The phase shifting transformer is the best tool to reach this goal [1].

In using shifting transformers, two unique configurations have an interest [1]

i. Operation of load flow between parallel transmission lines with a shifting transformer in one of them
ii. A single transmission line containing a shifting transformer connects two otherwise independent power networks.

3.5 Rectifier Transformers

In the rectifier transformer, the diodes or thyristors are in the same tank. Usually, voltage regulation is added.

Rectifier transformers can be used in industrial applications that high direct current is necessary, such as [5]:

1. DC traction
2. Melting operation
3. Electrolysis.

and, etc.

The kind of application influences the type design.

i. Thyristors which are connected in bridge type form for high voltages
ii. Interphase connection for low voltage, high current applications
iii. Number of pulses (6, 12 and, higher with phase shifting)
iv. Eddy current and harmonic issues.

No-load tap changers or on-load tap changers are used for voltage regulation. Fine levels for regulating the voltage can be achieved by using saturable reactors on the secondary side, and regulation units could be built separately or in.

Various transformer configurations are available, including [6]:

- On-load or off-load tap changers
- Three-phase bridge-type rectifier
- Double Delta-star three-phase, five-leg rectifier transformer
- Cooling options including ONAN, ONAF, OFWF, OFAF, ODAF.

Figure 3.3 shows a three-phase rectifier transformer.

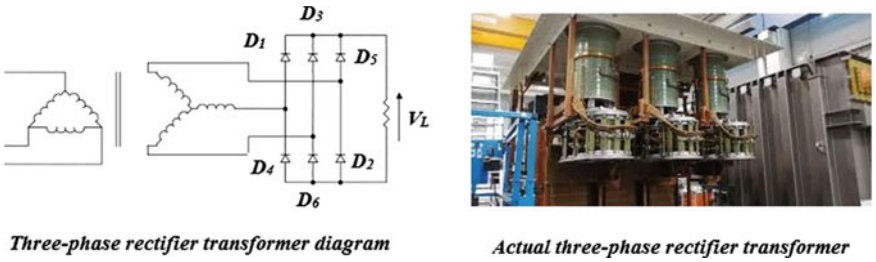

Fig. 3.3 A three-phase rectifier transformer

3.6 Dry-type Transformers

In dry-type transformers, the insulation surrounding windings is gas or dry compound.

There are two types of dry transformers [7]:

1. Cast Resin Dry Type Transformer (CRT)
2. Vacuum Pressure Impregnated Transformer (VPI).

3.6.1 Dry-type Transformer (Cast Resin)

In areas polluted with high moisture, the CRT can be used because both primary winding and secondary winding are sealed by resin (epoxy) and protect the windings against moisture. Cast resin transformers rating is from 25 kVA to 12.5 MVA with F class of insulation (90 °C temperature rise). Advantages of CRT:

1. Low loss and low partial discharge; therefore, it has good efficiency
2. The insulation of its winding is non-inflammable; therefore, it has zero risk of fire hazards and can be installed indoors
3. It can be installed inside of IP 45 enclosure as outdoor
4. It is non-hygroscopic.

3.6.2 Vacuum Pressure Impregnated Transformer

VPI transformer is made of insulation material with a shallow risk of fire. VPI transformer windings are constructed of strips or foil as a continuous layer for lower voltage ratings. However, a higher voltage rating is made of disks in series or parallel connections to reach the voltage and power rating levels [7]. The insulations of the VPI windings are impregnation and free of void and are constructed from the polyester resin of the *H* class. The core and primary and secondary windings are encapsulated inside a protective vacuum box safely. It is highly protected against

moisture, and pollution cannot affect it. VPI transformer rating is available for 5 kVA to 30 MVA with insulation grades F (155 °C) and H (180 °C). It's with Protection up to IP56.

VPI transformer advantages are:

1. Its mechanical strength is high
2. Its insulation is void free
3. Its temperature has no fluctuation
4. Its maintenance is easy
5. It has fewer fire risks.

3.6.3 Dry-type Transformers Application

This type of transformer is usually used in the following cases:

Industries in the fields of gas and oil and other chemical industries

- Areas that are sensitive environment
- Area with risk of fire
- Those substations are located in inner-city areas
- Substations are located underground or indoors
- Substations for use in renewable generation networks.

Figure 3.4 shows dry-type transformers.

3.6.4 Essential Factors for Designing Dry-type Transformers

The essential factors for designing dry-type transformers are:

1. Type of Insulation:

Insulation with the class of F or H usually is used for insulating both sides windings; because F or H class can withstand higher temperatures; i.e., 155 and 180 °C for insulation of F class and H class respectively. Insulation of winding usually is a varnished, and polyester resin. More than withstanding high temperature, the dielectric stress, mechanical stress, and strength against thermal shocks are essential [7].

2. Conductor material:

Copper conductor and aluminum conductor are used, but it should be noted that the mechanical strength of a coil which is made of copper is more than coil which is made of aluminum.

Fig. 3.4 Dry-type transformers

3. Material selection for core:

Core material should be selected so that its loss (hysteresis) will be low. Material of core must possess high permeability and less hysteresis loss, and generally, silicon steel, CRGO, etc. are used.

4. Voltage regulation:

In order to keep voltage regulation in good status, the leakage reactance of dry-type transformer is kept within 2% during design.

More than the above factors, it should keep in mind during the designing stage that loss (core losses + windings loss) must be as low as possible in order to keep the temperature within the permissible limits.

3.7 Instrument Transformer

In order to isolate the main primary circuit from secondary measuring and control equipment, the instrument transformers are used [1, 8]. The instrument transformers' levels of magnitudes are reduced to lower safe levels. There are two categories of instrument transformers: voltage transformer (VT) and current transformer (CT). The primary voltage transformer connects in parallel with the monitored circuit, and the

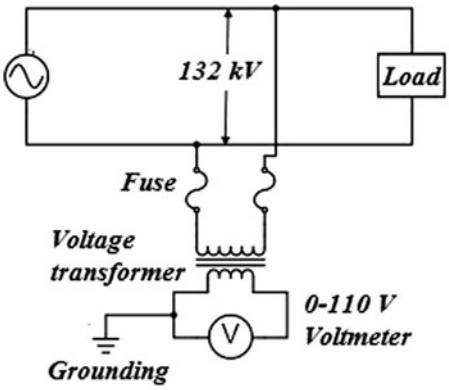

(a)- Voltage transformer connection diagram (b)- Voltage transformer

Fig. 3.5 The voltage transformer

primary winding of the current transformer is connecting in series with the monitored circuit. The output level of the VT is 100 V, 110 V, or 120 V and the output level of the CT is 1 A or 5 A.

Measuring and monitoring devices are often connected to the secondary side of instrument transformers.

Figure 3.5 shows the voltage transformer.

Figure 3.6 shows the current transformer.

3.7.1 Advantages of Instrument Transformers

1. The high AC voltages and currents can be monitored using a small rating measuring instrument, i.e., 1 A or 5 A, 110 or 120 V
2. By application of the VT and CT transformers, standardization of measuring instruments can be achieved
3. Therefore the cost of the measuring instruments is reduced, and a new one can replace the measuring instrument which is damaged
4. VT and CT isolate the HV circuit from measuring devices that highly reduce the required insulation of measuring devices and protective circuits and prepare adequate safety for operators
5. An instrument transformer can connect several measuring devices to the network

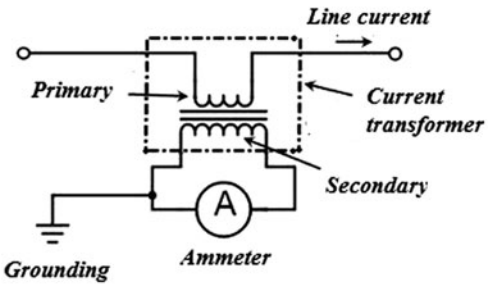

(a)- Current transformer connection diagram

(b)- Current transformer

Fig. 3.6 The current transformer

6. The voltage and the current level are low in the measuring and protective circuit. Therefore, the power consumption in the measuring and protective circuits is low.

3.8 Step-voltage Regulators

The voltage of the distribution line fluctuates significantly during the days and nights; therefore, due to this problem, it is not easy to guarantee the voltage quality [9].

Two methods are available for adjusting the primary voltage: i. adjusting the tap of the main transformer tap, ii. adjusting the voltage by compensating the reactive power.

By adjusting the tap for the main transformer, the voltage magnitude is not changing, but the system power distribution is also changing. This proposed main transformer tap changer is adjusted concerning the system load to keep the output voltage of the substation at a predetermined value. As the voltage of the bus of the substation is fixed, it is not guaranteed that the voltage at a long distance from the substation is on the required value. Several lines go out of the substation, and each line has its load curve and voltage drop, which are different from the others; therefore, all lines' voltages are not guaranteed to be at the required value.

Therefore, there is no strong flexibility in this method of voltage regulation.

For complex feeders, the voltage is high for buses close to the substation, but for those far from the substation is low. Sometimes transformers with a voltage range of 35 to 66 kV in the substations of rural areas are not equipped with an on-load voltage regulation facility, and the cost of changing them to on-load voltage regulation is high. The application of this type of voltage regulation can be limited. The voltage quality of the end users can be improved by using reactive power compensation.

The outdoor capacitor is used widely for voltage adjustment. For solving the voltage quality of distribution systems step-voltage regulator is helpful.

3.8.1 The Step-voltage Regulator Characteristics

- Voltage regulator can prepare a constant output voltage for variable load currents and input voltage
- According to the standard, it regulates voltage up to $\pm$ 10%
- Total steps 33, which per tap is 5/8% voltage
- In the raising direction of voltage, there are 16 steps. In the lowering direction of voltage also, there are 16 steps and a neutral position.

3.8.2 Three Basic Parts of a Step-voltage Regulator

- Autotransformer—A transformer in which part of one winding is common to both the primary and secondary winding
- Load tap-changer—This switch is designed for working under load to change a transformer coil's configuration
- Voltage regulator control—This control senses the system and automatically sends commands to the tap changer.

Figure 3.7 shows the diagram of a step-voltage regulator.
Figure 3.8 shows a single-phase step-voltage regulator.

3.9 Constant-voltage Transformers

Constant-voltage transformer (CVT) has been used for many years as a noise isolation device, but now it is used as a voltage sag protection device [1]. The CVT is a magnetic transformer with an individual construction with a capacitor parallel to the secondary winding. For an ordinary transformer, the primary and secondary winding are placed close to each other, and any change in primary winding will change the secondary voltage depending upon to turn ratio of the two windings.

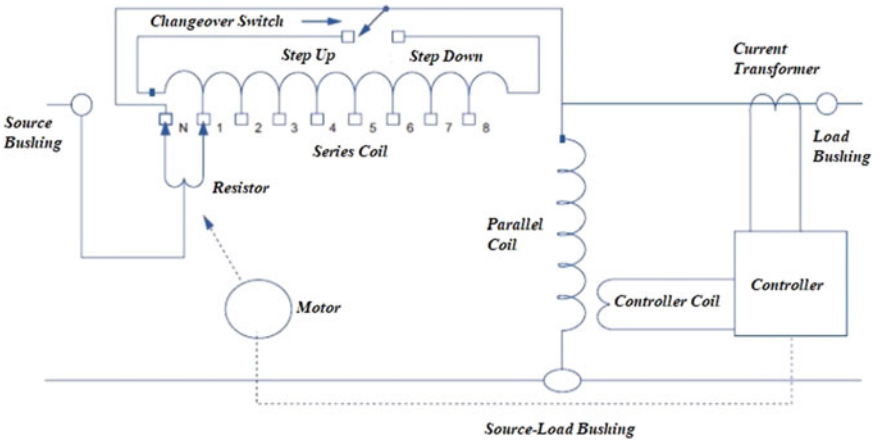

Fig. 3.7 The diagram of a step-voltage regulator

Fig. 3.8 A single-phase step-voltage regulator

However, these two windings are placed separately in a CVT, as shown in Fig. 3.9. To set up a field between the windings, a separate shunt path is provided between the two windings, but there is an air gap in the shunt path. A capacitor is also connected across suitable tapings of the secondary winding [10].

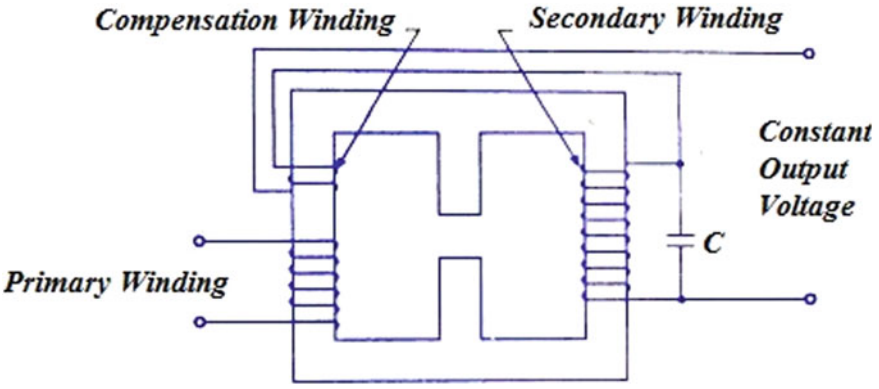

Fig. 3.9 Circuit diagram of CVT

3.9.1 Working Principle

- The constant-voltage transformer is a non–linear transformer, and it works according to the ferro–resonance principle
- The CVT operates in the magnetic saturation region and per ferro–resonance principle, so by any change in the input voltage, magnetic flux does not change, and output voltage remains constant. Simply, the ferro–resonance acts as a flux limiter, not a voltage regulator [11].

3.10 Autotransformers

An autotransformer (also autotransformer) is a transformer that has one winding. The prefix "auto" refers to a single winding that acts alone (Greek for "self"), not to any automatic mechanism [12].

3.10.1 Basic Relations

The different internal connection is the difference between a two-winding transformer and an autotransformer. In a two-winding transformer, total power exchange between primary and secondary through the magnetic circuit (core), but in an autotransformer, total power is transferred through both the magnetic circuit and electrical circuit due to the connection between low voltage and high voltage windings (Fig. 3.10).

For a two-winding transformer, the following relations can be written (symbols in the equations are shown in Fig. 3.10) [3].

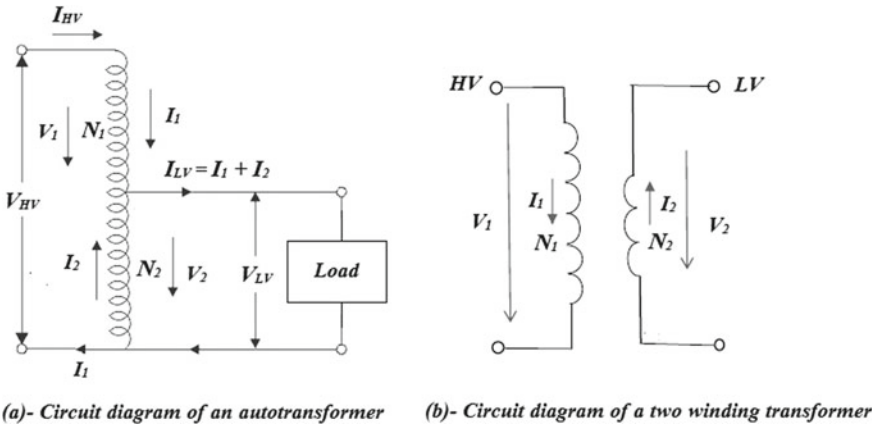

Fig. 3.10 Circuit diagrams of an autotransformer and a two-winding transformer

$$\frac{V_1}{V_2} = \frac{N_1}{N_2}; \quad I_1 N_1 = I_2 N_2 \tag{3.1}$$

For autotransformer, the relations are as follows:

$$V_{HV} = V_1 + V_2 = \left(\frac{N_1}{N_2} + 1\right) V_2 = \frac{N_1 + N_2}{N_2} V_{LV} \tag{3.2}$$

$$I_1 N_1 - I_2 N_2 = 0; \qquad I_{HV}(N_1 + N_2) - I_{LV} N_2 = 0 \tag{3.3}$$

$$\frac{V_{HV}}{V_{LV}} = \frac{N_1 + N_2}{N_2}; \qquad \frac{I_{HV}}{I_{LV}} = \frac{N_2}{N_1 + N_2} \tag{3.4}$$

The co-ratio of autotransformer is:

$$r = \frac{V_{HV} - V_{LV}}{V_{HV}} = \frac{I_{LV} - I_{HV}}{I_{LV}} = \frac{MVA_m}{MVA} \tag{3.5}$$

where:

MVA_m is power transferred through the magnetic circuit.

MVA is total power or name nameplate power.

The power ratio is:

$$\frac{Rating\ as\ an\ autotransformer}{Rating\ as\ a\ two\ winding\ transfomer} = \frac{V_{HV}}{V_{HV} - V_{LV}} \tag{3.6}$$

Fig. 3.11 A single-phase transformer

3.11 Single-Phase and Three-Phase Transformers

3.11.1 Single-phase Transformer

Single-phase transformer structure is quite simple concerning the three-phase transformer physical structure [13]. In a shell-type single-phase transformer, both sides windings are wound around the same magnetic core. In a core-type single-phase transformer, the low voltage winding and high voltage winding wound around two legs. The single-phase transformer can install in both single-phase and three-phase circuits by using three single-phase transformers as a three-phase transformer. A single-phase transformer may contain two windings, three windings, or more than three windings. Concerning the symmetrical operation of the power network, single-phase transformer is installed at the endpoint of the distribution system as distribution transformer. In the transmission network, by using three single-phase transformers, a three-phase transformer is built. Figure 3.11 shows a single-phase transformer.

3.11.2 Three-phase Transformer

Transformers of three-phase networks are mostly three-phase transformers that windings are placed on the magnetic core with three legs. Sometimes three-phase transformers are built by three single-phase transformers. Three-phase transformer's advantages compared to a single-phase transformer are:

- More efficient
- Lighter
- Smaller
- Less expensive
- It is occupied less space and needs less wiring.

For long-time use, a three-phase transformer made of three single-phase transformers are flexible under unbalanced load; one or more of the transformers can be replaced in malfunction operation, but the entire three-phase transformer should be replaced in malfunction operation. Only in exceptional cases three single-phase transformers are used most of the time, and three-phase transformers are used in three-phase networks.

Two types of three-phase transformers are used:

- Shell-type
- Core-type.

Manufacturers mostly make the core types of transformers. Different structures for different types of three-phase transformers are shown in Fig. 3.12.

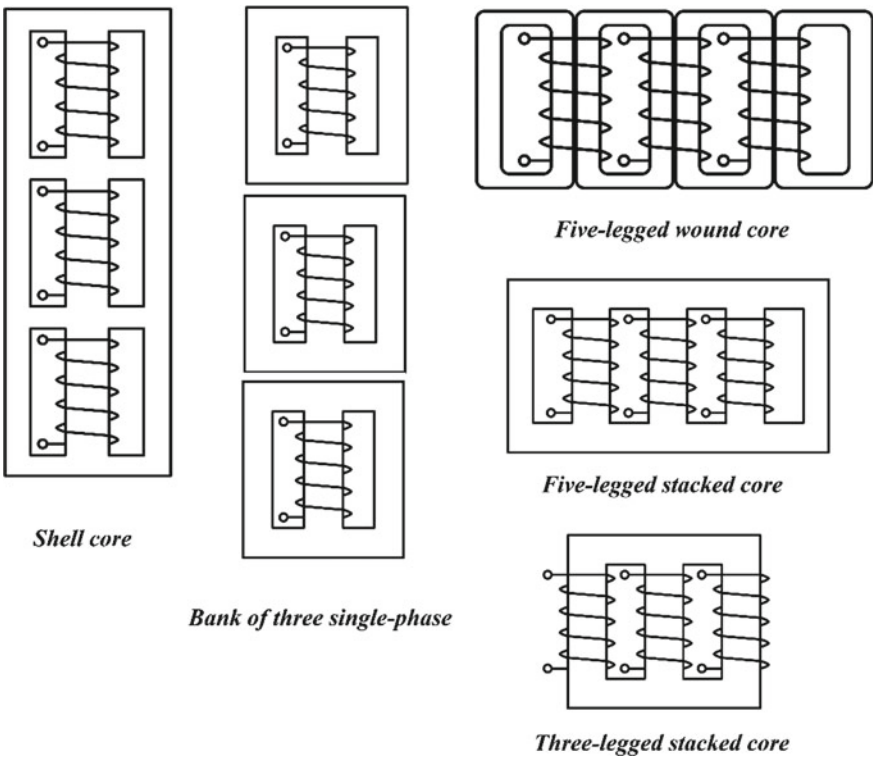

Fig. 3.12 The structure of different types of three-phase transformers

Transformers are designed in a way that the neutral end of the primary winding will be connected to the system ground. This connection must permanently be closed. By grounding the neutral of high voltage primary winding, the insulation of this winding can be graded and reduced the insulation at neutral.

Delta and/or wye connections of windings are standard connections for the three-phase transformers. Sometimes, zigzag connection transformers are used in the case of a high zero-sequence impedance requirement [13].

Angular phase shift in three-phase transformers, which is the phase angle between the phase voltage (line to neutral) of the high voltage side, which is reference, and the same voltage at low voltage terminal in degrees.

If the high-voltage terminal leads to the low-voltage terminal, the angle is positive.

The convention for the direction of voltage phasors rotation in transformers is always anti-clockwise. For indicating the angle of phase displacement, a 12 h' clock is used, and each hour represents 30° [13].

The following phenomenon can be seen in the delta connection of transformers:

- Showing a low impedance against third harmonics
- Delta connection can trap the ground fault current
- Voltage shifting problem on un-faulted phases during an unbalanced ground fault; this can exceed the un-faulted phase voltage more than the maximum rated voltage.

Zigzag connection of transformer is the special connection of transformer used in power networks [14]. This type of connection also is called "an interconnected star connection." This type has many features of both star and delta connections [14].

Figure 3.13 shows the diagram of a wye-zigzag connection transformer.

The zigzag transformer has six windings. There are three inner windings and three outer windings, and their connections are as Fig. 3.13.

Two windings of each phase have an equal number of turns, and their wound direction is opposite to cancel mismatch voltages.

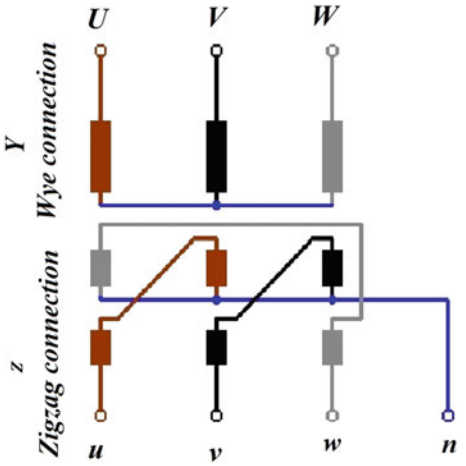

Fig. 3.13 The diagram of a wye-zigzag connection transformer

The zigzag connection of windings makes a phase shift of 30^0 between the outer winding voltage and the corresponding line to neutral voltage. The turns of zigzag winding are 15.47% more than conventional transformer turns to get the same voltage magnitude.

Zigzag transformer applications are:

1. Grounding transformer
2. Power electronic converters
3. Reference earthing or transformer for earthing
4. Cancellation of harmonic voltages.

Advantages of zigzag transformers:

With compared to the Scott transformer and other earthing transformers, the following advantages can be assigned to the zigzag transformer

1. The zigzag transformer is cheaper than the Scott transformer
2. Showing low impedance against zero sequence currents
3. Suppression of harmonic voltages
4. Providing good insulation between ground and component.

3.12 Power Transformers Protection

The main goal in transformer protection is detecting and protecting the transformer from both internal and external faults [15–17]. Conditions which leads to faults are:

1. Breakdown of insulation:

Ground fault or short in transformer are results of insulation breakdown. The insulation breakdown can damage the windings or the core of the transformer. Also a high pressure gas could produce which may damage the tank Breakdown in insulation of windings or in insulation between windings and core can be result of.insulation aging which is due to longtime overtemperature, oil contamination, partial discharge, transient overvoltages due lightning or switching in power system or high current due to external faults [15].

2. Insulation aging:

Insulation aging is a function of time and temperature. That section of the winding which has the highest temperature during operation (hot-spot) will have the greatest aging and shortest life. In controlled conditions the remaining life of transformer can not be predicted accurately as function of time and tempreture, therefore in actual operation conditions which these conditions are varying the prediction of remaining life is much more difficult. If transformer gets too hot, the cooling shall improve or to reduce the load to prevent aging acceleration. Short time moderate overtemperature is acceptable.

3. Overheating due to overexcitation:

With respect to lEG 60,076–1 guidelines [18], a power transiformer shall be capable of loaded up to nominal current under the applied voltage equal to 105% of its rated voltage. A transformer can be specified inorder to operate at a voltage up to 110% of rated voltage. During operation of a transformer under too high voltage or too low frequency, the core of transformer will be overexcited. The flux is passed through steel parts of transformer and heated up these steel parts more than normal condition which can damage the transformer.

Under rated loading current a transformer can withstand 105% of its rated voltage continuously and should be disconnected if the voltage is too high or the frequency is too low [15].

4. Oil leakage and contamination:

The oil responsibility in a transformer is acting as a part insulation and cooling systems. The service reliability of a power transformer is dependent on quality of oil. IEC 60,296 [19] is dealing with transformer oil and most important parameter of oil is its electrical strength because if the electrical strength of oil reduces due to water and impurities contaminant the insulation breakdown can occur. By testing the electrical strength of oil on site a quick check of oil condition can be achieved. Monitoring the oil level is also important because if the oil level gets too low the electrical breakdown can occur. Therefore an oil level monitor and a silica gel breather must be used for oil immersed transformers with an oil conservator.

5. Cooling reduction:

If natural cooling is not enough a forced cooling must be applied and an alarm shall be given if the cooling system stops. The oil temperature should be checked an proper action must be taken before the transformer.

Protection of transformer is divided into electrical and mechanical protections. Electrical protection is based on electrical parameters such as voltage, current, impedance and frequency, however mechanical protection is based on mechanical parameters such as pressure density, temperature and…

3.12.1 Electrical Protection of Power Transformers

1. Over current protection
2. Earth fault protection
3. Distance relay protection
4. Differential relay protection

5. Restricted earth fault protection
6. Overload protection
7. Over fluxing protection
8. Under voltage and over voltage protection.

3.12.2 Mechanical Protection of Power Transformers

1. Indicator for oil temperature
2. Indicator for winding temperature
3. Oil pressure relief.

3.12.3 Protection of Transformers Based on Transformer Modeling

Protecting power transformers from various electrical faults and abnormal operating conditions is of paramount importance to ensure their safe and reliable operation. Power transformer modeling provides valuable insights into the behavior of transformers under different fault scenarios, enabling engineers to design effective protection schemes. By analyzing key parameters, such as current, voltage, and temperature, power transformer modeling aids in the development of comprehensive and accurate protection strategies. In this section, we will explore the significance of power transformer modeling in the protection of transformers.

1. Overcurrent Protection:

Overcurrent faults, such as short circuits and overloads, pose a significant threat to power transformers. Power transformer modeling allows engineers to simulate and analyze the response of transformers under various overcurrent scenarios. By considering factors like fault magnitude, fault location, and transformer impedance, the models can accurately predict the current flow and resulting stresses on the transformer windings. This information helps in selecting and coordinating protective devices, such as fuses, circuit breakers, and relays, to quickly isolate the faulted section and prevent extensive damage to the transformer.

2. Differential Protection:

Differential protection is commonly employed to detect internal faults within a power transformer. It relies on comparing the current entering and leaving the transformer windings. Power transformer modeling plays a crucial role in optimizing differential protection schemes by simulating the behavior of transformers during internal fault conditions. By accurately modeling the transformer's winding configuration, impedance, and tap changer operation, engineers can determine appropriate settings for the differential relays. Power transformer modeling also aids in assessing the

sensitivity and selectivity of the protection scheme, ensuring reliable fault detection and discrimination.

3. Overvoltage Protection:

Overvoltage events, such as lightning strikes and switching transients, can impose excessive voltage stress on power transformers, potentially leading to insulation failure.

Power transformer modeling facilitates the analysis of overvoltage phenomena by simulating the transformer's response to various transient conditions. By considering factors such as the transformer's insulation level, voltage withstand capability, and transient performance, engineers can design and implement protective devices like surge arresters and voltage limiters to divert and suppress overvoltage surges. Power transformer modeling also assists in evaluating the effectiveness of protective measures in mitigating overvoltage stress and preserving the transformer's insulation integrity.

4. Thermal Protection:

Excessive temperature rise is a significant concern for power transformers, as it can degrade insulation materials and reduce the transformer's lifespan. Power transformer modeling enables the accurate simulation of thermal behavior by considering parameters such as loading conditions, ambient temperature, cooling systems, and thermal time constants. By predicting the temperature distribution within the transformer components, engineers can establish appropriate thermal protection measures, including temperature sensors, thermal relays, and cooling system control strategies. Power transformer modeling aids in determining optimal loading guidelines and operating limits to prevent thermal stress and ensure the transformer operates within its safe temperature range.

3.13 Life Expectancy of Transformers

Transformers are main part of power systems, they have essential role in prepare reliable electrical energy as well they are a high cost equipment. Nowadays, society need more reliable energy therefore the reliability, availability and cost efficiency of power supply are so important. The transformers operate under high electric fields and also temperature is a limiting factor for loading the transformers. The transformer insulation should tolrate high electric stresses, high electromechanical forces and high temperatures. The life time of transformer essentially depends on the qualitly of paper-oil insulation. The expected life of transformers which is defined by manufacturers is 25 to 40 years. Many of in service transformers are now reaching this limit, and it could be helpful to estimate their remaining life. This is essential to prevent unwanted outage of transformers. In order to make a decision for replaceing or maintenance of transformer it is essential to know the condition of transformer [20–23].

3.13.1 Life Expectancy of Power Transformers Based on Power Transformer Modeling

Power transformers play a critical role in electrical power systems by facilitating the efficient transmission and distribution of electrical energy. As integral components of these systems, it is crucial to understand the life expectancy of power transformers to ensure their reliable operation. In recent years, power transformer modeling has emerged as a valuable tool for estimating the lifespan of these vital devices. By analyzing various factors that affect their longevity, such as loading conditions, thermal stresses, and insulation aging, power transformer modeling provides valuable insights into their operational lifespan.

The life expectancy of a power transformer can be affected by numerous factors, both external and internal. External factors include ambient temperature, atmospheric conditions, and the quality of maintenance and service practices. Internal factors involve the transformer's design, materials used, and the efficiency of its cooling system. Traditional approaches to estimating the life expectancy of power transformers have relied on historical data, empirical formulas, and statistical analysis. While these methods have their merits, power transformer modeling offers a more comprehensive and accurate approach.

Power transformer modeling leverages advanced mathematical techniques, computer simulations, and computational analysis to predict the life expectancy of transformers. These models incorporate a wide range of parameters and variables, allowing engineers to simulate the behavior of power transformers under various operating conditions. By considering factors such as load profiles, temperature variations, and electrical stresses, power transformer models can estimate the cumulative effects of these variables on the device's aging process.

One crucial aspect of power transformer modeling is the consideration of thermal stresses. Transformers are subjected to significant thermal cycling during their operation, which leads to thermal expansion and contraction of their components. Over time, these thermal stresses can degrade the insulation materials, affect the mechanical integrity of the transformer, and reduce its overall life expectancy.

Power transformer modeling enables engineers to analyze the impact of thermal cycling on different transformer components and make informed decisions regarding materials, insulation systems, and cooling mechanisms to improve longevity.

Another essential factor addressed by power transformer modeling is the aging of insulation materials. Insulation degradation is a major concern in power transformers and can be influenced by temperature, electrical stresses, and the presence of contaminants. By incorporating models that simulate the aging process of insulation materials, engineers can assess the rate of degradation and predict when insulation replacement or maintenance may be required. This proactive approach helps utilities and asset managers to optimize maintenance schedules, reduce downtime, and extend the operational lifespan of power transformers.

Furthermore, power transformer modeling facilitates the identification of potential operational issues that may lead to accelerated aging and reduced life expectancy.

By conducting virtual tests and simulations, engineers can evaluate the impact of different scenarios, such as overload conditions, voltage fluctuations, and short circuits. This allows for the development of preventive measures and the implementation of appropriate protective devices to mitigate potential risks.

In addition to the general considerations discussed above, it is worth noting that the life expectancy of power transformers can vary depending on the type of connection employed in the electrical power system. Three common types of connections for power transformers are three-phase Y-Y, Y-delta, and delta configurations. Each of these connections has unique characteristics that can impact the longevity of the transformer.

Three-phase Y–Y Connection:

In a three-phase Y–Y connection, both the primary and secondary windings are connected in a Y (star) configuration. This connection offers several advantages, such as the ability to handle unbalanced loads and reduce harmonic distortion. Regarding the life expectancy of transformers in a Y–Y configuration, it generally depends on factors such as load imbalance, voltage imbalances, and the quality of neutral grounding.

Load imbalances in the Y–Y configuration can result in circulating currents within the transformer windings, leading to increased heating and potentially reducing the transformer's lifespan.

Similarly, voltage imbalances can cause uneven distribution of magnetic flux within the core, resulting in increased core losses and additional heating. Proper design considerations, including adequate neutral grounding and effective measures to balance loads and voltages, can help mitigate these issues and improve the life expectancy of transformers in a three-phase Y–Y connection.

Y-Delta Connection:

The Y-delta connection, also known as a star-delta connection, involves connecting the primary winding in a Y configuration and the secondary winding in a delta configuration. This connection is often used in systems where the primary voltage level is higher than the secondary voltage level. The life expectancy of transformers in a Y-delta configuration is influenced by factors such as voltage stresses, harmonics, and unbalanced loads.

Voltage stresses occur during switching operations or under transient conditions, particularly on the primary side of the transformer. These voltage stresses can cause insulation breakdown and accelerate the aging process. Effective surge protection and voltage regulation measures can help mitigate these stresses and extend the life expectancy of transformers in a Y-delta connection. Additionally, harmonic distortion resulting from nonlinear loads can cause additional heating and insulation degradation. Proper filtering and mitigation techniques should be employed to minimize the impact of harmonics on transformer life expectancy.

Delta Connection:

In a delta connection, both the primary and secondary windings are connected in a delta configuration. Delta-connected transformers are commonly used in systems where the voltage levels remain the same on both sides. The life expectancy of transformers in a delta configuration is influenced by factors such as winding insulation, winding protection, and fault conditions.

Winding insulation plays a crucial role in the life expectancy of delta-connected transformers. The insulation must be designed to withstand the higher voltages present in delta connections. Adequate protection against overcurrent and fault conditions is also essential to prevent excessive heating and insulation breakdown. Fault events, such as short circuits, can subject the transformer windings to high mechanical and thermal stresses, potentially reducing the transformer's operational lifespan.

Proper fault protection devices and coordinated protection schemes should be implemented to minimize the impact of fault conditions on transformer life expectancy.

In addition to the considerations discussed earlier, it is important to address the life expectancy of power transformers when subjected to non-sinusoidal waveforms typically associated with power electronic circuits. Power electronic devices, such as rectifiers, inverters, and converters, generate non-sinusoidal waveforms due to their switching operations. These waveforms often contain harmonics and transients that can impact the performance and longevity of power transformers.

The life expectancy of transformers in the presence of non-sinusoidal waveforms is influenced by several factors related to the waveform characteristics and the design of the transformer itself. Some key considerations include harmonics, high-frequency components, thermal stresses, insulation aging, and stray losses.

Harmonics:

Non-sinusoidal waveforms produced by power electronic circuits often contain harmonics, which are integer multiples of the fundamental frequency. Harmonics can cause additional heating in the transformer due to increased core losses and eddy current losses. This additional heating can lead to accelerated insulation aging and reduce the transformer's operational lifespan. Proper filtering techniques, such as harmonic filters and line reactors, should be employed to mitigate the effects of harmonics and minimize their impact on the transformer's life expectancy.

High-frequency Components:

Power electronic circuits can generate high-frequency components in addition to the fundamental frequency. These high-frequency components can induce additional losses in the transformer, particularly in the windings and core. The increased losses contribute to higher temperatures and can lead to thermal degradation of the transformer's insulation. Special attention should be given to the design of transformer windings, including the selection of suitable conductor materials and insulation systems capable of withstanding high-frequency currents and minimizing losses.

Thermal Stresses:

Non-sinusoidal waveforms can subject the transformer to rapid and frequent changes in load, resulting in thermal cycling. These thermal stresses can affect the integrity of the transformer's insulation materials and lead to premature aging.

Adequate cooling systems and proper thermal management strategies should be implemented to dissipate the additional heat generated by non-sinusoidal waveforms and ensure the transformer remains within its safe operating temperature limits.

Insulation Aging:

The presence of non-sinusoidal waveforms can accelerate the aging process of transformer insulation materials. The increased stress on the insulation due to harmonics, high-frequency components, and thermal cycling can lead to the breakdown of insulation systems. The choice of suitable insulation materials and periodic monitoring of insulation condition are crucial to ensure the longevity of transformers operating in power electronic circuits.

Stray Losses:

Non-sinusoidal waveforms can give rise to additional stray losses in the transformer, particularly in the windings and magnetic core. These losses result from eddy currents induced by high-frequency components and harmonic content. Minimizing stray losses through proper design techniques, such as the use of laminated cores and optimized winding arrangements, can help reduce the impact of non-sinusoidal waveforms on transformer life expectancy.

The life expectancy of power transformers operating in power electronic circuits with non-sinusoidal waveforms is influenced by factors such as harmonics, high-frequency components, thermal stresses, insulation aging, and stray losses. Proper design considerations, including suitable insulation materials, thermal management strategies, filtering techniques, and mitigation of stray losses, are essential to ensure the transformer can withstand the additional stresses imposed by non-sinusoidal waveforms. By addressing these considerations, power electronic circuits can be effectively integrated with power transformers, promoting their reliable operation and extending their operational lifespan in the presence of non-sinusoidal waveforms.

In conclusion, the life expectancy of power transformers can be influenced by various factors specific to each configuration. Load imbalances, voltage stresses, harmonics, insulation design, and fault conditions are among the key considerations. By understanding these factors and implementing appropriate measures, such as load balancing, voltage regulation, surge protection, harmonic mitigation, and fault protection, the life expectancy of power transformers can be optimized based on proper modeling procedure.

References

1. J. H. Harlow, *Electric Power Transformer Engineering* (CRC Press, 2004)
2. M. J. Heathcote, *The J & P Transformer Book*, 13th edn (Elsevier, 2007)
3. F. Zhu, B. Yang, *Power Transformer Design Practices* (CRC Press, 2021)
4. S. D. Myers, J. J. Kelly, R. H. Parrish, A guide to transformer maintenance, in *Transformer Maintenance Institute Division*, 2nd edn (S. D. Myers Inc., Ohio, USA, 1988)
5. S. M. Fadyen, What is a rectifier transformer, https://myelectrical.com/notes/entryid/121/what-is-a-rectifier-transformer
6. Rectifier transformers, https://www.gegridsolutions.com/hvmv_equipment/catalog/rectifier_transformers.htm
7. Electrical 4 U, What is dry-type transformer, www.electrical4u.com/dry-type-transformer/, Last update: 27 Oct. 2020
8. Electrical 4 U, Instrument Transformers: What is it? (and their Advantages), https://www.electrical4u.com/instrument-transformers/, Last update: 26 Oct. 2020
9. Rockwill Electric Group, *Basic Knowledge of Step Voltage Regulator*, https://www.cnrockwill.com/technical/basic-knowledges-of-step-voltage-regulator, Last update: 24th Dec. 2020
10. Circuits Today, *CVT-Constant Voltage Transformer*, https://www.circuitstoday.com/cvt-constant-voltage-transformer
11. Electrical Revolution, *Constant Voltage Transformer—Construction & Working*, www.myelectrical2015.com/2019/04/constant-voltage-transformer.html, Last update: 26 April 2019
12. Electrical 4 U, Auto Transformer: What is it? (Definition, Theory & Diagram), https://www.electrical4u.com/what-is-auto-transformer/, Last update: 12 July 2020
13. K. Shaarbafi, Transformer modeling guide, Report by Teshmont consultants LP, Alberta (2014)
14. Instrumentation Tools, Advantages and applications of zigzag transformer, https://instrumentationtools.com/advantages-applications-zig-zag-transformer/
15. R. Nylen, Power transformer protection: application guide, A GO3-5005E, ABB Relays (1988)
16. Types of transformer protection, https://electengmaterials.com/types-of-transformer-protection/ (2022)
17. D. Das, All about transformer protection and transformer protection circuits, https://circuitdigest.com/article/all-about-transformer-protection-and-transformer-protection-circuits (2020)
18. IEC 60076-1:2011, Power transformers—Part 1: General (2011)
19. IEC 60296:2020, Fluids for electrotechnical applications–mineral insulating oils for electrical equipment (2020)
20. W. D. A. G. Hillary et al., A tool for estimating remaining life time of a power transformer, in *2017 Moratuwa Engineering Research Conference (MERCon), Moratuwa, Sri Lanka* (May 2017)
21. C. Gamez, Power transformer life. Transform. Mag. **1**(1) (2014)
22. J. Foros, When should I replace an old transformer? https://blog.sintef.com/sintefenergy/when-should-i-replace-an-old-transformer (Oct. 2021)
23. T. Benadum, 6 Signs you might need to replace your oil filled transformer, ELSCO Transformers, elscotransformers.com/blog/6-signs-you-might-need-to-replace-your-oil-filled-transformer (June 2019)

Chapter 4
Transformer Core Modeling

4.1 Introduction

The behavior of ferromagnetic cores in transformers is characterized by nonlinear and frequency-dependent properties such as saturation, hysteresis, and eddy currents. These effects introduce complexities in the modeling of transformers, particularly in the low and mid-frequency range [1]. Saturation and hysteresis lead to waveform distortion and power losses in the iron core, respectively. While saturation is the most significant effect in transformer modeling for many studies, hysteresis and eddy current effects play a crucial role in certain transient analyses. This chapter focuses on the modeling approaches for iron cores in power transformers.

The phenomena of saturation and hysteresis are fundamental properties of ferromagnetic materials [2]. As the applied magnetic force increases, the magnetic moments within the iron core tend to align with the field until the material becomes fully saturated, unable to contribute further to the increase in magnetic flux density. Hysteresis, on the other hand, arises from the residual flux density stored in the iron, requiring overcoming when the current changes direction. The relationship between magnetic flux density (B) and magnetic field intensity (H) in ferromagnetic materials is nonlinear and multivalued due to saturation and hysteresis, respectively. Analytically describing these material characteristics is challenging, so empirical curves, such as the B-H curve or hysteresis loop, are commonly used to represent them. Modeling transformer saturation and hysteresis becomes necessary when the flux exceeds the linear region.

This chapter explores the modeling of transformer cores and delves into the concepts of saturation and hysteresis. It discusses the formation of hysteresis loops, the impact of irregular magnetic fields, and the construction of magnetization curves or saturation curves. Different modeling approaches, including linear approximation, piecewise linear approximation, and hysteresis models, are introduced. Among the hysteresis models, the Jiles-Atherton (JA) model and the Preisach model are discussed, highlighting their equations and parameters. These models provide

B. Vahidi and R. A. Naghizadeh, *Principles and Modeling of the Power Transformers*, Energy Systems in Electrical Engineering,
https://doi.org/10.1007/978-981-99-5796-5_4

insights into accurately representing hysteresis and capturing minor loops in the magnetic core. The chapter concludes by comparing the JA and Preisach models and discussing their respective advantages and limitations.

4.2 Saturation and Hysteresis

The saturation and hysteresis phenomena are fundamental properties of ferromagnetic materials [2]. As the applied magnetizing force on an iron core is increased, the domain magnetic moments tend to align with the applied magnetic field. This continues until all the magnetic moments are aligned with the applied field; at this point, they can no longer contribute to increasing the magnetic flux density, and the material is said to be fully *saturated.*

Hysteresis occurs because of residual flux density stored in the iron that must be overcome when the current changes direction. Due to saturation and hysteresis effects, the relationship between B and H for a ferromagnetic material is both nonlinear (due to saturation) and multivalued (due to hysteresis). In general, the characteristics of the material cannot be described analytically. They are commonly presented in graphical form as a set of empirically determined curves based on test samples of magnetic materials or steel sheets. The most common curve used to describe a magnetic material is the *B-H curve* or *hysteresis loop.* Transformer saturation or hysteresis should be modeled if the flux will exceed the linear region.

Suppose the net flux density of the core in Fig. 4.1 is zero. Applying the magnetic field H shown in Fig. 4.2a implies a flux density B as shown in Fig. 4.2b. At the initial moments, little increase in B is observed because more H is required to move some magnetic domain walls and align them with the B direction. After that, B increases substantially due to the easier domain wall motions with increasing H. These convenient alignments continue until most of the domain walls are aligned with H. At this point, more nearly alignment of the domain walls with the magnetic field requires much greater values of the magnetic field, and B increases with a slow slope and the iron core approach magnetic saturation.

If the coil current is gradually reduced, some domains aligned to the applied H will relax back to their crystal orientation while most remain in their position as H is reduced to zero. This position maintaining domain walls exhibits a residual flux density Br or remains in the iron core. An opposite magnetic field H_c or coercively is required to overcome the domain inertia and reduce the flux density to zero. The path continues from $(-H_c,0)$ point to the $(-\hat{H}, -\hat{B})$ and so on. Eventually, a closed B-H loop is formed, known as a hysteresis loop. This loop is swiped in each cycle after reaching a steady-state condition. If the applied magnetic field H has an irregular form like Fig. 4.3a, some minor hysteresis loops appear in the B-H plane of Fig. 4.3b.

A family of hysteresis loops can be formed in the steady state conditions for the different values of the magnetic field or $\hat{H}$ as shown in Fig. 4.4. If the tips of the loops in this figure are joined, a curve is formed, called a magnetization curve or a

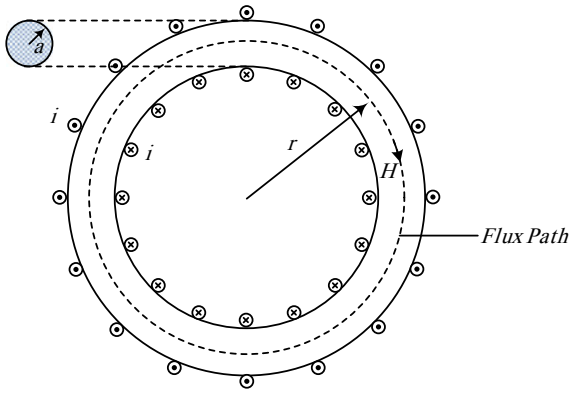

Fig. 4.1 Toroidal magnetic core structure with magnetic field path

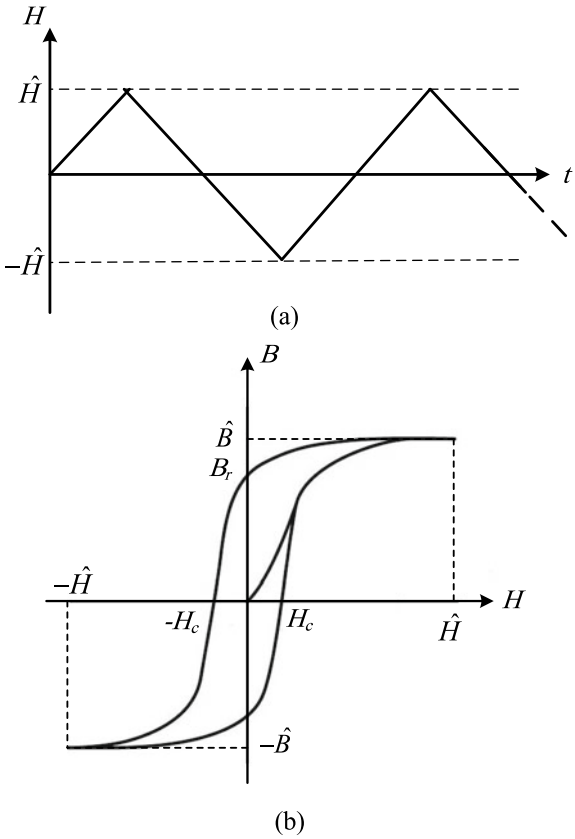

Fig. 4.2 **a** Time-varying magnetic field intensity and **b** the resultant *B-H* hysteresis loop.

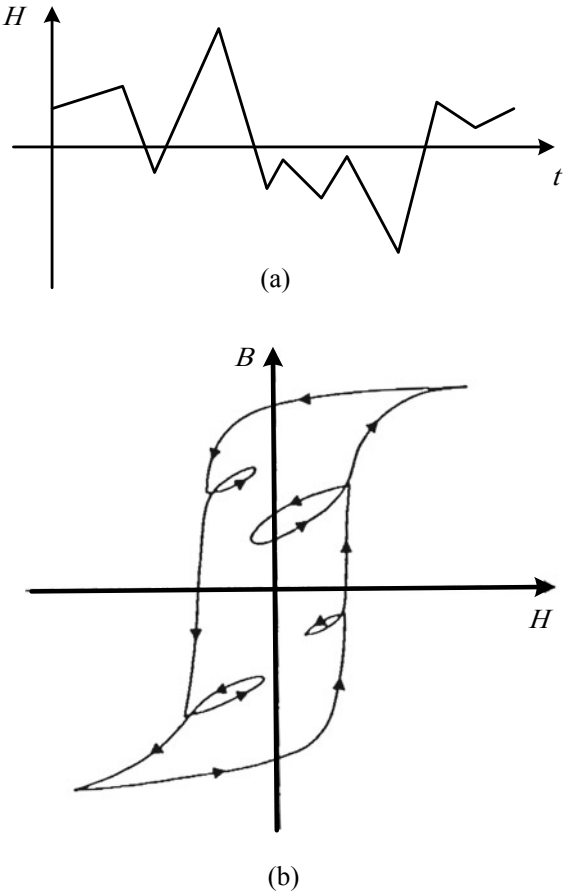

Fig. 4.3 **a** An irregular time-varying magnetic field, **b** and minor hysteresis loops due to reversals in magnetic field H

hysteretic curve. This curve is practically extracted from V_{rms}-I_{rms} curves with no-load losses in the open-circuit test of the power transformers at a rated frequency in standard open-circuit tests. More specific tests have been developed for a direct limb-by-limb calculation of a multi-phase transformer's saturation and loss curves. These tests are based on the transformers single-phase or DC excitation, which can only be performed in a controlled laboratory environment.

The magnetization curve can be used solely for practical or simulation purposes in which magnetic core losses are modeled separately or ignored.

Since the magnetic curve is nonlinear, a simplifying approximation can be used to analyze magnetic systems. Suppose a typical magnetization curve of a steel sheet in Fig. 4.5. Although this curve is nonlinear, the *B-H* characteristic can be approximated by a straight line expressed by the following relation:

$$B = \mu_r \mu_0 H \tag{4.1}$$

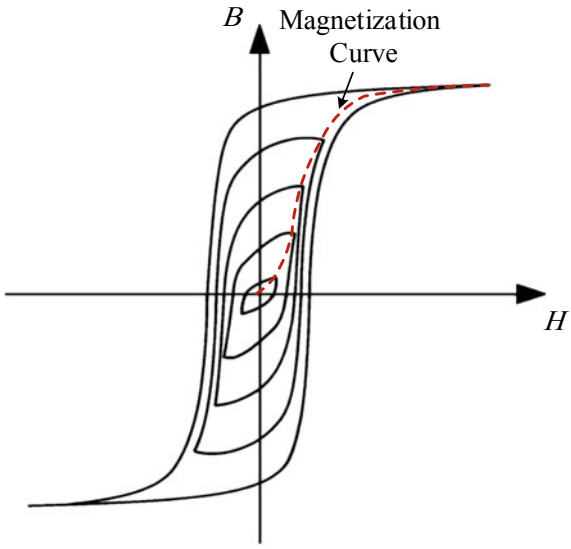

Fig. 4.4 Family of hysteresis loops in steady-state and constructing the magnetization or saturation curve

To improve the accuracy of representing the nonlinear characteristic of the magnetic core behavior, the magnetization curve can be described by a piecewise linear function or can be represented by a proper function (e.g., by a two-term polynomial relationship $H = aB + bB^p$) as a reasonable approximation of the hysteretic curve. In most transient programs, the saturation characteristic is represented by a piece-wise linear approximation with usually two lines (Fig. 4.5). Increasing the number of lines would not lead to significant accuracy improvements, except for

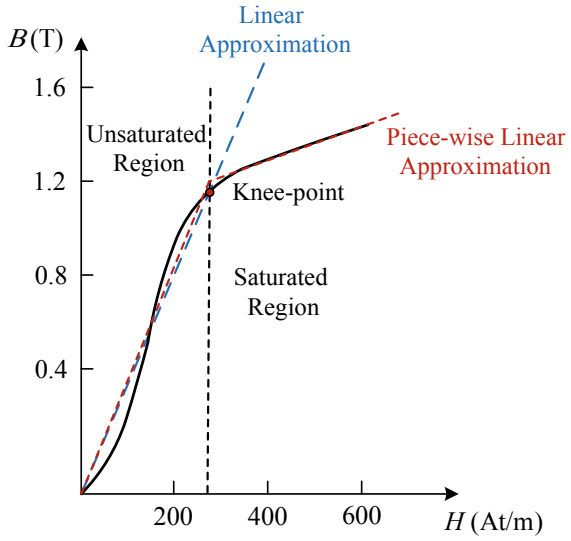

Fig. 4.5 Nonlinear magnetization curve of a steel sheet and the linear and piece-wise linear approximations

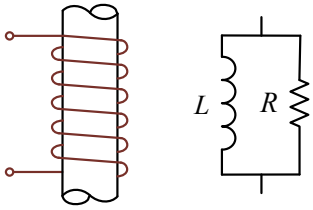

Fig. 4.6 Modeling the magnetic core with linear inductance and resistance

the studies in which a more accurate representation of the magnetization curve is required (e.g., Ferro resonance). The slope of the line in the saturated region beyond the knee point is considered the air core inductance in λ-i saturation curves. This slope is shallow compared to the inductance or slope in the unsaturated region.

The dimensionless coefficient of the $\mu 0$ in (4–1) or μ_r is called the relative permeability of the magnetic material. This parameter indicates the flux density in the material relative to that which would occur in the case of an air core for the same magnetic field density.

This approach leads to the representation of the magnetic core with a linear inductance. A linear resistance can also model the core losses parallel to the linear inductor. Therefore, the simplest model of a magnetic core can be developed, as shown in Fig. 4.6, which can be used for analytical purposes.

4.3 Modeling of Hysteresis

The phenomenon of hysteresis has been attracting the attention of many investigators for a long time. The reason is that the hysteresis phenomenon is encountered in many different areas of science and engineering. Representing the hysteresis for magnetization in electrical engineering applications is crucial for accurately representing magnetic core behavior and determining the magnetic core's residual flux values. In addition, hysteresis modeling provides significant damping in long-term dynamic transients, especially in the case of Ferro resonance. The scope of magnetization and hysteresis modeling is basically to determine B (φ or λ) values concerning H (i or MMF) values or vice-versa (that are known as inverse hysteresis models).

The proposed approaches for modeling hysteresis can be divided into three main categories 1) physics-based models, 2) mathematical models, and 3) simple models. The physical models used by physicists are developed using the detailed physical description of magnetic material properties and consider very small-scale energies. Mathematical models are based on a macroscopic description of phenomena and are used for designing electric machines. These models relate microstructural characteristics to the macroscopic responses of the magnetic material to outside magnetic fields. Simple models are based on a path tracing approach and ignore the underlying physics. These models are constructed based on scaling a primarily defined hysteresis loop.

Physical models are too cumbersome with a high level of detail and so complicated to be considered in transformer modeling studies. The simple models require limited input data, but the main disadvantage of this modeling approach is the inaccurate representation of minor or sub-hysteresis loops. Consequently, mathematical models are preferred to represent sub-loops and remanent flux better. Several hysteresis models are proposed in the literature, and among them, the Jiles-Atherton (JA) and Preisach models can represent minor loops and demagnetization properly. Comparing these two models shows that the Preisach model is generally more accurate than the JA model in corresponding with the measurements and representing minor loops. The Preisach model requires several measurements with different conditions to determine the model parameters, while JA model parameter determination is more straightforward and accessible. JA model is preferred in most studies due to its less computational burden and more straightforward parameter determination. However, the Preisach model is sometimes preferred over the JA model, especially if a more accurate representation of the hysteresis is required. Both of these models are discussed in this chapter.

4.3.1 Jiles-Atherton Hysteresis Model

The Jiles-Atherton (JA) model is in the form of a set of non-linear and first-order ordinary differential equations [3, 4]. It makes this model relatively easy to use for representing hysteresis loops of magnetic materials. This model is formed based on magnetic quantities B, H, M, and μ and is used to describe the nonlinear magnetization of electrical steel with a focus on the characteristics of a single sheet. The model parameters can be extracted from measured hysteresis loops with an Epstein frame or an analogous technique. The level of details can be significantly reduced when the interest is on the average response of the entire transformer core formed by a stack of laminations. The JA model has recently been considered for modeling magnetic core behavior in power system transients.

The equations of the classical JA model are described in this section. The total magnetization (M) has been split into two components, including irreversible and reversible magnetization, as follows:

$$M = M_{rev} + M_{irr} \tag{4.2}$$

The following ordinary differential equation describes the irreversible component:

$$\frac{\mathrm{d}M_{irr}}{\mathrm{d}H} = \frac{M_{an} - M_{irr}}{k\delta - \alpha(M_{an} - M_{irr})} \tag{4.3}$$

where δ is a directional parameter that is introduced to distinguish between the ascending and the descending part of the hysteresis loop, which is determined by:

$$\delta = sign(\mathrm{d}H/\mathrm{d}t) \tag{4.4}$$

M_{an} is the anhysteretic magnetization provided by the Langevin function:

$$M_{an} = M_s\left[\coth\left(\frac{H+\alpha M}{a}\right) - \frac{a}{H+\alpha M}\right] \tag{4.5}$$

The reversible component M_{rev} is given by:

$$M_{rev} = c(M_{an} - M_{irr}) \tag{4.6}$$

The inverse form of the JA model is preferred for power transformer simulation purposes in transient programs. This model calculates the magnetic field H from the known magnetic induction B. This procedure makes this model preferable for time domain simulations that use nodal matrix formulation. If B is considered as the independent or the input variable, the inverse JA model can be developed as [4]:

$$\frac{\mathrm{d}M}{\mathrm{d}B} = \frac{(1-c)\frac{\mathrm{d}M_{irr}}{\mathrm{d}B_e} + \frac{c}{\mu_0}\frac{\mathrm{d}M_{an}}{\mathrm{d}H_e}}{1+\mu_0(1-c)(1-\alpha)\frac{\mathrm{d}M_{irr}}{\mathrm{d}B_e} + c(1-\alpha)\frac{\mathrm{d}M_{an}}{\mathrm{d}H_e}} \tag{4.7}$$

where:

$$\frac{\mathrm{d}M_{irr}}{\mathrm{d}B_e} = \frac{M_{an} - M_{irr}}{\mu_0 k\delta} \tag{4.8}$$

where $H_e = H + \alpha M$, and $B_e = \mu_0 H_e$ is the effective magnetic induction. Using (4–4), the derivative of anhysteretic magnetization can be determined as:

$$\frac{\mathrm{d}M_{an}}{\mathrm{d}H_e} = \frac{M_s}{a}\left[1 - \coth^2\left(\frac{H_e}{a}\right) + \left(\frac{a}{H_e}\right)^2\right] \tag{4.9}$$

The constants a, α, k, c, and M_s are the parameters of the JA model. It should be noted that the parameters of the inverse and original JA models are the same. The parameter a quantifies inter-domain coupling in A/m, and α quantifies domain walls density in the magnetic material. k quantifies the average energy required to break the pinning site in the magnetic material in A/m while c is the magnetization reversibility and, finally, M_s is the saturation magnetization in A/m. An appropriate method should be implemented to determine these parameters with proper measurements in saturated conditions accurately. Open-circuit test reports of the power transformers are usually the only data available to determine the Jiles-Atherton parameters.

A procedure can be developed to calculate H (which is used to determine the output current by Ampere's law) from B, which is determined by integrating the input voltage signal. The numerical procedure of hysteresis mode calculation is depicted

in Fig. 4.7 [5]. In this figure, e is the voltage across the nonlinear inductor, and i is the current through this element.

Since the magnetic core goes into deep saturation in some studies, like the inrush current, the anhysteretic function plays an important role. The classical Langevin

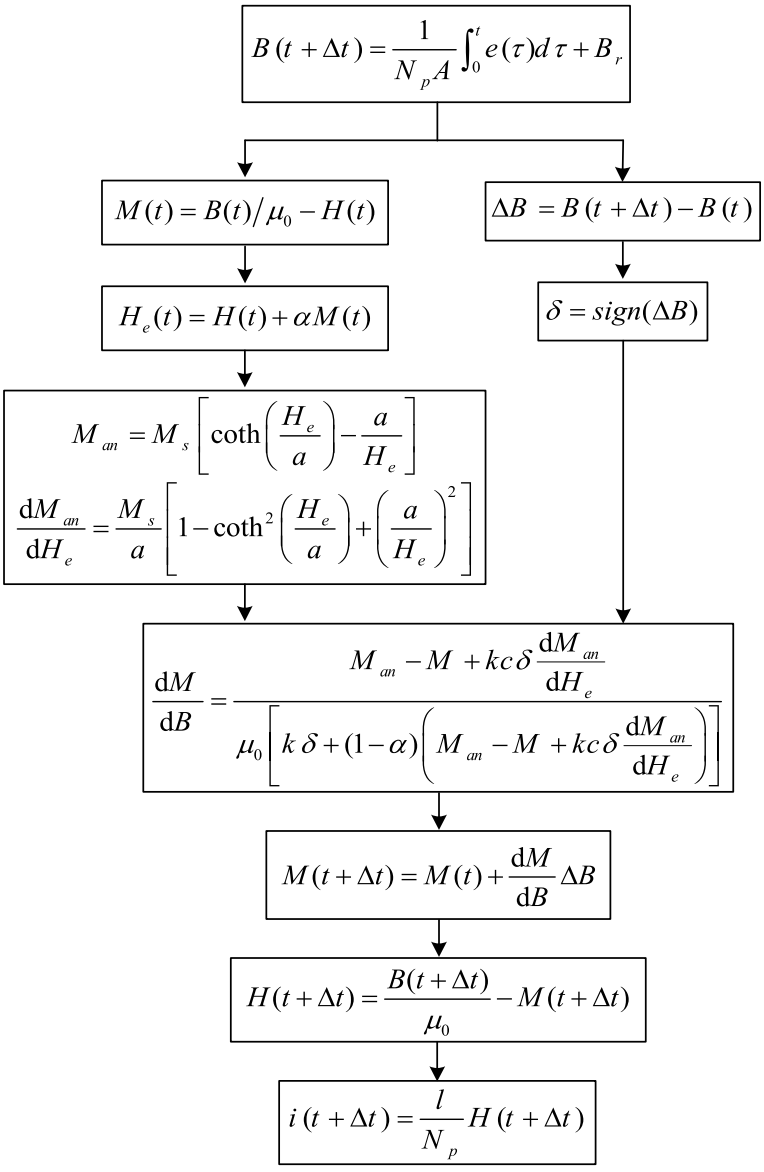

Fig. 4.7 Numerical procedure for calculation of current using inverse JA hysteresis model

function is proposed by Jiles and Atherton, which requires two parameters to determine (i.e., M_s and a). Some other proposed functions can be found in the literature, which is used mostly for fitting the core's saturation curves without considering the hysteresis phenomenon. However, to improve the JA model accuracy for inrush current simulation, the following function, which is proposed for current transformer modeling, is used here:

$$M_{an} = M_s \frac{a_1 H_e + H_e^b}{a_3 + a_2 H_e + H_e^b} \tag{4.10}$$

where a_1, a_2, a_3, and b are the parameters of the proposed function. Consequently, the derivative of M_{an} concerning H_e is given by:

$$\frac{\mathrm{d}M_{an}}{\mathrm{d}H_e} = M_s \frac{a_1 a_3 + b a_3 H_e^{b-1} + (b-1)(a_2 - a_1) H_e^b}{(a_3 + a_2 H_e + H_e^b)^2} \tag{4.11}$$

The advantage of modeling the anhysteretic magnetization curve using (4–11) compared to the Langevin function is that the additional parameters in the proposed function make it more flexible to obtain more accurate results. Like parameter a in the original JA model (known as the shape parameter), the newly introduced parameters (i.e., a_1, a_2, a_3, and b) are used to fit the anhysteretic curve of the transformer core, and they don't have a clear physical interpretation. Implementing an efficient optimization algorithm is very significant to use the advantages of the modified function [5].

4.3.2 Preisach Model

The classical Preisach hysteresis model has been used for magnetization and other fields of applications. This model is constructed as a superposition of the most straightforward hysteresis operators with simple rectangular hysteresis loops [6, 7].

The Preisach model is composed of an infinite set of hysteresis operators or relays $R_{\alpha\beta,}$ each of which can be depicted as a rectangular hysteresis loop on the input–output diagram, as shown in Fig. 4.8. The parameters α and β with the condition of $\alpha \geq \beta$ correspond to "off" and "on" threshold values of the input, respectively. The outputs of the hysteresis relay operators may only include two values, + 1 and -1. In other words, these operators can be considered as two-position relays with "up" and "down" positions corresponding to $R_{\alpha\beta} = +1$ and $R_{\alpha\beta} = -1$, respectively.

To understand the operation of the hysteresis operator, initially suppose that x is less than α, then the output y would be "off." As x increases, the output remains low until x reaches β, which switches to "on." Further increasing of x causes no change. If x is decreased, y does not go low until x reaches α again. It is apparent that the relay operator $R_{\alpha\beta}$ takes the path of a closed elementary rectangular hysteresis loop, and its subsequent state depends on its past state. The mathematical description of

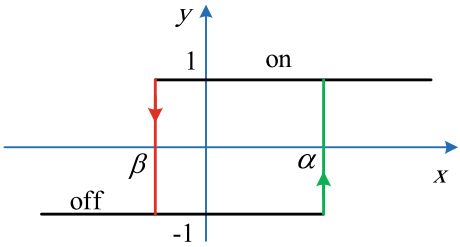

Fig. 4.8 An elementary rectangular hysteresis operator

the elementary hysteresis loop can be expressed as:

$$y(x) = \begin{cases} +1 & if\ x \geq \alpha \\ -1 & if\ x \leq \beta \\ S & if\ \beta < x < \alpha \end{cases} \tag{4.12}$$

where $S = $ -1 if in the last time x was outside the region $\alpha < x < \beta$, it was in the region $x \leq \alpha$; and $S = +1$ if in the last time, x was outside $\alpha < x < \beta$ and it was in the region $x \geq \beta$.

Along with the set of operators, $R_{\alpha\beta}$ consider an arbitrary weight function $\mu(\alpha,\beta)$ which is often known as the Preisach function. The classical Preisach model can be expressed by:

$$y(t) = \iint_T \mu(\alpha, \beta) R_{\alpha\beta}[x(t)]\mathrm{d}\alpha\mathrm{d}\beta \tag{4.13}$$

The Preisach function has finite support within some triangles T on the α-β plane, and this function would be equal to zero outside the triangles. To understand the basic properties of the model, a brief geometric interpretation is provided here based on Fig. 4.9. There is a one-to-one correspondence between $R_{\alpha\beta}$ operators and (α,β) points in the half plane $\alpha \geq \beta$. Based on this demonstration in Fig. 4.9a, the triangle T is subdivided into two sets of S^+ and S^- in which $R_{\alpha\beta}$ is $+1$ and -1, respectively. The border L between S^+ and S^- is a staircase line; its vertices are formed according to local maxima and minima of x at previous time intervals. The study of hysteresis on the system level is enabled by considering an infinitude set of hysteron spread over the limiting triangle (Fig. 4.9b), in which each coordinate pair corresponds to specific threshold values (α_i, β_i).

The Preisach model can be geometrically interpreted over the $\alpha \geq \beta$ half-plane, as shown in Fig. 4.10, such that output, y, is the fraction of the limiting triangle in which hysteron relays are on.

Changes to input, x, result in swipes on the limiting triangle (left-hand column). When x decreases, the hysteron relays are turned off by swiping to the left, and when x increases, hysteron relays are turned on by swiping up. The output y corresponds to the fraction of the hysteron relays on (the right-hand column).

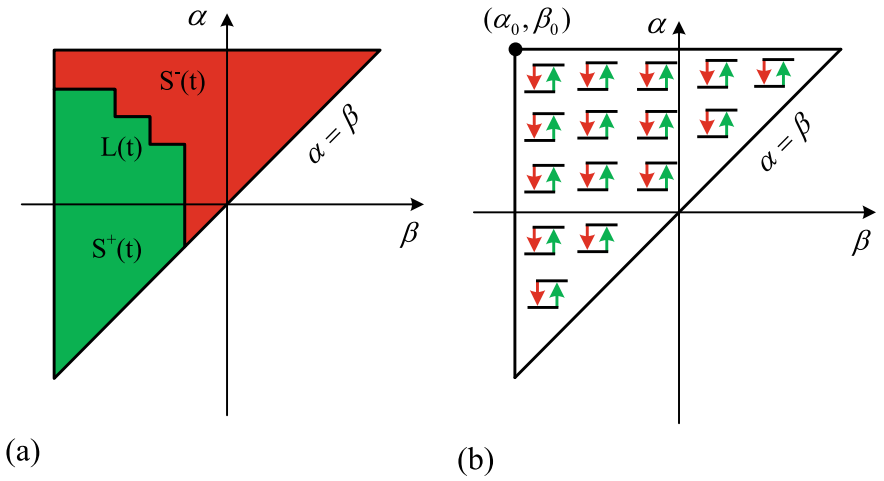

Fig. 4.9 **a** Interpretation of the Preisach Model and the limiting triangle, **b** Infinite set hysteron spread over the limiting triangle.

The Preisach function $\mu(\alpha,\beta)$ can be determined from the set of experimentally measured "first-order transition (reversal) curves" attached to the outer rising branch, as shown in Fig. 4.11.

The appropriate formulae are:

$$y(\alpha, \beta) = y_\alpha - y_{\alpha\beta} \tag{4.14}$$

$$\mu(\alpha, \beta) = -\frac{1}{2}\frac{\partial^2 y(\alpha, \beta)}{\partial\alpha\partial\beta} \tag{4.15}$$

This model is known as the classical or linear Preisach model, which allows fitting the set of first-order transition curves. A nonlinear version of the Preisach model is proposed, which is naturally more accurate than the classical linear model. This model allows experimentally measured first- and second-order transition curves while the classical linear model only allows for fitting the first-order transition curves.

A set of hysteresis operators is again considered, represented by rectangular hysteresis loops. A new set of step operators $\hat{\lambda}_\alpha$ is also needed, which are defined as follows:

$$\hat{\lambda}_\alpha(x) = \begin{cases} -1 \; if \; x < \alpha \\ +1 \; if \; x > \alpha \end{cases} \tag{4.16}$$

Two new weight (distribution) functions, $\mu(\alpha,\beta,x)$ and $\nu(\alpha)$ are used, and then the nonlinear Preisach model is given by:

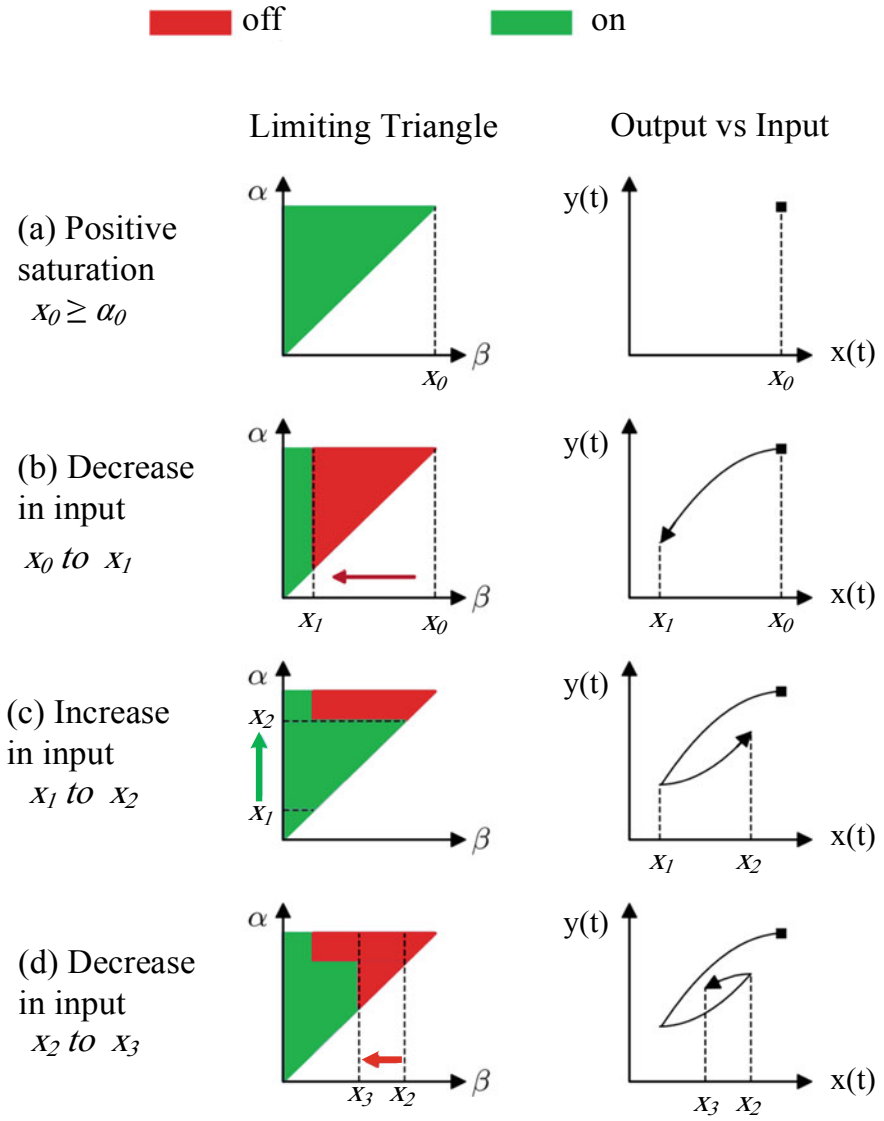

Fig. 4.10 Modeling hysteresis with the concept of limiting triangle and hysteron

$$y(t) = \hat{\Gamma}(x(t)) = \iint_T \mu(\alpha, \beta, x(t)) R_{\alpha\beta}[x(t)] d\alpha d\beta + \int_{-\infty}^{+\infty} v(\alpha) \hat{\lambda}(x(t)) d\alpha \tag{4.17}$$

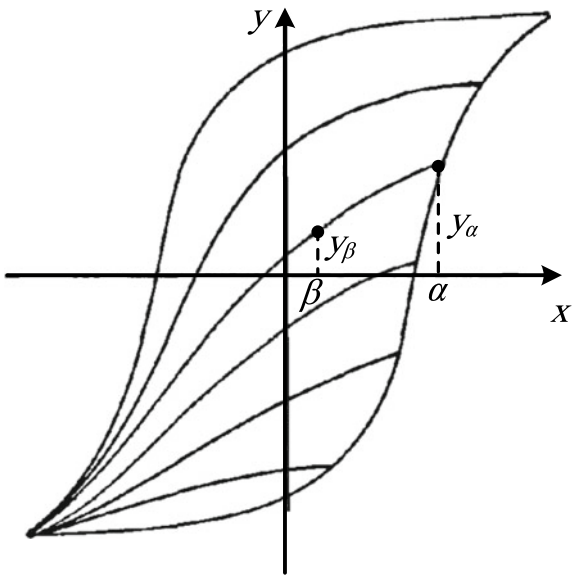

Fig. 4.11 First-order transition curves

Since the distribution function $\mu(\alpha,\beta,x)$ depends on the input's current value, $x(t)$, the model is known as the nonlinear Preisach model. In addition, a second term on the right-hand side of (4–17) is a fully reversible component for representing the hysteresis nonlinearity. The inability of the classical Preisach model to account for reversible processes is a significant deficiency that is not the case for the nonlinear model [8].

4.4 Modeling of Core Losses

When an alternating voltage is applied to a transformer winding, an alternating magnetic flux is induced in the core. The alternating flux cause hysteresis and eddy currents within the electrical steel sheets, causing heat to be generated in the core. Heating of the core due to the applied voltage is called no-load loss (or iron loss or core loss). The term "no-load" is well descriptive because the core is heated regardless of the amount of load on the transformer. If the applied voltage is varied, the no-load loss is roughly proportional to the square of the peak voltage, as long as the core is not taken into saturation. The current that flows when a winding is energized is called the "exciting current" or "magnetizing current," consisting of a real and reactive component. The real component delivers power for no-load losses in the core.

The reactive current delivers no power but represents energy momentarily stored in the winding inductance. Typically, the exciting current of a distribution transformer is less than 0.5% of the rated current of the energized winding. Accuracy is reduced

in estimating the magnetizations curve if the nonlinearity of the no-load losses is not considered. Therefore, many studies have essential accurate core loss representation of power transformers. This section is dedicated to modeling iron core losses in power transformers with different levels of accuracy.

The total core loss is separated into two components: hysteresis and eddy current losses. The phenomenological concept of core loss separation where total power loss P_{core} at a given magnetizing frequency is expressed as:

$$P_{core} = P_{hyst} + P_{eddy} \tag{4.18}$$

P_{hyst} is the hysteresis loss component, and P_{eddy} is the eddy current loss component. The hysteresis loss is the area of the quasi-static hysteresis loop multiplied by the magnetizing frequency.

A discussion is presented here to understand the eddy current phenomena in the magnetic cores of the power transformers. The hysteresis curves discussed earlier in this chapter are only valid for slowly varying phenomena because it is assumed that the magnetic field is distributed uniformly in the core. In practice, a change in the magnetic field introduces eddy currents in the core laminations. Therefore, the flux density will be lower than the normal magnetization curve. The flux distribution in the core laminations will change depending on the change in frequency.

Consequently, the flux will be confined to a thin layer near the lamination surface. The thickness of this layer decreases as the frequency increases. The circulation of eddy current in core laminations introduces additional losses. This is why the transformer cores are built up from many thin parallel laminations. Therefore, the eddy current losses are frequency-dependent. Only the loss effects of the eddy currents are essential in most low-and mid-frequency studies discussed in this section. A more accurate impedance representation of the magnetic core considering eddy current effects is discussed in the next chapter.

The component P_{eddy}, the dynamic loss component, is assumed to be the sum of a classical contribution P_{clc} and an excess eddy current loss component P_{exc} [9]. In the case of a perfectly homogeneous material (without magnetic domains), there are no excess losses, and P_{eddy} reduces to the rigorously calculable classical loss P_{clc}. The simplest way to represent the core losses is to use resistances.

The use of resistances for modeling iron losses is based on a semi-empirical description of the loss components. The core losses include hysteresis and eddy current losses are nonlinear and cannot be modeled by a linear resistance. These two core loss components are often modeled separately. The magnetic saturation can be modeled with a nonlinear inductance. The combination of magnetic saturation and core loss components leads to a model shown in Fig. 4.12.

For the sake of simplicity, hysteresis losses can be neglected as they represent a small contribution to the total losses, and eddy current losses are assumed proportional $\left(\hat{B}\, f\right)^2$ [10]. This assumption leads to a convenient representation using a simple linear resistance. The model of a nonlinear inductance with a parallel constant resistance is reported to be accurate within 5% up to several kHz.

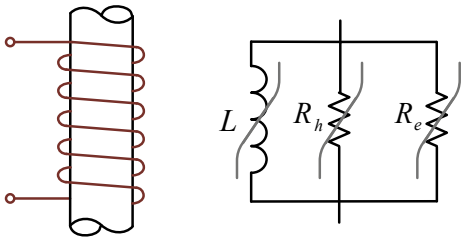

Fig. 4.12 Modeling of a nonlinear iron-core inductor (L) with hysteresis (R_h) and eddy current (R_e) loss components

To achieve a more accurate representation, the following expression can be used, which is based on the properties of magnetic material [11]:

$$p_{core}(t) = p_{hyst}(t) + \frac{\sigma d^2}{12}\left(\frac{dM}{dt}\right)^2 + \sqrt{\sigma G S_{sh} V_0}\left|\frac{dM}{dt}\right|^{\frac{3}{2}} \tag{4.19}$$

$$P_{core} = W_h(M_{\max}) f + \frac{\pi^2}{6}\sigma d^2 (M_{\max} f)^2 + 8\sqrt{\sigma G S_{sh} V_0}(M_{\max} f)^{\frac{3}{2}} \tag{4.20}$$

where M is the average magnetization in the laminations, d is the lamination thickness, S_{sh} is the lamination cross-sectional area, σ is the conductivity of the magnetic material, G is a dimensionless geometrical factor, and V_0 is a phenomenological parameter. The hysteresis loss is based on the hysteresis loop area ($W_h(M_{\max})$ or, in fact $W_h(B_{\max})$) as follows:

$$W_h(M_{\max}) \propto B_{\max}^2 \tag{4.21}$$

Therefore, the core loss can be expressed by the following equation, which is known as the Bertotti equation:

$$P_{core} = k_h B_{\max}^2 f + \frac{\pi^2}{6}\sigma d^2 (M_{\max} f)^2 + 8\sqrt{\sigma G S_{sh} V_0}(M_{\max} f)^{3/2} \tag{4.22}$$

where k_h is the coefficient of the hysteresis losses. The implementation of this equation in the frequency or time domain is challenging. If the flux is assumed to be uniformly distributed over the cross-sectional area of a core limb, the following relations between magnetic flux and electrical voltage can be expressed:

$$\frac{\mathrm{d}M}{\mathrm{d}t} \propto \frac{\mathrm{d}\phi}{\mathrm{d}t} \propto v(t) \tag{4.23}$$

$$B(t) \propto \phi(t) \propto M(t) \propto \int v(t)\mathrm{d}t \tag{4.24}$$

Based on the above assumptions, the following relations can be obtained:

$$P_{cls} \propto B_{\max}^2 f^2 \tag{4.25}$$

$$P_{exc} \propto B_{\max}^{1/5} f^{1/5} \tag{4.26}$$

For a sinusoidal flux, we have:

$$\lambda_{\max} = \frac{V}{\sqrt{2}\pi f} \tag{4.27}$$

$$B_{\max}^n f^n \propto V^n \tag{4.28}$$

And finally, the total core current and core loss can be expressed as a function of voltage:

$$i_{core\_tot}(t) = i_{hyst}(t) + k_c v(t) + k_e \sqrt{v(t)} \tag{4.29}$$

$$p_{core}(t) = p_{hyst}(t) + k_c v(t)^2 + k_e v(t)^{3/2} \tag{4.30}$$

It should be mentioned that $i_{hyst}(t)$ can be obtained using a hysteresis model. These equations can be used to model the core loss dynamically and accurately in time domain simulations. In the frequency domain, the core loss power can be obtained as a function of frequency f and B_{max} as follows:

$$P_{core} = k_h B_{\max}^S f + k_c (B_{\max} f)^2 + k_e (B_{\max} f)^{3/2} \tag{4.31}$$

where k_h, $k_{c,}$ and k_e are constant coefficients of static hysteresis loss, classic eddy current loss, and excessive eddy current loss, respectively, and S is the Steinmetz coefficient. This equation can be re-written as follows:

$$P_{core} = K_h V^S f^{1-S} + K_c V^2 + K_e V^{3/2} \tag{4.32}$$

K_h, K_c, and K_e are similar to k_h, $k_{c,}$ and k_e but with different values. With the typical assumption of $S = 2$, we have:

$$P_{core} = K_h \frac{V^2}{f} + K_c V^2 + K_e V^{3/2} \tag{4.33}$$

$$P_{core} = K_h' B_{\max} V + K_c V^2 + K_e V^{3/2} \tag{4.34}$$

The accuracy of Bertotti equations is affected by core saturation with the three constant coefficients. Therefore, a more sophisticated approach can be used to enhance the accuracy of core loss representation with modification of coefficients as follows [12]:

$$k_h = k_{h3} B_{\max}^3 + k_{h2} B_{\max}^2 + k_{h1} B_{\max} + k_{h0} \tag{4.35}$$

$$k_c = k_{c3} B_{\max}^3 + k_{c2} B_{\max}^2 + k_{c1} B_{\max} + k_{c0}. \tag{4.36}$$

$$k_e = k_{e3} B_{\max}^3 + k_{e2} B_{\max}^2 + k_{e1} B_{\max} + k_{e0}. \tag{4.37}$$

Several measurements can obtain the required coefficients in an open-circuit test of the transformer with different saturation levels.

References

1. J. A. Martinez, B. A. Mork, Transformer modeling for low- and mid-frequency transients—a review. IEEE Trans. Power Del. **20**(2) II, 1625–1632 (2005)
2. C.P. Steinmetz, On the law of hysteresis. Proc. IEEE **72**(2), 196–221 (1984)
3. D. C. Jiles, D. L. Atherton, Ferromagnetic hysteresis. IEEE Trans. Magn. MAG-**19**(5), 2183–2185 (1983)
4. D.C. Jiles, D.L. Atherton, Theory of ferromagnetic hysteresis. J. Magn. Magn. Mater. **61**(1–2), 48–60 (1986)
5. R.A. Naghizadeh, B. Vahidi, S.H. Hosseinian, Parameter identification of Jiles-Atherton model using SFLA. COMPEL **31**(4), 1293–1309 (2012)
6. I. D. Mayergoyz, Mathematical models of hysteresis. IEEE Trans. Magn., MAG-**22**(5), 603–608 (1986)
7. D.A. Philips, L.R. Dupre, J.A. Melkebeek, Comparison of Jiles and Preisach hysteresis models in magnetodynamics. IEEE Trans. Magn. **31**(6 pt 2), 3551–3553 (1995)
8. Chiesa N, Power Transformer Modeling for Inrush Current Calculation, Ph.D. dissertation (Department of Electric Power Engineering, Norwegian University of Science and Technology, Norway, 2010)
9. G. Bertotti, General properties of power losses in soft ferromagnetic materials. IEEE Trans. Magn. **24**(1), 621–630 (1988)
10. G. Bertotti, M. Pasquale, Physical interpretation of induction and frequency dependence of power losses in soft magnetic materials. IEEE Trans. Magn. **28**(5), 2787–2789 (1992)
11. G. Bertotti, *Hysteresis in Magnetism for Physicists, Materials Scientists, and Engineers* (Academic Press, San Diego, CA, USA, 1998)
12. Y. Zhang, M. C. Cheng, P. Pillay, A Novel Hysteresis Core Loss Model for Magnetic Laminations. EEE Trans. Energy Con. **26**(4), 993–999 (2011)

Chapter 5
Low- and Mid-Frequency Modeling of Transformers

5.1 Introduction

Modeling power transformers is a complex task, mainly due to the multitude of topologies and the nonlinear and frequency-dependent behavior of various parameters involved. Numerous specifications, behaviors, and phenomena need to be accurately represented in transformer modeling, including different core and coil configurations, self- and mutual inductances, leakage fluxes, skin and proximity effects in coils, ferromagnetic core saturation, hysteresis and eddy current losses in the iron core, and capacitive effects [1]. Given this array of nonlinear and frequency-dependent behaviors and the significant impact transformers have on power system transient events, it becomes crucial to adequately model and determine the parameters of power transformers for effective power system simulations and studies.

Transformers can be approached using various methods in the low- and mid-frequency ranges, making transformer simulation a broad and diverse topic [2, 3]. A transformer can be conceptualized as a circuit composed of branches and nodes, incorporating resistances, inductances, and capacitances. Resistances are employed to represent copper and core losses in the windings and magnetic core, while inductances are used to model the magnetic flux paths within the air or iron core components. Furthermore, the capacitive behavior exhibited by the transformer becomes particularly significant at higher frequencies. Developing a single comprehensive model capable of accurately representing every transient situation across the entire frequency range, from DC to several MHz, is exceedingly difficult and impractical. Hence, an appropriate model must be adopted for each specific study.

The purpose of this chapter is to establish transformer models for investigating low- and mid-frequency transients, with a focus on addressing magnetic saturation effects, nonlinearities, and loss representation, which are critical concerns in these scenarios. The transformer's low- and mid-frequency models consist of two main components: the iron core and the windings. In Chap. 4, we have already presented the modeling of the iron core. Therefore, the objective of this chapter is to delve into

B. Vahidi and R. A. Naghizadeh, *Principles and Modeling of the Power Transformers*, Energy Systems in Electrical Engineering,
https://doi.org/10.1007/978-981-99-5796-5_5

the modeling of transformer windings and explore their integration with the iron core models to establish a comprehensive transformer model.

5.2 Transformer Models and Frequency Ranges

Transformer models are fundamental tools used in various fields of engineering to understand and analyze the behavior of systems operating at different frequency ranges. These models are particularly essential in electrical engineering, where they are employed to study the characteristics and performance of power systems. This section provides an overview of power transformer modeling approaches and the importance of the frequency range in selecting the appropriate model.

5.2.1 State of the Art of Transformer Modeling

This section aims to provide an overview of the state-of-the-art techniques and methodologies employed in power transformer modeling for low and mid-frequency transients.

5.2.1.1 Equivalent Circuit Models

Another widely employed technique for power transformer modeling is the use of equivalent circuit models. These models represent the transformer as a set of electrical components, such as resistors, inductors, and capacitors. The parameters of the equivalent circuit are derived from the physical characteristics of the transformer, including winding arrangement, core geometry, and material properties. The transient response of the transformer is then obtained by solving the circuit equations. Various modifications and refinements have been proposed to enhance the accuracy of these models, such as including frequency-dependent parameters and accounting for core losses. This chapter focuses on this type of modeling that finds extensive application in electrical circuit simulation tools, such as the Electromagnetic Transients Program (EMTP).

5.2.1.2 Electromagnetic Modeling

One of the primary approaches in power transformer modeling is based on electromagnetic field theory. Electromagnetic models describe the transformer's behavior by solving Maxwell's equations to determine the distribution of electric and magnetic fields within the device. Finite Element Analysis (FEA) and Boundary Element Method (BEM) are widely used numerical techniques for solving these equations,

allowing accurate calculation of transformer responses under transient conditions. These methods consider the geometric complexity of the transformer windings, core, and magnetic materials.

5.2.1.3 Numerical Time-Domain Simulation

To capture the dynamic behavior of power transformers during low and mid-frequency transients, time-domain simulation techniques are commonly used. These simulations involve solving the differential equations that describe the transformer's electrical and magnetic behavior using numerical integration methods. Finite Difference Method (FDM), Finite Volume Method (FVM), and Finite Element Method (FEM) are some of the numerical techniques employed in time-domain simulations. These methods provide a comprehensive understanding of the transformer's transient response, accounting for phenomena like winding transposition, core saturation, and hysteresis effects.

5.2.1.4 Multi-Physics Coupling

Power transformers are complex devices that involve the interaction of various physical phenomena, such as electromagnetics, heat transfer, and mechanical stress. To capture the complete transient behavior, multi-physics coupling techniques have gained attention in recent years. These approaches integrate the electromagnetic models with additional modules for thermal analysis, mechanical stress analysis, and fluid dynamics. The coupling of these different physical domains enables a more accurate representation of transformer behavior during transient events and can be useful for investigating thermal and mechanical effects.

5.2.1.5 Data-Driven Approaches

With the advent of big data and machine learning techniques, data-driven approaches have also found application in power transformer modeling for low and mid-frequency transients. These methods utilize historical operational data, such as voltage and current waveforms, along with corresponding transformer response, to develop empirical models or predictive algorithms. Machine learning algorithms like artificial neural networks, support vector machines, and random forests have been employed to learn the complex relationships between input variables and transformer behavior. Data-driven approaches can complement traditional modeling techniques and provide insights into transformer performance in various transient scenarios.

5.2.2 *Frequency Ranges in Transformer Modeling*

Frequency range refers to the span of frequencies over which a system or device can operate effectively and exhibit reliable behavior. Transformer models are specifically designed to capture the electrical, magnetic, and electromagnetic properties of transformers within specific frequency ranges. Understanding the limitations and capabilities of transformer models in different frequency ranges is crucial for accurate analysis, design, and optimization of transformer-based systems. The selection of the frequency range depends on the type of the transient. Several types of transients can occur in power systems those can be caused by faults, switching operations, lightning strokes, load variations, etc. The transients are usually classified based on the frequency contents including:

(1) Low-frequency transients (DC to 1 kHz)
(2) Mid-frequency transients (50 or 60 Hz to 10 kHz)
(3) Fast front transients (10 kHz to 1 MHz)
(4) Very fast front transients (100 kHz to 50 MHz).

Any range of the above frequency ranges corresponds to some specific transient phenomena in the power system. For example, inrush current, ferroresonance, controller interactions, and harmonic interactions are known as low-frequency transients. Mid-frequency transients are caused by the energization or de-energization of power system components like the energization of transmission lines and capacitors or the de-energization of transformers, reactors, and the faulted parts of the power system. Mid-frequency transient studies are useful for insulation coordination, determination of arrester characteristics, calculation of transient recovery voltages, and evaluation of transient mitigation solutions. Fast front transients are mainly caused by the lightning strokes on overhead transmission lines and substations. The related transient studies are used for transmission line and substation design and overvoltage protection of lines and equipment. Very fast front transients mainly occur in gas-insulated substations (GIS) due to switchings.

Transformer models have to include different levels of details for the frequency range of interest. According to the frequency range of the studied transients, there are two main categories for the transformer model including low- and mid-frequency and high-frequency models. This separation is generally based on considering the ferromagnetic behavior of the magnetic core.

The depth of penetration of the electromagnetic waves decreases with increasing frequency and the magnetic flux tends to appear at the surface of the core mostly. Based on this physical behavior, the nonlinear behavior of the core can be ignored in high frequencies while the capacitances become more effective. On the other hand, the ferromagnetic core plays an important role in low frequencies while the capacitances can be ignored. Transient phenomena below the first winding resonance (several kHz) including ferroresonance, most switching transients (e.g. transformer energization), geomagnetically induced currents, and harmonic interactions are examples of low- and mid-frequency studies of the transformers.

Several approaches have been proposed for modeling transformers in low-and mid-frequency transients. Two standard classical approaches include BCTRAN, and the saturable transformer component (STC). These models have been used in transient programs for several decades and their parameters are mainly extracted from short-circuit measurements. They represent the winding structure of a transformer and the iron core model has to be externally connected to them to construct a propped model.

5.3 Classical Transformer Models

Standard transform models are available in ATP/EMTP and other transient program libraries. These models are briefly described in this section.

5.3.1 BCTRAN Model (Matrix Representation)

BCTRAN has been presented in [4] primarily for the matrix representation of 3-phase *n*-winding transformers as mutually coupled coils. This representation assumes symmetry and can be used to consider the inter-winding coupling in both steady-state and transient studies.

Since there are multiple windings in a power transformer, it is convenient to use a matrix representation approach for modeling, which could be especially useful for implementation in simulation programs.

Therefore, branch resistance and inductance matrices [**R**] and [**L**] represent multiple windings' resistances and self and mutual inductances. The voltage equation of the transformer, taking into account the exciting current, can be expressed based on the following equations in time and frequency (phasors) domains, respectively:

$$[\mathbf{v}] = [\mathbf{R}][\mathbf{i}] + [\mathbf{L}]\frac{\mathrm{d}}{\mathrm{d}t}[\mathbf{i}] \tag{5.1}$$

$$[\mathbf{V}] = [\mathbf{R}][\mathbf{I}] + \mathrm{j}\omega[\mathbf{L}][\mathbf{I}] \tag{5.2}$$

The slight difference between each matrix element pair X_{ii} and X_{ij} or the short circuit reactances in the reactance matrix ($[\mathbf{X}] = \mathrm{j}\omega[\mathbf{L}]$) contain the information of the exciting transformer current. A very high accuracy has to be used to input the numerical values to prevent losing the short circuit reactances and avoid forming an ill-conditioned matrix. The reverse form of the above equations or branch matrix formulation can be written as:

$$[\mathbf{I}] = [\mathbf{Y}][\mathbf{V}] \quad or \quad [\mathbf{V}]=[\mathbf{Z}][\mathbf{I}] \tag{5.3}$$

This form of the equation is used in BCTRAN (and TRELEG) approach in EMTP-type programs. This model accurately presents leakage fluxes between windings and can be easily implemented in an EMTP-type program (BCTRAN routine in ATP/EMTP). The admittance or impedance matrix for the coupled coils can easily be derived from commonly available standardized test data. The nonlinear components for representing core losses, magnetization, saturation, and hysteresis can be added externally to the terminals of the winding nearest to the transformer core as a set of parallel nonlinear resistances or inductances. The admittance matrix formulation can be more easily formed by inspection without the inversion process.

For a better understand this model, suppose a single-phase transformer with n windings. The resistance and inductance parts of the impedance matrix need to be separated for time-domain modeling. Therefore, the BCTRAN model can be expressed at the time domain in expanded form as:

$$\begin{bmatrix} v_1 \\ v_2 \\ \vdots \\ v_n \end{bmatrix} = \begin{bmatrix} R_{11} & R_{12} & \cdots & R_{1n} \\ R_{21} & R_{22} & \cdots & R_{2n} \\ \vdots & \vdots & & \vdots \\ R_{n1} & R_{n2} & \cdots & R_{nn} \end{bmatrix} \begin{bmatrix} i_1 \\ i_2 \\ \vdots \\ i_n \end{bmatrix} + \begin{bmatrix} L_{11} & L_{12} & \cdots & L_{1n} \\ L_{21} & L_{22} & \cdots & L_{2n} \\ \vdots & \vdots & & \vdots \\ L_{n1} & L_{n2} & \cdots & L_{nn} \end{bmatrix} \frac{\mathrm{d}}{\mathrm{d}t} \begin{bmatrix} i_1 \\ i_2 \\ \vdots \\ i_n \end{bmatrix} \tag{5.4}$$

Since the nonlinearities are not taken into account in this model, the [**R**] and [**L**] matrixes in the above equations are symmetric, and [**R**] is diagonal.

An open-circuit test cannot practically obtain the elements of these matrixes. For example, consider a single-phase two-winding transformer with the total short circuit impedance 0.004 + j 0.08 pu with j99.96 pu magnetizing inductance. The equivalent circuit of this transformer is shown in Fig. 5.1.

The matrix equation of this transformer in pu for steady-state is:

$$\begin{bmatrix} V_1 \\ V_2 \end{bmatrix} = \left[\begin{bmatrix} 0.002 & 0 \\ 0 & 0.002 \end{bmatrix} + \begin{bmatrix} 100 & 99.96 \\ 99.96 & 100 \end{bmatrix} \right] \begin{bmatrix} I_1 \\ I_2 \end{bmatrix} \tag{5.5}$$

And for the time domain or transient solution, we have:

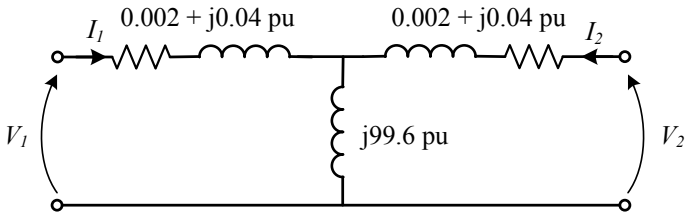

Fig. 5.1 Equivalent circuit of a single-phase transformer

$$\begin{bmatrix} v_1 \\ v_2 \end{bmatrix} = \frac{1}{S_{Rated}} \left[\begin{bmatrix} 0.002V_{B1}^2 & 0 \\ 0 & 0.002V_{B2}^2 \end{bmatrix} \begin{bmatrix} i_1 \\ i_2 \end{bmatrix} + \frac{1}{2\pi f} \begin{bmatrix} 100V_{B1}^2 & 99.96V_{B1}V_{B2} \\ 99.96V_{B1}V_{B2} & 100V_{B2}^2 \end{bmatrix} \frac{\mathrm{d}}{\mathrm{d}t} \begin{bmatrix} i_1 \\ i_2 \end{bmatrix} \right] \tag{5.6}$$

where S_{Rated} is the rated MVA of the transformer, V_{B1} and V_{B2} are the rated voltages of the windings in kV, and f is the rated frequency of the transformer. If all quantities are to be referred to one side, then the voltages V_1 and V_2 should be set equal.

BCTRAN model can be easily extended for three-phase transformers. Each coil of a single-phase transformer becomes three coils on core legs 1, 2, and 3 in a three-phase design (Fig. 5.2).

For the extension of (4.1) for three-phase transformers, each scalar element of [**Z**] should be replaced by 3 × 3 sub-matrixes, including self and mutual impedances; Z_S and Z_M as the following form:

$$\begin{bmatrix} Z_S & Z_M & Z_M \\ Z_M & Z_S & Z_M \\ Z_M & Z_M & Z_S \end{bmatrix} \tag{5.7}$$

Z_S is the self-impedance of each phase or leg, and Z_M is the mutual impedance between the two other phases or legs.

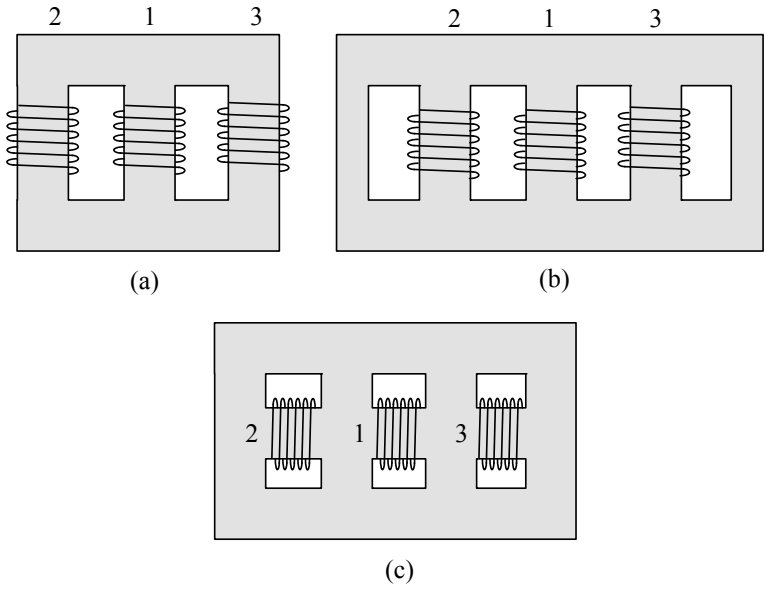

Fig. 5.2 Three-phase transformers designs; **a** Three-legged core design, **b** Five-legged core design, and **c** Shell-type design

Although the above matrix is asymmetric, data for considering such conditions are not usually available. Therefore, the matrix is supposed to be symmetric for simplicity. The self and mutual impedances can be conventionally calculated by symmetrical component theory in which the positive and zero sequence impedances are defined as Z_1 and $Z_{0,}$ respectively:

$$Z_s = \frac{1}{3}(Z_0 + 2Z_1) \tag{5.8}$$

$$Z_M = \frac{1}{3}(Z_0 + Z_1) \tag{5.9}$$

The magnetic core model can also be added to any BCTRAN model to construct the complete transformer model [5, 6]. A three-phase three-winding transformer model is shown in Fig. 5.3 as an example. The winding terminals in this model are the terminals of a coupled RL network which is the implementation of $[\mathbf{Y}]$ $([\mathbf{Z}]^{-1})$. The core model should be added to the transformer representation and attached to the external terminals of a winding. As mentioned earlier, it is recommended to connect the magnetic core model to the winding closest to the core. This winding usually has the lowest rated voltage among the other transformer windings.

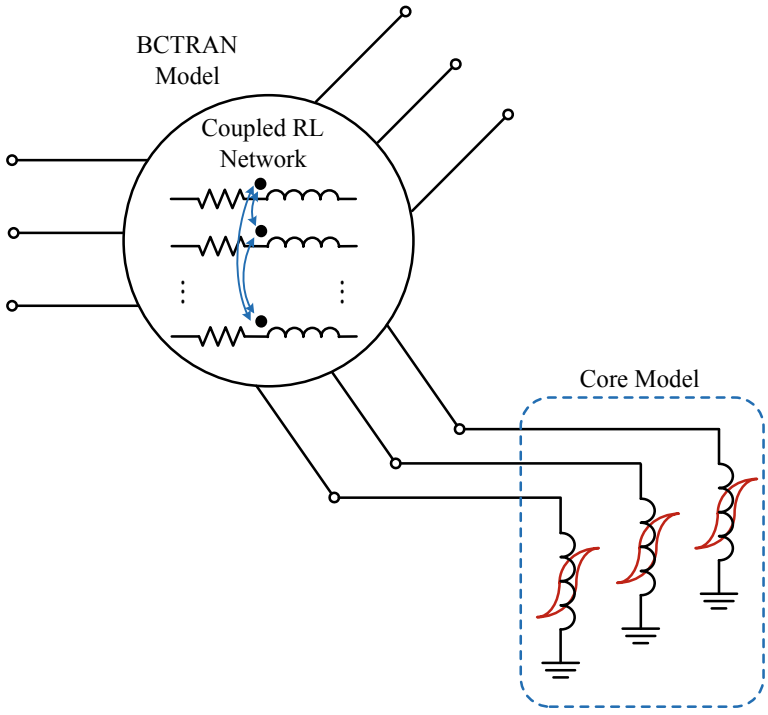

Fig. 5.3 Three-phase three-winding BCTRAN transformer model

The BCTRAN model is generally reliable and has been tested for a wide range of transient phenomena with acceptable accuracy. Since the cross-admittances always have positive values, this model does not have stability issues. The BCTRAN model does not have a practical limitation for the number of phases and windings. However, the external attachment of the core model to the short circuit network and across a winding is not topologically correct. It can introduce errors for transients that involve core saturation, e.g., Ferro resonance conditions.

5.3.2 *Saturable Transformer Model*

The Saturable Transformer Model (STC) model is the essential transformer element in transient electromagnetic programs, also known as the star representation of the transformer. Each winding is modeled with its resistance in series with its leakage inductance connected through ideal transformers to consider the voltage ratios.

The model of the transformer core (magnetizing branch) is connected in parallel at the common connection or the star point. The simplest STC model is the well-known model for the single-phase two-winding transformer, as shown in Fig. 5.4. Three-phase transformer models are also developed from this representation with a proper connection of primary and secondary windings.

The resulting circuit for a single-phase transformer with n windings is shown in Fig. 5.5. This model is not valid for $n > 3$, which leads to numerical instability in some cases due to the negative value for series reactances.

In the general case, the multi-phase STC model can be developed using the BCTRAN model by [**R**] and $[\mathbf{L}]^{-1}$ matrix to represent coupling between phases, as shown in the following equation:

$$[\mathbf{L}]^{-1}[\mathbf{v}] = [\mathbf{L}]^{-1}[\mathbf{R}][\mathbf{i}] + \frac{\mathrm{d}}{\mathrm{d}t}[\mathbf{i}] \tag{5.10}$$

As mentioned earlier, the inductance or [**L**] matrix can be formed only if the exciting current is not ignored. But on the reverse mode, the $[\mathbf{L}]^{-1}$ matrix can always be determined regardless of exciting current considerations without the possibility of being ill-conditioned. Therefore, the transformer core can be easily modeled with an externally parallel branch connected to the star point.

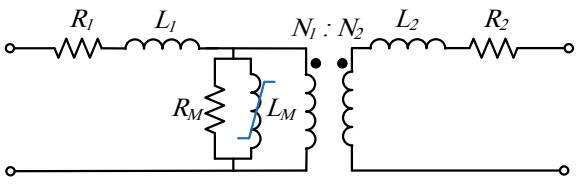

Fig. 5.4 Simple STC model for single-phase two-winding transformer

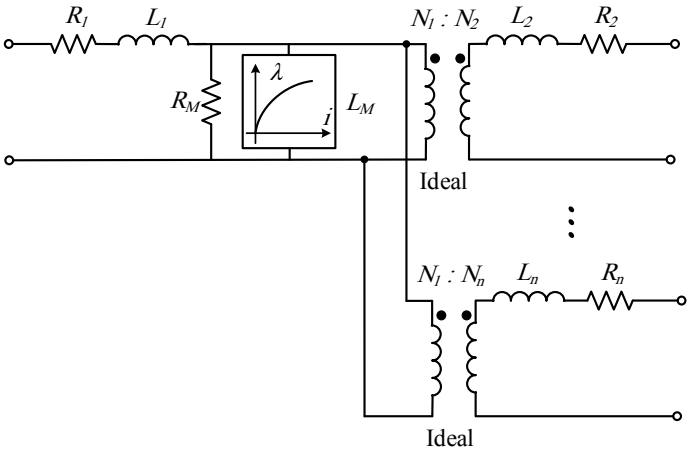

Fig. 5.5 Saturable transformer component with n windings

Since the magnetizing inductances are much larger than the short-circuit inductances, they can also be connected to the related winding terminals. It should be mentioned that this approach has a stability problem in the case of three-winding transformers, and severe numerical instability happens in time domain simulation if one of the leakage inductances becomes negative. Therefore, this model has limited capabilities in modeling multi-winding transformers.

5.4 Topology-Based Models

As mentioned earlier, BCTRAN and STC have substantial limitations for accurate and stable representation of transformers. A proper and accurate transformer model for low- and mid-frequency studies must be based on a topologically correct or topology-based representation of the magnetic and winding structure. Topology-based models are constructed concerning the core and winding topology and design. Therefore, unlike the classical modeling methods, the topology-based models of each specific core design are different. This modeling is based on discretizing the transformer construction geometry into flux paths or tubes. There are two main categories of topology-based models, including magnetic and duality-based models.

An equivalent magnetic circuit is used in magnetic models to represent transformers. An interface is required between the magnetic model and the electric circuit connected to the transformer winding terminals. An equivalent dual electric circuit is used in duality-based models, which extracted similarities between electric and magnetic systems. The main characteristic of such a dual electric circuit is that it can be directly connected to an electric network in simulation programs. Both methods

are suitable for representing transformers with any core structure and winding number and arrangements.

It is worth mentioning that some hybrid models are also introduced for transformer modeling based on building a connection between BCTRAN models for windings and magnetic or duality-based models for the core construction [7–10]. Magnetic and duality-based models are described here.

5.4.1 Magnetic Models

Magnetic models of transformers can be directly developed using inductance or reactance elements. Any transformer's structure can be converted into a magnetic circuit. As in illustration, a magnetic equivalent of a single-phase two-winding transformer is shown in Fig. 5.6. The accuracy of the magnetic circuit mainly depends on assumptions for decomposing the magnetic structure to an equivalent circuit with lumped parameters. Nonlinear reactances represent the core, and linear reactances are used for modeling air paths of the leaking magnetic fluxes.

Providing a suitable interface between the electric network and the transformer is not easy in this method. Windings can be used for providing such interconnection between magnetic and electric systems, which are described by:

$$v(t) = \mathrm{d}\lambda(t)/\mathrm{d}t \tag{5.11}$$

$$i(t) = mmf(t)/N \tag{5.12}$$

The core and winding losses cannot be directly included in the magnetic circuit. Therefore, these losses are modeled by resistors in the winding terminals. For example, R_{Cu1} and R_{Fe1} represent winding and core losses in Fig. 5.6. The core losses can be represented by a nonlinear (e.g. voltage-dependent) resistance to provide more accuracy. Many simplifying assumptions should be made to aggregate the hysteresis and eddy current losses in winding terminals instead of core legs or yokes. Therefore, it is difficult to allocate core losses in suitable locations in this approach.

5.4.2 Duality-Based Models

Implementing the reluctance model described in the previous section in electromagnetic transient programs is not easy because the magnetic and electric networks must be mutually interconnected. The magnetic model is suitable for analysis of the transformer itself without its interface with the related electrical circuit.

But magnetic models can be used with the duality transformation to construct an equivalent dual electric circuit based on the reluctance model.

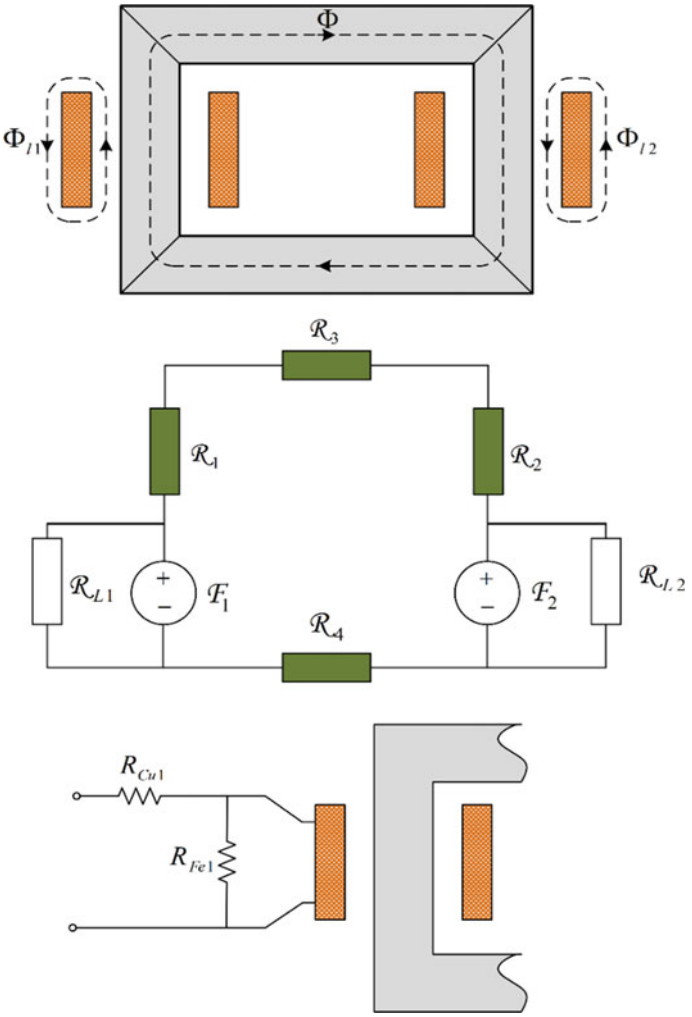

Fig. 5.6 Magnetic circuit modeling of a two-winding transformer

The resultant model is a purely electric circuit that can be easily connected to other elements of an electric network in an electromagnetic transient programs environment [11]. Resistances can also be connected parallel to the inductances to represent core losses properly. Therefore, it is convenient to model the core losses according to the topology of the transformer core. Consequently, the principle of duality can be used for constructing a topologically correct model based on a magnetic circuit model. Maxwell equations can be used to define the general rules for synthesizing magnetic circuits:

$$\nabla.\vec{D} = \rho\upsilon \tag{5.13}$$

$$\nabla.\vec{B} = 0 \tag{5.14}$$

$$\nabla \times \vec{E} = -\frac{\partial \vec{B}}{\partial t} \tag{5.15}$$

$$\nabla \times \vec{H} = \vec{J} + \frac{\partial \vec{D}}{\partial t} \tag{5.16}$$

Equation (5.14) shows that all flux paths must be closed loops; in other words, the net input flux to any defined surface with the winding must be equal to the net output flux of that surface. The electric potential and magnetic flux change rate are related by (5.15). In the case of an ideal short circuit in a winding ($E = 0$), the net flux passing on a surface enclosed by the winding must be zero. In addition, the space charge and displacement current $\left(\partial \vec{D}/\partial t\right)$ are supposed to be zero in transformer modeling. Therefore, Eq. (5.16) can be simplified as $\nabla \times \vec{H} = \vec{J}$ follows. This equation means that the magnetic field is related to the winding current. A winding without current is considered neutral by a magnetic field and cannot change the flux paths. This case is an open circuit, and the flux can freely pass through the enclosed surface without change.

The induced voltage in an open circuit winding is defined by the net input or net output flux through the surface enclosed by the winding according to (5.15). To satisfy the Maxwell equations, at least one magnetic inside and one outside magnetic branch must be available from the same circuit. In addition, each node must be connected to at least two magnetic branches to form at least one loop (or mesh).

There is no approximation in converting a magnetic circuit to its dual electric circuit using duality transformation. Some basic duality conversions are described here. The flux is established by magnetomotive force or *mmf* in the magnetic circuit that is described $\Phi = \mathscr{F}\Lambda$ by can be converted to its dual phenomena in an electric circuit by $v = L\mathrm{d}i/\mathrm{d}t$ which describes creating electromotive force or emf by the time rate of the current. The magnetism across a variable magnetic potential (M) is the dual of variable electric current (i), and the magnetic through variable magnetic flux (Φ) is the dual of the electric potential across a variable voltage (v).

The basic equivalent components in duality transformation are shown in Fig. 5.7. the electric dual of magnetic permeance (Λ) is an inductance (L), and the electric dual of an mmf source (F) is an electric current source (i). The duality principles for the transformation of series and parallel components are illustrated in Fig. 5.8.

An illustrating example for implementing the topological method for a simple structure to construct a dual circuit is depicted in Fig. 5.9. As shown in this figure, the magnetic structure is first discretized or decomposed, forming a magnetic circuit. The leakage flux is ignored in this example. Hypothetical knots are defined at the center of each mesh of the magnetic circuit and numbered. A "0" is also defined externally. Then, a line between different knots is drawn according to the following rules to construct the topology of the equivalent electric circuit:

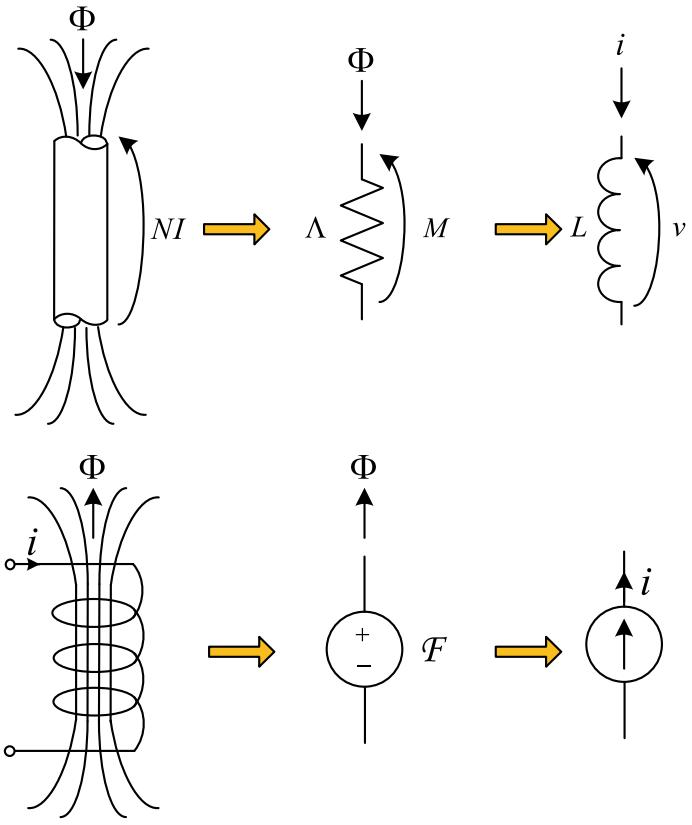

Fig. 5.7 Equivalent components in duality transform

- The line can only cross the magnetic elements (permeance and MMF sources), not the connections between them.
- To connect two knots, the line must cross only one single element.
- Every single element must only be crossed once by a single line
- All elements must be crossed once by a line.
- Every single knot must have at least two connections.

The discretization of the magnetic structure and construction of the magnetic circuit is the most sensitive step. The magnetic flux paths must be correctly identified and represented by linear or nonlinear reluctance for air and iron core. The flux paths in the core parts have high permeability providing a preferred route for the magnetic flux. The magnetic field can leak into the open space outside the core. Therefore, different magnetic circuits are constructed due to different winding configurations.

These rules are implemented here to draw the flux paths shown by the dashed lines in Fig. 5.9. These lines are the electric connections between the dual electric components in the dual circuit. The core is assumed linear, and the core losses and

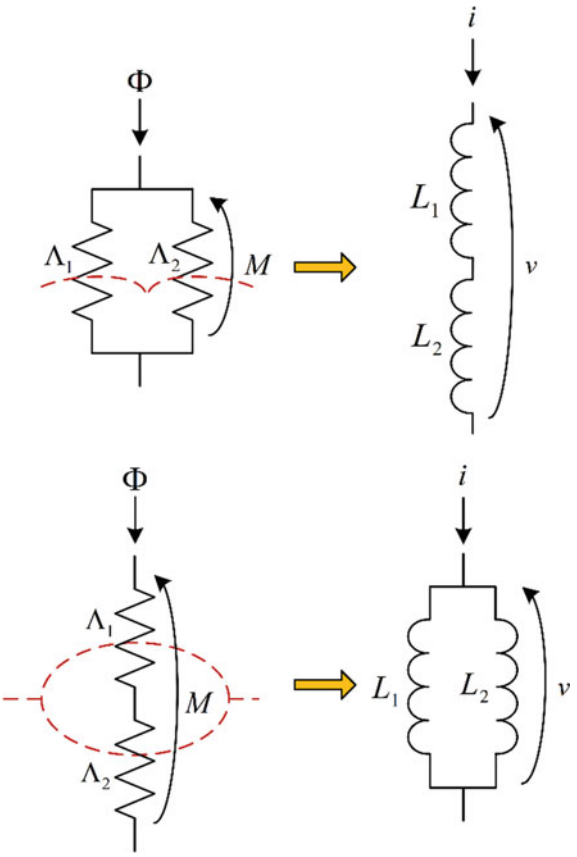

Fig. 5.8 Series and parallel connections in duality transform

leakage inductances are ignored. Other examples of this approach are presented as follows.

5.4.2.1 Single-Phase Transformer with Air Gap

A hypothetical single-phase transformer with an air gap is depicted in Fig. 5.10. The leakage fluxes are ignored in this example. The flux paths in the core ate modeled with nonlinear inductances to represent saturation and/or hysteresis effects, while the air gap is modeled with a linear inductance. Parallel resistances are also included in parallel with nonlinear inductances to represent core losses in each part of the core. Modeling the magnetic core described in the previous chapter.

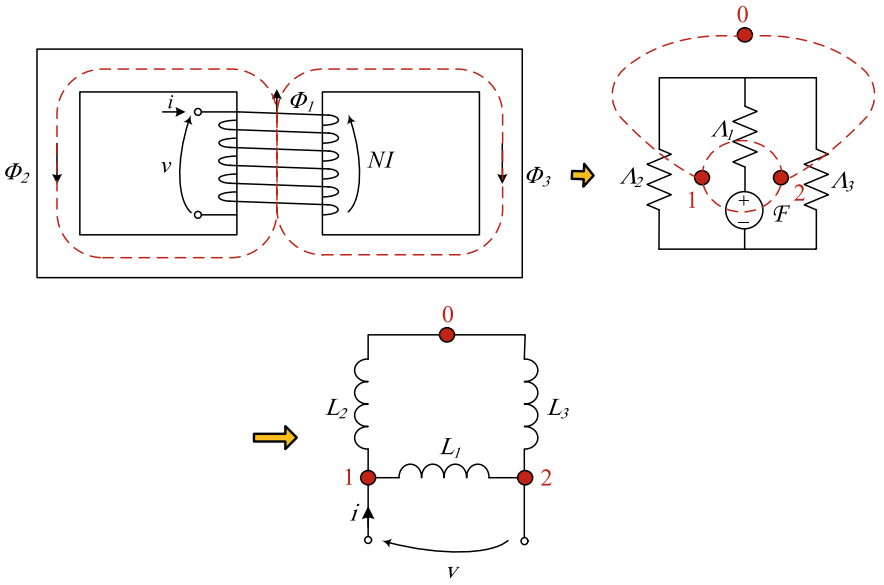

Fig. 5.9 The procedure of driving a dual electric circuit

5.4.2.2 Single-Phase Transformer Without Air-Gap

Another example is depicted in Fig. 5.11 for a single-phase core type transformer with two windings. The resultant dual electric circuit is shown at the bottom of this figure. The leakage flux paths are modeled using linear inductances. In contrast, the core's flux paths (divided into four sections) are modeled with nonlinear inductances to represent saturation and/or hysteresis effects.

Parallel resistances are also included in parallel with nonlinear inductances to represent core losses in each part of the core. The procedure for determining leakage inductance is presented in the following section.

5.4.2.3 Single-Phase Shell-Type Transformer

An equivalent dual circuit for a single-phase shell-type transformer is extracted in this section. The steps of the procedure to establish a topological electrical equivalent model of this transformer are described here. The transformer structure and the flux path discretization are shown in Fig. 5.12. The linkage flux path goes through the iron core to provide coupling between two windings. This path has nonlinear magnetic behavior with high permeability in normal conditions. When the iron core is saturated, the permeability decreases to μ_0.

They determine the magnetic coupling between windings and the open-circuit characteristics of the transformer. The leakage flux paths are closed outside the iron

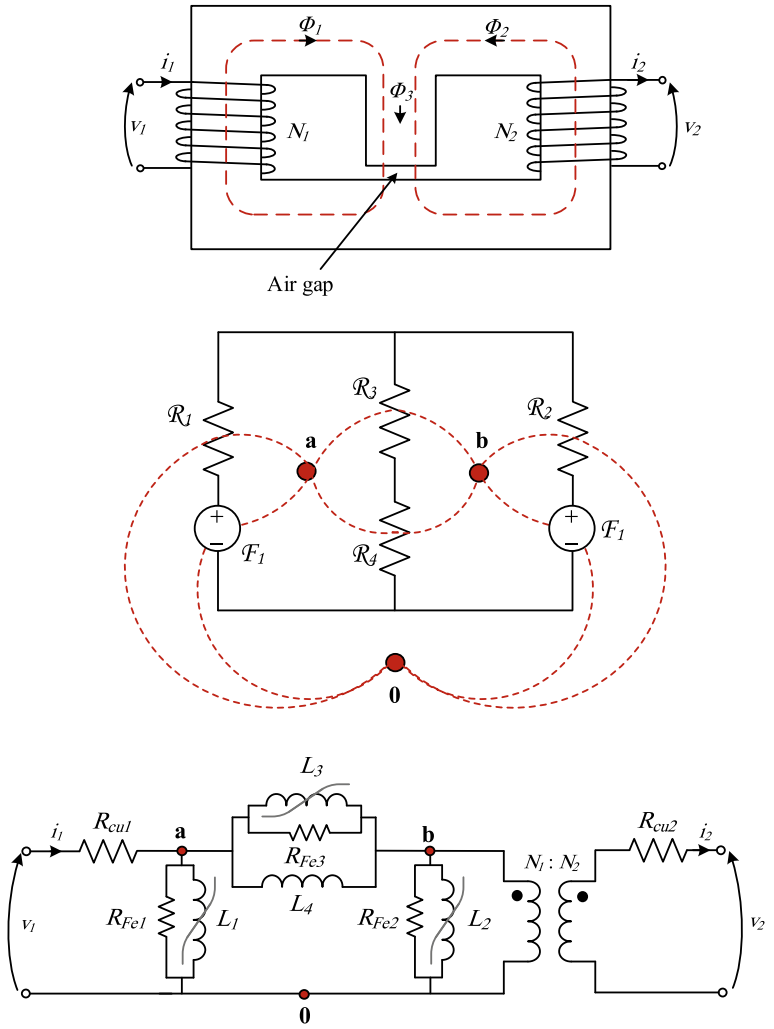

Fig. 5.10 Development of an equivalent electric circuit for a single-phase transformer with air gap based on duality

core in the air with the linear permeability of μ_0. The space between windings is the most critical part of the leakage paths due to the high magnetic energy density and the short-circuit characteristic. A critical leakage path is identified between the innermost winding and the related core leg. This particular path plays a vital role in the saturated condition to consider the non-ideal adhesion of this winding to the core leg. The coupling between the windings due to the leakage flux can be ignored.

The magnetic circuit is also shown in Fig. 5.12. Each path has a related linear or nonlinear reactance. Windings are represented by MMF sources in series in the leg.

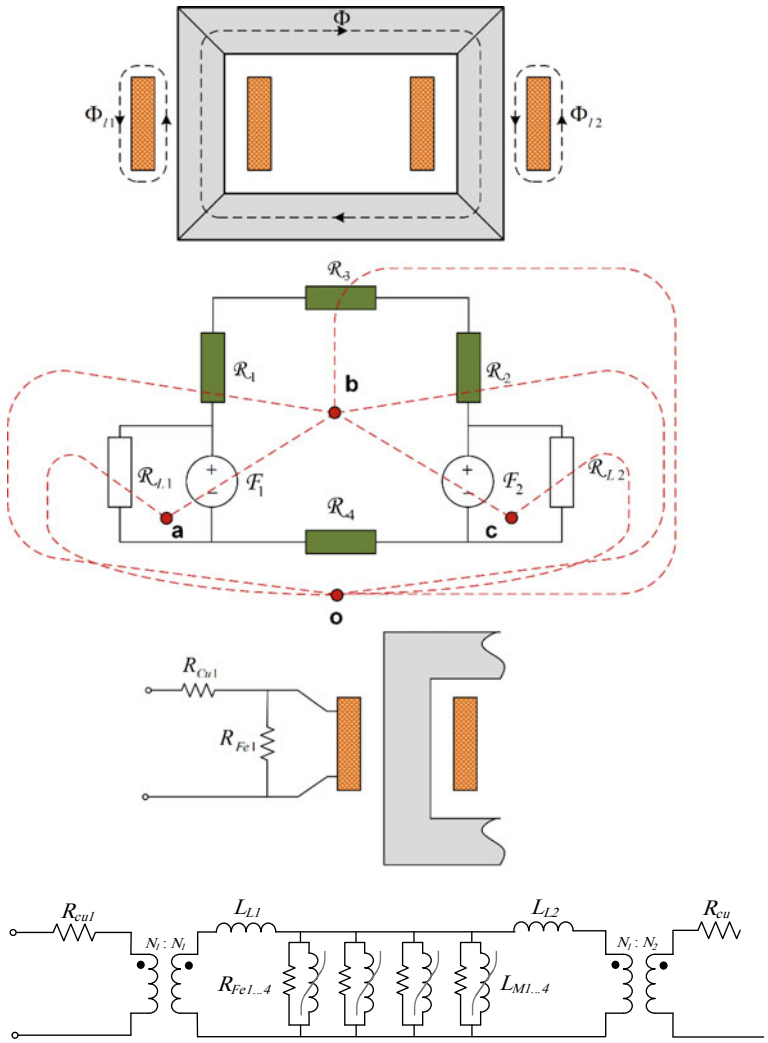

Fig. 5.11 Development of an equivalent electric circuit for a single-phase transformer based on duality

The innermost winding (F_1) encloses only the leg flux path represented by R_{Leg} and the leakage flux path between itself and the leg represented by R_{c1}. The difference between the magnetic flux of winding 2 and winding 1 flows in the leakage reluctance R_{12}. The linkage flux is divided into two paths in the yokes represented by a single equivalent reluctance R_{Yoke}.

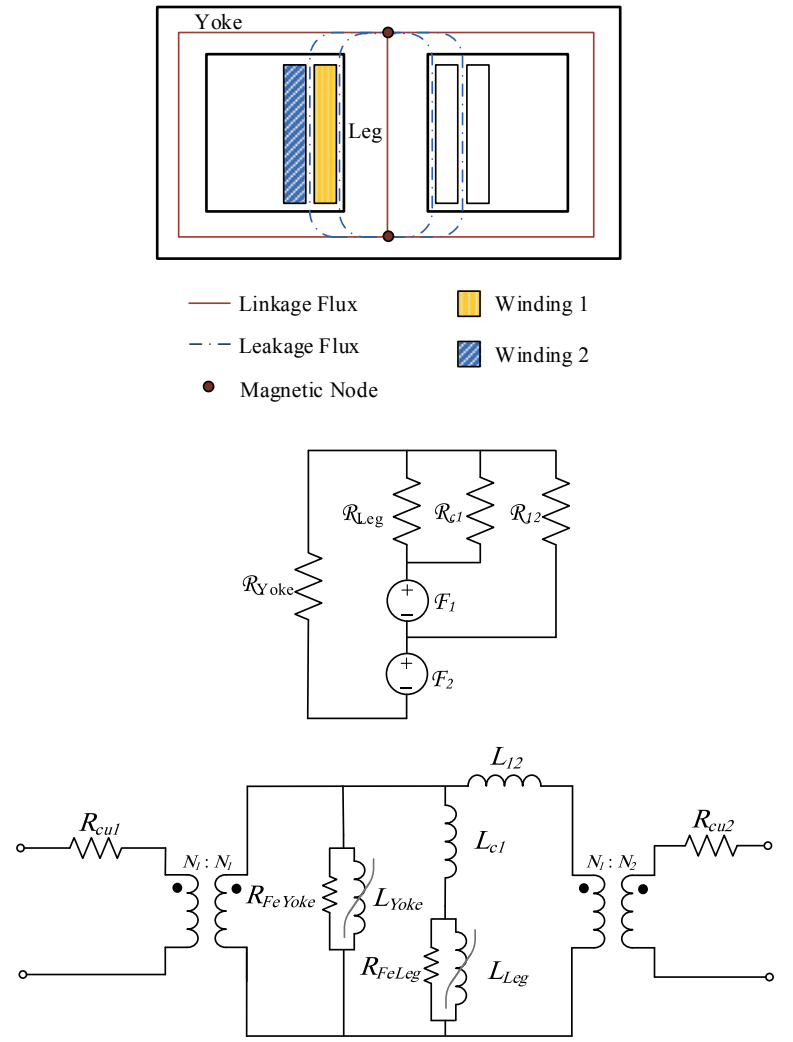

Fig. 5.12 Equivalent dual electric circuit of a shell-type 1-phase 2-winding transformer

5.4.2.4 Three-Phase Transformer

An equivalent circuit for a three-phase three-winding core-type (three-legged) transformer is derived in this section. The magnetic core of such transformer is shown in Fig. 5.13. The first step is discretising the magnetic structure, as shown by the dashed lines in Fig. 5.13.

Six magnetic nodes are determined in this transformer. These points are departure points of the magnetic flux paths and determine the discretization level of the structure. A higher number of magnetic nodes lead to a more complex model.

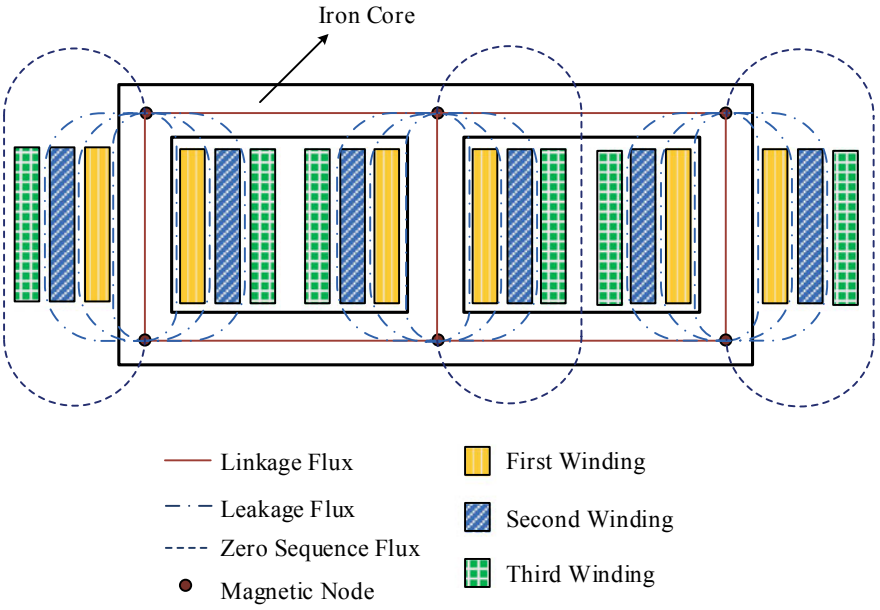

Fig. 5.13 Structure and discretization of the flux paths of a 3-phase, 3-legged 3-winding transformer

The flux paths shown in Fig. 5.13 are described here. The linkage flux paths go through the iron core to provide coupling between phases. They determine the magnetic coupling between phases. The coupling between phases due to the leakage flux can be ignored. Zero-sequence paths are defined for homopolar magnetic fluxes that flow through the tank and oil and describe the zero-sequence characteristics of the transformer. These paths are linear with the permeability of μ_0 in the case of a three-legged transformer. In the case of a five-legged transformer, these fluxes mainly flow in the outer legs and have non-linear characteristics.

The magnetic meshes are formed by drawing the flux paths. The magnetic circuit is shown in Fig. 5.14. The three bottom magnetic nodes are expanded to put these MMF sources in series. The innermost winding (F_1) encloses only the leg flux path represented by R_{Leg} and the flux path between itself and the leg represented by R_{c1}.

The difference between the magnetic flux of winding 2 and winding 1 flows in the leakage reluctance $R_{12,}$ and the difference between the magnetic flux of winding 3 and winding 2 flows in the leakage reluctance R_{23}.

The final step is to convert the magnetic circuit into the equivalent electric circuit shown in Fig. 5.15. The MMF sources are converted to ideal transformers with winding resistance in series. The core model is the equivalent circuit represented by nonlinear inductances, including L_{Leg} and L_{Yoke}. The leakage is modeled by linear inductances, including L_{c1}, L_{12}, and $L_{23,}$ and the zero-sequence characteristic is represented by L_0.

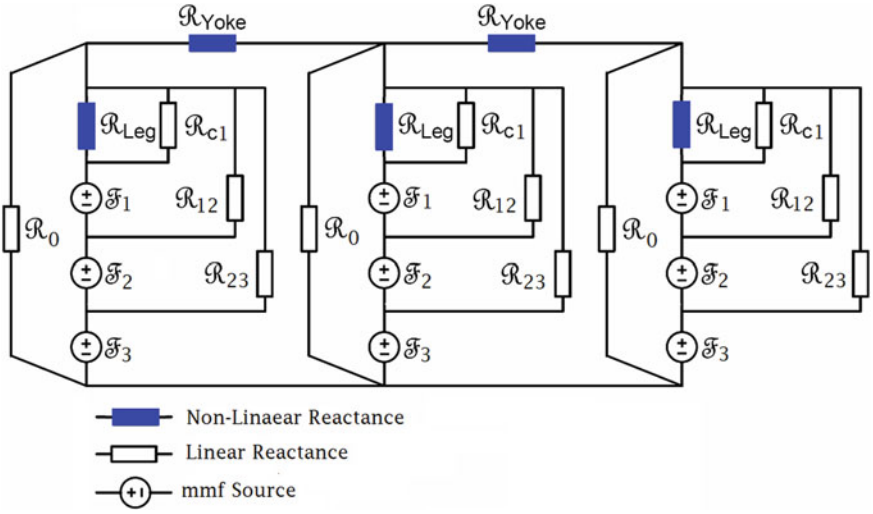

Fig. 5.14 The dual magnetic circuit of a 3-phase, 3-legged 3-winding transformer

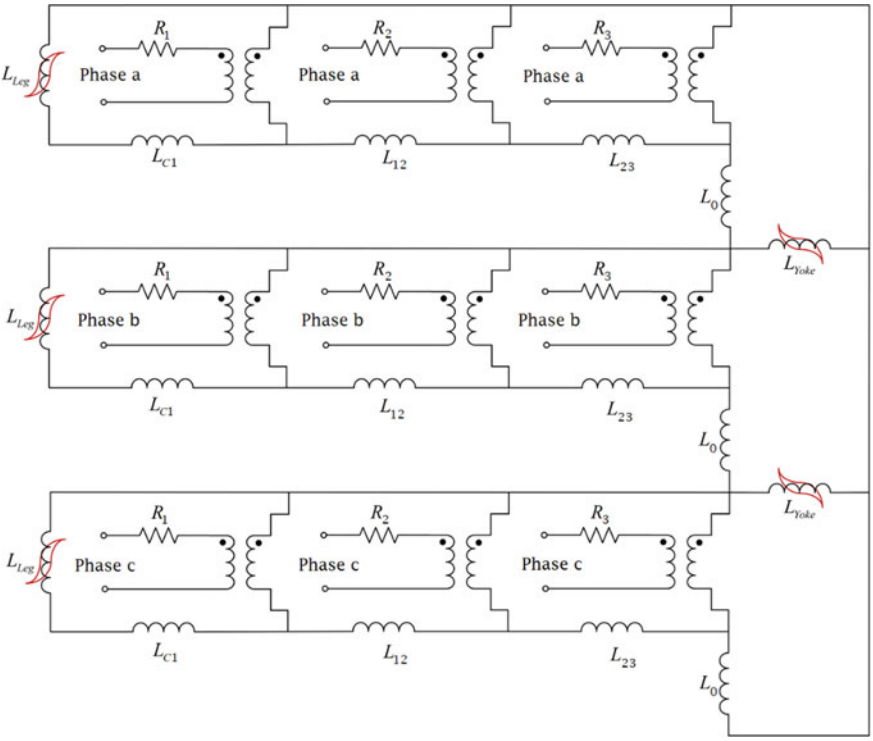

Fig. 5.15 Equivalent dual electric circuit of a core-type 3-phase 3-winding transformer

Finally, the magnetic circuit is converted into the dual electric equivalent circuit shown at the bottom of Fig. 5.12. The MMF sources are represented by ideal transformers with winding resistance in series. Nonlinear inductances including L_{Leg} and L_{Yoke} represent the magnetic core model. Linear inductances including Lc1 and L12 model the leakage paths.

5.4.2.5 Determination of the Leakage Inductance

The leakage inductances represent the leakage flux paths in dual electric circuits. In this section, an expression for leakage inductance for two concentric windings (Fig. 5.16) is derived. This procedure can be used for other topologies [12–16]. This figure is a cross-section of two winding, and a magnetic core on the right side which is not shown.

If we apply Ampere's Law $\left(\oint \vec{\mathbf{H}}.\mathrm{d}\vec{\mathbf{l}} = \oint \vec{\mathbf{J}}.\mathrm{d}\vec{\mathbf{A}}\right)$ to the path shown on the left side of Fig. 5.16 in winding 1 we have:

$$Hz = Ni\frac{y}{d_1} \quad \Rightarrow \quad H = \frac{Niy}{zd_1} \ \text{A/m} \quad \text{for } 0 < z < d_1 \tag{5.17}$$

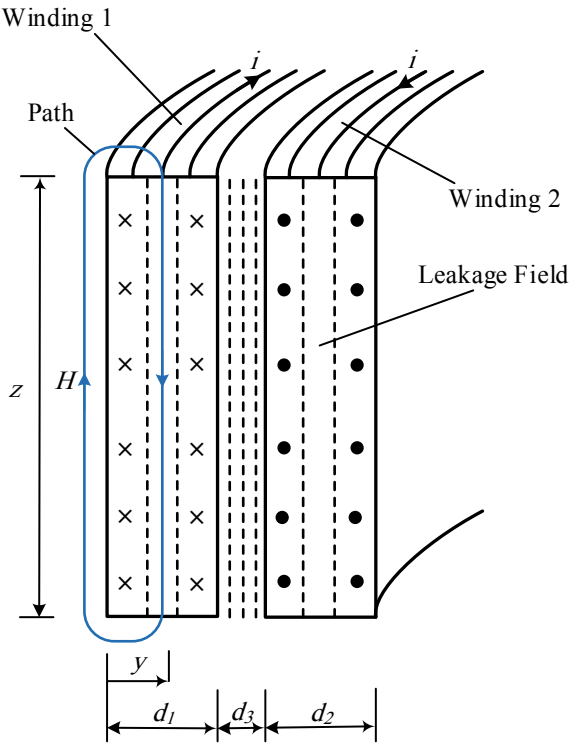

Fig. 5.16 Leakage paths and dimensions in two concentric windings for calculating leakage inductance

For the path between the windings:

$$H = \frac{Niy}{z} \quad \text{A/m} \quad \text{for } d_1 < z < (d_1 + d_3) \tag{5.18}$$

And for the path within winding 2:

$$\begin{aligned} H &= \frac{Ni}{z}(d_1 + d_2 + d_3 - z) \quad \text{A/m} \\ &\text{for } (d_1 + d_2) < z < (d_1 + d_2 + d_3) \end{aligned} \tag{5.19}$$

Suppose l is the mean circumferential length of the winding turns. Then, the stored energy in volume V of the magnetic field H is expressed by:

$$\begin{aligned} W &= \frac{1}{2}\mu_0 \int H^2 \mathrm{d}V \\ &= \frac{1}{2}\mu_0 \int_0^{d_1+d_2+d_3} H^2 z l dy \\ &= \frac{1}{2}\frac{\mu_0 N^2 i^2 l}{z}\left(\frac{d_1}{3} + d_2 + \frac{d_3}{3}\right) \quad J \end{aligned} \tag{5.20}$$

Since $W = 1/2\left(Li^2\right)$ the leakage inductance for the windings is:

$$L = \frac{\mu_0 N^2 l}{z}\left(\frac{d_1}{3} + d_2 + \frac{d_3}{3}\right) \quad H \tag{5.21}$$

5.5 Capacitive Effects and Higher Frequencies

Power transformer modeling at higher frequencies necessitates a comprehensive understanding of capacitive effects, which play a critical role in the behavior and performance of transformers operating in this frequency range [17]. As the frequency increases, capacitive effects become more pronounced, influencing the electrical characteristics and overall performance of transformers. In this section, we explore the significance of capacitive effects and their implications for power transformer modeling in higher frequency applications.

The windings of a transformer have three capacitive effects including winding to earth or core (also known as terminal, shunt, or stray capacitances), winding to winding capacitance, and turn-to-turn capacitance. These capacitive effects have to be included for accurate simulation of some transients in low- and mid-frequency range or mostly in high-frequency transients. They can be externally added to any obtained equivalent circuit like winding resistance or core losses.

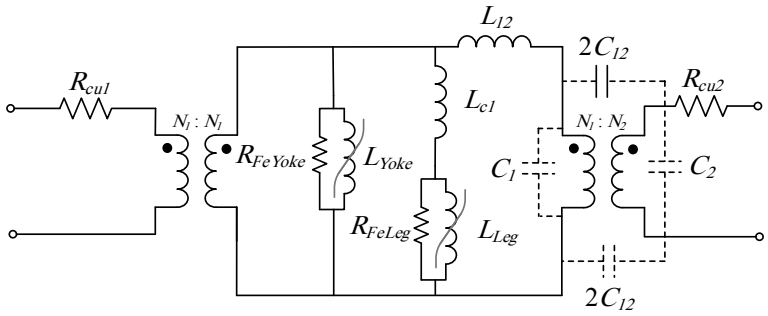

Fig. 5.17 Adding terminal capacitance and capacitance between windings in the equivalent circuit of a single-phase shell-type transformer

The modeling of winding stray capacitances is important for the higher frequencies and the calculation of residual magnetic fluxes but may be omitted in other studies. The magnetic residual flux of the core can be significantly influenced by the stray capacitances of the transformer and any other shunt capacitance in the connected circuit. The residual flux is observed to decrease in presence of large shunt capacitances. Therefore, it is necessary to include capacitances if the adopted transformer model can calculate residual fluxes. The winding shunt capacitances are standardly measured and available in test reports. Winding to winding capacitances are important in high-frequency or fast and very fast front transients studies to calculate the capacitive voltage transfer between windings from one side to another. The winding stray capacitances (C_1 and C_2) and winding to winding capacitance (C_{12}) can be included in the equivalent electric circuit driven by the duality concept as shown in Fig. 5.17 as an example for a single-phase shell-type transformer.

Turn-to-turn capacitance is used in high-frequency transformer modeling and the distribution of voltage surges in windings. To enhance accuracy, some approaches have proposed adding a single capacitor to the iron core model to represent the turn-to-turn winding capacitance effect. The capacitive effects are generally more critical in high-frequency models of the transformers, which are discussed in Chap. 6.

5.6 State of the Art of Low- and Mid-Frequency Models

In recent years, significant progress has been made in the field of power transformer modeling, with a specific focus on low and mid-frequency transients. This section aims to provide an overview of the state-of-the-art techniques and methodologies used in power transformer modeling for these types of transients.

Computer modeling and simulation of power transformers are complex due to the interactions of electric and magnetic fields in a non-linear environment consisting of materials like iron, oil, paper, and copper. Power transformers exhibit different behaviors when subjected to various excitations throughout their operational

lifespan. The state-of-the-art methods for modeling power transformers in the context of low and mid-frequency transients encompass a wide range of techniques and methodologies. These include electromagnetic modeling, equivalent circuit models, time-domain simulations, multi-physics coupling, and data-driven approaches. By employing these advancements, engineers and researchers can analyze and predict the performance of power transformers under different operating conditions, leading to improved system reliability and more efficient design practices.

Several research efforts have been undertaken to propose more accurate models in recent years. Of particular interest to power system modelers are accurate transformer models compatible with Electromagnetic Transient Programs (EMTP-type) tools. Ideally, a transformer model should be constructed using the existing capabilities of EMTP-type tools.

The principle of duality is recognized as a physically sound technique for obtaining circuit-based models of power transformers. As discussed earlier, this method offers the advantage of converting the physical magnetic circuit of an electromagnetic device into its dual electric circuit, which is suitable for simulation in EMT-type programs using standard circuit elements. Duality models effectively describe the distribution of magnetic flux in the core and windings, providing valuable information about the electromagnetic behavior of all transformer construction elements.

There are other modeling possibilities available to represent the physics of magnetic circuits in time-domain simulations, such as bond graphs, magnetic circuit equations, gyrator-capacitors, and mutators.

However, some of these techniques are challenging to implement in EMTP-type programs. Recently, a proposal for implementing mutators using commonly available coupled R-L branches has been introduced, offering an alternative to the duality transformation for representing magnetic circuits. It has been demonstrated in various studies that the models can differ significantly depending on the iron-core geometries and/or winding configurations of the transformers.

Another aspect of transformer modeling concerns eddy currents induced during high-frequency transients. These currents result in a nonuniform distribution of magnetic flux in the iron core and nonuniform current distribution in the windings. Conventional representations of eddy current losses in transformer cores, used for steady-state studies at 50/60 Hz, consist of a constant resistor in parallel with a magnetizing inductor, while dynamic eddy currents in the windings are disregarded. However, this constant resistance model is not accurate for many types of transient studies. Mid-frequency, high-frequency, and even some low-frequency studies, such as ferroresonance, require an accurate representation of the frequency-dependent effects of eddy currents in the windings and core.

The goals of modeling eddy current effects are to accurately represent the eddy losses and the nonuniform distribution of leakage flux within the transformer windings. A common method for obtaining a high-frequency transformer model is to replace lumped leakage inductances with ladder-type equivalent circuits. The synthesis of a realizable equivalent circuit involves two main steps: selecting a suitable model configuration that aligns with the frequency response of the winding

and accurately calculating the circuit parameters. Currently, there is no optimum-order fully dual model available for transformer windings that not only matches the terminal behavior but can also be constructed using only elements already available in EMTP-type programs.

Literature review shows that recent research efforts aim to propose a unified and widely accepted model for transformers capable of reproducing their behavior under all low-frequency operating conditions. Numerous duality-derived transformer models exist, each with slight or significant variations from one another. Researchers are striving to develop models that accurately represent all low-frequency transients for transformers, including normal operation, inrush currents, short-circuits, out-of-phase synchronization, geomagnetic-induced currents, ferroresonance, and harmonics.

It should be noted that these sophisticated approaches often result in ad-hoc models tailored to specific transformers with different winding geometries or core structures. However, a unified model can be derived for a particular type of transformer that is capable of reproducing all low- and mid-frequency transients. Some top recent and advanced works in this area are provided in the references ot this chapter.

References

1. J.A. Martinez, B.A. Mork, Transformer modeling for low- and mid-frequency transients-a review. IEEE Trans. Power Del. **20**(2 II), 1625–1632 (2005)
2. A. Rezaei-Zare, Enhanced transformer model for low- and mid-frequency transients—Part I: model development. IEEE Trans. Power Deliv. **30**(1), 307–315 (2015)
3. A. Rezaei-Zare, Enhanced transformer model for low- and mid-frequency transients—Part II: validation and simulation results. IEEE Trans. Power Deliv. **30**(1), 316–325 (2015)
4. V. Brandwajn, H.W. Dommel, I.I. Dommel, Matrix representation of three-phase n-winding transformers for steady-state and transient studies. IEEE Trans. Power App. Syst. PAS-101(6), 1369–1378 (1982)
5. M. Yang, R. Kazemi, S. Jazebi, D. Deswal, F. de León, Retrofitting the BCTRAN transformer model with nonlinear magnetizing branches for the accurate study of low-frequency deep saturating transients. IEEE Trans. Power Deliv. **33**(5), 2344–2353 (2018)
6. G.R. Slemon, Equivalent circuits for transformers and machines including non-linear effects, in *Proceedings of the Institution of Electrical Engineers IV*, vol. 100 (1953), pp. 129–143
7. Nicola Chiesa, *Power Transformer Modeling for Inrush Current Calculation.* Ph.D. dissertation, Department of Electric Power Engineering, Norwegian University of Science and Technology, Norway (Jun 2010)
8. S. Jazebi et al., Duality derived transformer models for low-frequency electromagnetic transients—Part I: topological models. IEEE Trans. Power Deliv. **31**(5), 2410–2419 (2016)
9. S. Jazebi et al., Duality-derived transformer models for low-frequency electromagnetic transients—Part II: complementary modeling guidelines. IEEE Trans. Power Deliv. **31**(5), 2420–2430 (2016)
10. J. Zhao et al., Topological transient models of three-phase, three-legged transformer. IEEE Access **7**, 102519–102529 (2019)
11. S.R. Pordanjani, M. Naïdjate, N. Bracikowski, M. Fratila, J. Mahseredjian, A. Rezaei-Zare, Electromagnetic modeling of transformers in emt-type software by a circuit-based method. IEEE Trans. Power Deliv. **37**(6), 5402–5413 (2022)

12. Q. Wu, S. Jazebi, F. de Leon, Parameter estimation of three-phase transformer models for low-frequency transient studies from terminal measurements. IEEE Trans. Magn. **53**(7), 1–8 (2017)
13. M. Lambert, M. Martínez-Duró, J. Mahseredjian, F. de León, F. Sirois, Transformer leakage flux models for electromagnetic transients: critical review and validation of a new model. IEEE Trans. Power Deliv. **29**(5), 2180–2188 (2014)
14. S. Jazebi, F. de León, Experimentally validated reversible single-phase multiwinding transformer model for the accurate calculation of low-frequency transients. IEEE Trans. Power Deliv. **30**(1), 193–201 (2015)
15. M. Lambert, F. Sirois, M. Martinez-Duro, J. Mahseredjian, Analytical calculation of leakage inductance for low-frequency transformer modeling. IEEE Trans. Power Deliv. **28**(1), 507–515 (2013)
16. F. de León, J.A. Martinez, Dual three-winding transformer equivalent circuit matching leakage measurements. IEEE Trans. Power Del. **24**(1), 160–168 (2009)
17. A. Rezaei-Zare, Equivalent winding capacitance network for transformer transient analysis based on standard test data. IEEE Trans. Power Deliv. **32**(4), 1899–1906 (2017)

Chapter 6
High-Frequency Modeling of Power Transformers

6.1 Introduction

Transformers can be subjected to different overvoltages, which have a frequency of a few Hz to several MHz. It has been found that transformers can be damaged due to the resonance of a part of winding excited by specific switching or lightning transient in the power system network. To avoid the exposition of the transformer to such stresses, the critical situations should be investigated using the physical winding models. In this regard, the accurate high-frequency modeling of the transformer is crucial for determining the internal resonance phenomena [1, 2].

About 50 years ago, the hazard of resonance for transformers was cleared. Suppose one input frequency copes with one of the natural frequencies of winding. In that case, the resonance phenomenon occurs, and due to an overvoltage, the winding can be damaged. Winding protection can not be successful by installing a surge arrester. As we know, the natural frequencies of winding are related to the inverse of the nominal voltage of transformers; therefore, as much as nominal voltage increases, the natural frequencies decrease and can be in the kHz range, so the probability of resonance increases [3, 4]. The natural frequencies of transformers are in the range of 5 kHz to several hundreds of kHz.

From a long time ago, it was evident that high-frequency resonance can occur inside the winding of transformers, but it was emphasized to do impulse tests on power transformers. Transformers' designers had been focused on impulsing waves and ignored frequencies of internal resonance, in which non-standard input waves could exist.

The exact characteristic of transformer frequency response can be used to prevent the occurrence of resonance in the windings. The transformer's frequency response can be determined by measurement, an old reliable method. Still, at the design stage, the frequency response is not available and, therefore, can not be used at the design stage. The best method for determining the resonance frequencies of winding is simulating them by an equivalent circuit consisting of capacitors, inductors, and

B. Vahidi and R. A. Naghizadeh, *Principles and Modeling of the Power Transformers*, Energy Systems in Electrical Engineering,
https://doi.org/10.1007/978-981-99-5796-5_6

losses [5, 6]. To remove the resonance condition, the resonance frequency of the transformer should be determined at the design stage, and the winding response to a wide range of inputs should be studied.

6.2 Literature Review

Many researchers have researched the high-frequency modeling of power transformers. In his research, E. Bjerkan [7] established a versatile and rigorous method for obtaining the high frequency model of transformer modeling. His purpose was to apply the model for sensitivity analysis of Frequency Response Analysis (FRA).

In his work, S. D. Cho [8] tried to improve topologically-correct duality-based models for three-phase autotransformers with five-legged, three-legged, or shell-form cores. In the laboratory, a distribution transformer is tested by lightning surges, and a high-frequency model of the transformer is proposed by K. Imdad [9].

M. Eslamian and B. Vahidi presented a new equivalent circuit for the winding of the transformer. In this model accurate representation of eddy current losses of the transformer at high frequencies is shown [10]. P. Mishra et al., in their paper, introduced hybrid modeling of the transformer.

This model is based on the theory of traveling waves. Also, the paper discusses the modeling and simulation of the transformer, which has disk-type winding [2]. X. Zhao et al. [11] proposed a detailed high-frequency circuit model for the transformer. In this model, they considered the winding structure, inter-turn capacitance, and all mutual inductances.

E. Bjerlan and H. K. Hoidalen [12] introduced a method for obtaining both internal and terminal models of power transformers at high frequency by FEM. This model is based on information on construction and uses the physical basis of frequency-dependent phenomena. K. Pedersen et al. [13] described how a great detailed internal model for a transformer can be achieved systematically with Matlab software and the technique of using it for transient analysis.

The input of their model is the characteristics of the cross section of the leg of a single transformer, and all turns and windings are included. By using the input data, a three-phase equivalent circuit is calculated. H. Quaddi et al. [14] work is the modeling of those transformers (three-phases) that are used in the railway substation. They propose a high-frequency model for the transformer, valid in the frequency range of 10 kHz to 30 MHz. Various impedances should be determined with reasonable accuracy.

Kh. Elkamouny et al. [15], to minimize the dimension and cost of a PV micro-inverter board, designed a high-frequency transformer that adopted the criteria of reliability and miniaturization. In their work, L. Brana et al. [16] introduced a high-frequency model for a transformer that can be integrated into a time-domain equivalent circuit. M. Heindl et al. [17] introduced a high-frequency model for large transformers to analyze the transient interaction phenomena between the power systems and transformers. A. Abu-Siada [18] used the FRA as a diagnostic tool to detect the

deformation of transformer winding. He used transformer high-frequency computer modeling together with FRA for this diagnostic.

Y. Yoon et al. [19] proposed a method for estimating transformer parameters using sweep frequency response analysis (SFRA) test data. At first, a model based on repetitive RLC sections and mutual inductances was introduced and then aligned the simulated SFRA curve with the measured one by adjusting parameters. Finally, the power transformer model can be attained by aligning the two curves. M. Hussain et al. [20] introduced a modified high-frequency model for transformers to study protection against lightning transients. This model is a modified version of the N. A Sabiha model [21] is based on the black box, two ports, and four-terminal network theory.

F. De León and A. Semlyen [22] modeled the losses of eddy current of a coil by Foster (series and parallel) and Cauer (series and parallel) circuits. The coil model is presented in references [23] and [24]. The equivalent circuit contains the main branch and several magnetically coupled loops to the main branch, representing the eddy currents. In the case of winding with multi-coil for precise modeling of eddy current losses, mutual resistance and mutual inductance should be considered, which does not apply to usual Foster or Cauer circuits.

In [25] Self resistances and mutual resistance are modeled by a series of Foster circuits and mathematical approximations, which is made the simulation complicated. The equivalent circuit, which is introduced in [23, 24], and [26], is one of the complete models of eddy current. Some other models can be found in [27, 28], and [29].

6.3 Transformer Winding Modeling

In this chapter, high-frequency modeling of the winding of the transformer is used, based on the modeling of Eslamian and Vahidi [10] and [1].

This model considers the high-frequency eddy current losses of the transformer. In this model, by using Foster circuits, the frequency-dependent impedance of the coil system is employed. The model's parameters are determined using the vector fitting method for rational approximation of the system impedance matrix. This model may be used for computing the high-frequency resonance inside the winding of the transformer in which the overvoltage is dependent on the damping effect of loss of the transformer. As the model parameters are constant lumped parameters, the model could be used for the computation of time domain transients by using the electromagnetic transients programs.

Till now, different methods have been used for modeling the eddy current losses in a transformer coil. This modeling is done by using Foster's circuit (series and parallel) [22] and Cauer's circuit (series and parallel) [30, 31]. The point is to be careful about winding containing several coils in which the mutual inductance and resistance should be considered, which can not be modeled by custom Foster and Dauer circuits.

In this chapter, by using Foster coupled series circuits, a model is introduced which can model the behavior of an actual winding containing several coupled coils at high frequency, including modeling the effects of eddy current. Also an effective method for determining model parameters by using the Vector Fitting program is introduced [32]. This method is fast enough and can be used for windings with several coils, and because of using the Vector Fitting, the equivalent circuit is passive and can be used in the software in the time domain. This model is an improved version of De Leon's model [25] which coupling between Foster's circuits is not shown mathematically but by mutual inductances. This model is slightly similar to Mobello's model in the point of view of parallel RL branches and ignores the coupling between inductances of auxiliary branches [26]. The introduced equivalent circuit is linear and is not considering hysteresis and saturation and can be used in the frequency range where the effects of nonlinearity of the core, such as hysteresis and saturation, can be neglected (over several kilo-Hertz).

6.4 Vector Fitting

According to [33] and [34], the impedance of any RL circuit can be written as follow:

$$Z(s) = b_0 + b_\infty s + \sum_{i=1}^{m} \frac{b_i}{s + \lambda_i} \tag{6.1}$$

where:

$s_i = -\lambda_i$ are negative real poles,

b_i are negative real residues,

b_0 and b_∞ are real positive constants.

The $Z(s)$ can be synthesized by a series Foster circuit like the one that is indicated in Fig. 6.1

where:

$$R_0 = b_0 + \sum_{i=1}^{m} \frac{b_i}{\lambda_i} \; L_0 = b_\infty \tag{6.2}$$

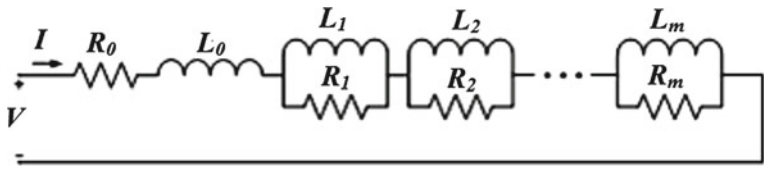

Fig. 6.1 Foster circuit

$$R_i = -\frac{b_i}{\lambda_i} \qquad L_i = \frac{R_i}{\lambda_i} \tag{6.3}$$

Therefore, if the frequency behavior of a winding can be measured or computed and a function such as Eq. (5.1) can be fitted, it can be synthesized by a series Foster circuit [1]. Vector Fitting is a method for impedance (or admitance) function fitting in the form of minor fractions [32]. Decades after introducing this method, Gustavsen and Semlyen they have developed it and other researchers from a different point of view; for example, [35] made it faster, [36] improved the pole relocating properties of Vector Fitting, and [37–39] applied the passivity to the final result.

According to a mathematical point of view, a model has the passivity criterion if all eigenvalues of the real part of the model impedance (or admittance) matrix are positive for all frequencies. A nonpassive model may result in unstable time-domain simulations for no apparent reason [10].

Generally, Vector Fiting is used for admittance function fitting, and its important application has been admittance fitting of transformers and synthesizing the equivalent circuit by RLC circuit [40–43] and can be used for impedance function fitting as well.

As there is no capacitance in an RL, the rational approximation of its driving-point impedance does not contain complex conjugate poles. However, Vector Fitting can do very well in this situation by fitting smooth impedance responses with rational functions with only negative real stable poles, which satisfies the passivity condition. It should be noted that the starting poles are complex conjugate pairs (distributed over the frequency range), and the real poles result from the subsequent iterative procedure. Due to the smoothness of the fitted function, Vector Fitting is fast enough and uses the least square error method [1].

6.5 Proposed Model

In this chapter, an equivalent circuit which is consisted of coupled series Foster circuits is introduced, which can model the frequency behavior of the system impedance matrix. The method for one winding can be used for a system with several coupled coils. Of course, determining the system's parameters is not as simple as a single winding, but by using Vector Fitting, the parameters for the system model can be obtained [1]. It should be noted that for a multi-terminal system, determining parameters is not as easy as for single winding, and the method will be discussed in the next section. The modeling process steps are:

1. Calculation of winding impedance matrix.
2. A certain number of common poles fit into the computed impedance matrix using Vector Fitting.
3. Determining the equivalent circuit parameters by using a particular procedure.

It should be noted that the winding impedance matrix is matric with complex elements that vary with frequency. These elements can be determined by measurement or electromagnetic computation. In the measurement method, due to the capacitance effect in the high-frequency range in this modeling, we used the Finite Element Method (FEM) for computing the elements of the impedance matrix by considering skin and proximity effects [1, 10]. Frequency behavior of impedance matrix of winding can be modeled by coupled Foster series circuits in a way that impedance is seen from the terminal of inductive branches of equivalent circuit is not constant and is a function of frequency. The equivalent circuit is shown in Fig. 6.2.

The mutual inductances between different branches are not shown in this picture for the sake of clarity, but they exist. The mutual inductances between Foster circuits for coils number I and j are shown in Fig. 6.3. In this figure, the coupling between auxiliary inductaces of Foster circuits is neglected [1].

According to the physical point of view is correct because most of the current is passing through the series inductances; therefore, coupling between them is more than coupling between auxiliary inductances. By neglecting coupling between auxiliary inductances, the equivalent circuit will be smaller, and the parameters are less, which

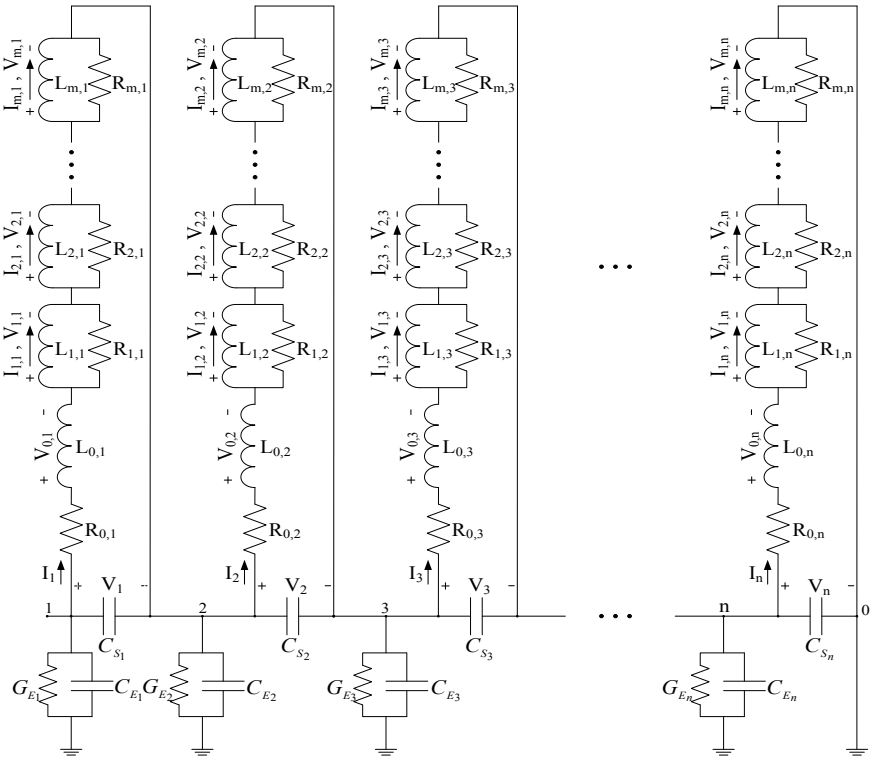

Fig. 6.2 The introduced equivalent circuit for transformer winding [1]

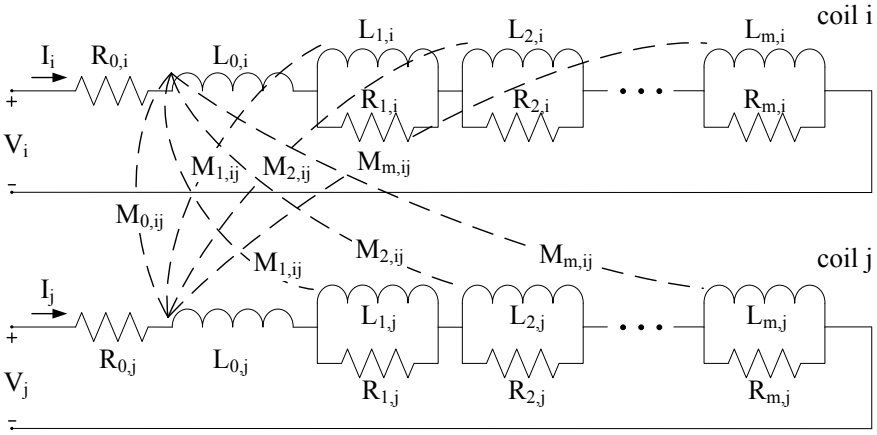

Fig. 6.3 Equivalent circuit for two coupled coils [1]

makes the computation less; this assumption also is used by [26]. Another assumption is needed in order to allow the equivalent model can be realized by the results of the impedance fitting process [1, 10].

Each RL block of the system $(R_{i,j}, L_{i,j})$. produces a real negative pole $(-R_{i,j} / L_{i,j})$, and the corresponding blocks in Foster circuits can produce the same poles:

$$\frac{R_{i,j}}{L_{i,j}} = \frac{R_{i,k}}{L_{i,k}} \quad , \; i = 1..m \quad , \; j, k = 1..n \tag{6.4}$$

From (6.4) can judge that ratio of resistance to the inductance of corresponding blocks (e.g., all first blocks, all second blocks,….) is a real value; this assumption also is used by [25].

As seen in Fig. 6.3, the third suggestion needs to be used for finding parameters of the circuit uniquely by Vector Fitting. It is assumed in Fig. 6.6; the mutual inductances between the series inductance of the ith circuit and the auxiliary inductances of the jth circuit $(M_{k,ij}\,, k = 1..m)$ are correspondingly equal to the mutual inductances between the series inductance of the jth circuit and the auxiliary inductances of the ith circuit.

Figure 6.2 is an equivalent circuit of a transformer winding that contains n coils, and the equivalent circuit is made of n coupled Foster circuits of m order. The number

of independent parameters due to mutual inductances between two Foster circuits is m + 1 (Fig. 6.3).

Voltages and currents relationship is as follows:

$$\begin{bmatrix} \overline{V}_0 \\ \overline{V}_1 \\ \overline{V}_2 \\ \cdots \\ \overline{V}_m \end{bmatrix} = \begin{bmatrix} s\mathbf{L_0} & s\mathbf{M_1} & s\mathbf{M_2} & \cdots & s\mathbf{M_m} \\ s\mathbf{M_1^T} & s\mathbf{L_1} & 0 & \cdots & 0 \\ s\mathbf{M_2^T} & 0 & s\mathbf{L_2} & \cdots & 0 \\ \cdots & \cdots & \cdots & \cdots & \cdots \\ s\mathbf{M_m^T} & 0 & 0 & \cdots & s\mathbf{L_m} \end{bmatrix} \begin{bmatrix} \overline{I} \\ \overline{I}_1 \\ \overline{I}_2 \\ \cdots \\ \overline{I}_m \end{bmatrix} \tag{6.5}$$

where:

$\overline{V}_i$ (order $= n \times 1$) is the voltage vector of corresponding inductances (series and auxiliary) of Foster circuits.

$$\overline{V}_i = \begin{bmatrix} V_{i,1} \\ V_{i,2} \\ \vdots \\ V_{i,n} \end{bmatrix} \quad , \; i = 0..m \tag{6.6}$$

$\overline{I}_i$ (order $= n \times 1$) is the current vector of corresponding inductances (series and auxiliary) (note: $\overline{I}_0$ is equal to $\overline{I}$) of Foster circuits.

$$\overline{I}_i = \begin{bmatrix} I_{i,1} \\ I_{i,2} \\ \vdots \\ I_{i,n} \end{bmatrix} \quad , \; i = 0..m \tag{6.7}$$

$\mathbf{L_0}$ (order $= n \times n$) is matrix inductance of series inductance elements of Foster circuits.

$$\mathbf{L_0} = \begin{bmatrix} L_{0,1} & M_{0,12} & \cdots & M_{0,1n} \\ M_{0,12} & L_{0,2} & \cdots & M_{0,2n} \\ \cdots & \cdots & \cdots & \cdots \\ M_{0,1n} & M_{0,2n} & \cdots & L_{0,n} \end{bmatrix} \tag{6.8}$$

$\mathbf{L_i}$ (order $= n \times n$) is a diagonal matrix containing the self-inductance of ith blocks of Foster circuits.

$$\mathbf{L_i} = \begin{bmatrix} L_{i,1} & 0 & \cdots & 0 \\ 0 & L_{i,2} & \cdots & 0 \\ \cdots & \cdots & \cdots & \cdots \\ 0 & 0 & \cdots & L_{i,n} \end{bmatrix} \tag{6.9}$$

Matrix $\mathbf{M_i}$ is symmetrical (order $= n \times n$) and contains the mutual inductances between the series inductances and the inductances of ith blocks of the Foster circuits.

$$\mathbf{M_i} = \begin{bmatrix} 0 & M_{i,12} & \cdots & M_{i,1n} \\ M_{i,12} & 0 & \cdots & M_{i,2n} \\ \cdots & \cdots & \cdots & \cdots \\ M_{i,1n} & M_{i,2n} & \cdots & 0 \end{bmatrix} \tag{6.10}$$

Another matrix equation for the relation of voltages and currents of RL branches can be written as follow:

$$\begin{bmatrix} \overline{V}_1 \\ \overline{V}_2 \\ \cdots \\ \overline{V}_m \end{bmatrix} = \begin{bmatrix} \mathbf{R_1} & -\mathbf{R}_1 & 0 & \cdots & 0 \\ \mathbf{R}_2 & 0 & -\mathbf{R}_2 & \cdots & 0 \\ \cdots & \cdots & \cdots & \cdots & \cdots \\ \mathbf{R}_m & 0 & 0 & \cdots & -\mathbf{R}_m \end{bmatrix} \begin{bmatrix} \overline{I} \\ \overline{I}_1 \\ \overline{I}_2 \\ \cdots \\ \overline{I}_m \end{bmatrix} \tag{6.11}$$

where:

$\mathbf{R_i}$ (order $= n \times n$) is a diagonal matrix that contains resistance of ith blocks of Foster circuits.

$$\mathbf{R_i} = \begin{bmatrix} R_{i,1} & 0 & \cdots & 0 \\ 0 & R_{i,2} & \cdots & 0 \\ \cdots & \cdots & \cdots & \cdots \\ 0 & 0 & \cdots & R_{i,n} \end{bmatrix} \tag{6.12}$$

Also, the following equation can be written for terminals of Foster circuits.

$$\overline{V} = \mathbf{R_0}\overline{I} + \sum_{i=0}^{m} \overline{V}_i \tag{6.13}$$

where:

$\mathbf{R_0}$ (order $= n \times n$) is a diagonal matrix that contains series resistance of the Foster circuits.

By combining Eqs. (6.5), (6.11), and (6.13), the following equation can be obtained:

$$\begin{bmatrix} \overline{V} \\ 0 \\ 0 \\ \cdots \\ 0 \end{bmatrix} = \begin{bmatrix} \mathbf{Z_0} + \sum_{i=0}^{m} \mathbf{R_i} & s\mathbf{M_1} - \mathbf{R_1} & s\mathbf{M_2} - \mathbf{R_2} & \cdots & s\mathbf{M_m} - \mathbf{R_m} \\ s\mathbf{M_1} - \mathbf{R_1} & s\mathbf{L_1} + \mathbf{R_1} & 0 & \cdots & 0 \\ s\mathbf{M_2} - \mathbf{R_2} & 0 & s\mathbf{L_2} + \mathbf{R_2} & \cdots & 0 \\ \cdots & \cdots & \cdots & \cdots & \cdots \\ s\mathbf{M_m} - \mathbf{R_m} & 0 & 0 & \cdots & s\mathbf{L_m} + \mathbf{R_m} \end{bmatrix} \begin{bmatrix} \overline{I} \\ \overline{I}_1 \\ \overline{I}_2 \\ \cdots \\ \overline{I}_m \end{bmatrix} \tag{6.14}$$

The relationships between voltages and currents of terminals of the system can be obtained from Eq. (6.14) as follow:

$$\overline{V} = \mathbf{Z}\,\overline{I} = (\mathbf{A} - \mathbf{B}\,\mathbf{C^{-1}}\,\mathbf{B^{T}})\,\overline{I} \tag{6.15}$$

where:

Z is the winding impedance matrix seen from the coils' output terminals.

The other matrices in (6.15) are as follow:

$$\mathbf{A} = \mathbf{Z_0} + \sum_{i=0}^{m} \mathbf{R_i} \tag{6.16}$$

$$\mathbf{B} = \left[\, s\mathbf{M_1} - \mathbf{R_1}\ s\mathbf{M_2} - \mathbf{R_2} \cdots s\mathbf{M_m} - \mathbf{R_m} \,\right] \tag{6.17}$$

$$\mathbf{C} = \begin{bmatrix} s\mathbf{L_1} + \mathbf{R_1} & 0 & \cdots & 0 \\ 0 & s\mathbf{L_2} + \mathbf{R_2} & \cdots & 0 \\ \cdots & \cdots & \cdots & \cdots \\ 0 & 0 & \cdots & s\mathbf{L_m} + \mathbf{R_m} \end{bmatrix} \tag{6.18}$$

As the **C** matrix is diagonal (due to neglecting the mutual inductances between auxiliary inductances) can be inversed easily; therefore, circuit equations can be written with the aid of Eq. (6.15). From (6.15) and with the aid of (6.16) to (6.18), the diagonal and non-diagonal elements of **Z** can be obtained as follows:

$$Z_{kk} = sL_{0,k} + R_{0,k} + \sum_{i=1}^{m} R_{i,k} - \sum_{i=1}^{m} \frac{R_{i,k}^2}{sL_{i,k} + R_{i,k}} - \sum_{i=1}^{m} \sum_{\substack{j=1 \\ j \neq k}}^{n} \frac{s^2 M_{i,kj}^2}{sL_{i,j} + R_{i,j}} \tag{6.19}$$

$$Z_{kl} = sM_{0,kl} + \sum_{i=1}^{m} \frac{sR_{i,k}M_{i,kl}}{sL_{i,k} + R_{i,k}} + \sum_{i=1}^{m} \frac{sR_{i,l}M_{i,kl}}{sL_{i,l} + R_{i,l}} - \sum_{i=1}^{m} \sum_{\substack{j=1 \\ j \neq k,l}}^{n} \frac{s^2 M_{i,kj}M_{i,lj}}{sL_{i,j} + R_{i,j}} \tag{6.20}$$

By using the following equations and with the aid of (6.4), the impedance elements can be written in partial fraction expansion forms as follows:

$$\frac{sMR}{sL + R} = \frac{R}{L}M - (\frac{R}{L})^2 \frac{M}{s + R/L} \tag{6.21}$$

$$\frac{s^2 M_1 M_2}{sL + R} = s\frac{M_1 M_2}{L} - \frac{R}{L}\frac{M_1 M_2}{L} + (\frac{R}{L})^2 \frac{(M_1 M_2)/L}{s + R/L} \tag{6.22}$$

The Z_{kk} can be written as follow:

$$Z_{kk} = \overline{d} + s\overline{e} + \sum_{i=1}^{m} \frac{\overline{c}_i}{s - a_i} \tag{6.23}$$

where:

$$a_i = -\frac{R_{i,k}}{L_{i,k}} \tag{6.24}$$

$$\overline{c}_i = -a_i^2 (L_{i,k} + \sum_{\substack{j=1 \\ j \neq k}}^{n} \frac{M_{i,kj}^2}{L_{i,j}}) \tag{6.25}$$

$$\overline{e} = L_{0,k} - \sum_{i=1}^{m} \sum_{\substack{j=1 \\ j \neq k}}^{n} \frac{M_{i,kj}^2}{L_{i,j}} \tag{6.26}$$

$$\overline{d} = R_{0,k} + \sum_{i=1}^{m} \frac{\overline{c}_i}{a_i} \tag{6.27}$$

The Z_{kl} can be written as follow:

$$Z_{kl} = \hat{d} + s\hat{e} + \sum_{i=1}^{m} \frac{\hat{c}_i}{s - a_i} \tag{6.28}$$

where:

a_i is the same as (6.24)

$$\hat{c}_i = -a_i^2 (2M_{i,kl} + \sum_{\substack{j=1 \\ j \neq k,l}}^{n} \frac{M_{i,kj} M_{i,lj}}{L_{i,j}}) \tag{6.29}$$

$$\hat{e} = M_{0,kl} - \sum_{i=1}^{m} \sum_{\substack{j=1 \\ j \neq k,l}}^{n} \frac{M_{i,kj} M_{i,lj}}{L_{i,j}} \tag{6.30}$$

$$\hat{d} = \sum_{i=1}^{m} \frac{\hat{c}_i}{a_i} \tag{6.31}$$

The Eqs. (6.23) and (6.28) are the main equations for determining the parameters of an equivalent circuit.

The reason for choosing these forms is to use rational function approximations, which Vector Fitting can obtain for computing the model's parameters [1].

6.6 Determining the Parameters of the Model

For determining the equivalent circuit parameters, we have to choose a way that the coefficients of partial fraction expansion of elements of the impedance of the equivalent circuit model [(6.23) and (6.28)] should be the same as their corresponding coefficients in the partial fraction expansion of the same element of impedance that obtained from the fitting by Vector Fitting.

A set of nonlinear equations is obtained, and the fixed-point iteration method can be used to solve them. Therefore, for the unknowns, at first, the proper initial values must be selected.

For selecting the initial values of resistances and self-inductances, at first, the coupling between Foster circuits is ignored. The values of R_0, L_0, R_i, and L_i are determined so that each un-coupled Foster circuit's terminal impedance equals the self-inductance of the corresponding winding coil. Assume that the output of Vector Fitting of impedance is as (6.32).

$$\mathbf{Z}(s) = \mathbf{D} + s\mathbf{E} + \sum_{i=1}^{m} \frac{\mathbf{C_i}}{s - a_i} \tag{6.32}$$

Then by ignoring the mutual inductances and using (6.19), the initial values of R and L for each Foster circuit can be obtained as follow:

$$R_{0,k}^{(0)} = \mathbf{D}(k,k) - \sum_{i=1}^{m} \frac{\mathbf{C_i}(k,k)}{a_i} \qquad L_{0,k}^{(0)} = \mathbf{E}(k,k) \tag{6.33a}$$

$$R_{i,k}^{(0)} = \frac{\mathbf{C_i}(k,k)}{a_i} \qquad L_{i,k}^{(0)} = -\frac{R_{i,k}^{(0)}}{a_i} \tag{6.33b}$$

These equations are similar to the equations of a single coil which is modeled by the Foster series circuit [Eqs. (6.2) and (6.3)]. Also, selecting initial values of mutual inductances between two Foster circuits should assume that only coupling exists between those two Foster circuits and there is not any coupling between other Foster circuits [1]. Therefore concerning Eq. (6.20), the initial values of mutual inductances can be obtained from the following equations.

$$M_{0,kl}^{(0)} = \mathbf{E}(k,l) \tag{6.34a}$$

$$M_{i,kl}^{(0)} = -\frac{\mathbf{C_i}(k,l)}{2a_i^2} \tag{6.34b}$$

The initial values for all impedance matrix elements (self and mutual) will be selected using the equations mentioned earlier. After selecting the initial values, the parameters will be determined in an iteration algorithm by using Eqs. (6.35a and 6.35b) [for self impedances] and (6.36) [for mutual impedances] (by using the results of Vector Fitting).

$$R_{0,k} = R_{0,k}^{(0)} \quad L_{0,k} = \mathbf{E}(k,k) + \alpha \sum_{i=1}^{m} \sum_{\substack{j=1 \\ j \neq k}}^{n} \frac{M_{i,kj}^2}{L_{i,j}} \tag{6.35a}$$

$$R_{i,k} = \frac{\mathbf{C_i}(k,k)}{a_i} + \alpha\, a_i \sum_{\substack{j=1 \\ j \neq k}}^{n} \frac{M_{i,kj}^2}{L_{i,j}} \quad L_{i,k} = -\frac{R_{i,k}}{a_i} \tag{6.35b}$$

$$M_{0,kl} = \mathbf{E}(k,l) + \alpha \sum_{i=1}^{m} \sum_{\substack{j=1 \\ j \neq k,l}}^{n} \frac{M_{i,kj} M_{i,lj}}{L_{i,j}} \tag{6.36a}$$

$$M_{i,kl} = -\frac{\mathbf{C_i}(k,l)}{2a_i^2} - \alpha \sum_{\substack{j=1 \\ j \neq k,l}}^{n} \frac{M_{i,kj} M_{i,lj}}{2L_{i,j}} \tag{6.36b}$$

R_i and L_i parameters for each element of self impedance and M_i parameters for each element of mutual impedance are updated by a method that the coefficients of the partial fraction expansion for the same impedance element result from Vector Fitting are obtained. It should be noted that the impedance matrix of a winding with n coils is a complex symmetrical matrix (order $= n \times n$) which contains n self impedance and n(n − 1)/3 mutual impedance. Therefore there is n(n + 1)/2 partial fraction expansions. In each iteration for each impedance (it means: Z_{ij} , $i = 1..n, j = 1..i$), the parameters for self-impedance are updated according to Eqs. (6.35a) and (6.35b). For updating parameters of mutual impedances, the Eqs. (6.36a) and (6.36b) are used [1]. As can be seen from Eqs. (6.35a, 6.35b) and (6.36a, 6.36b), a factor (α) which is called the variable under-relaxation factor, is used in the equations. The α factor is used to ensure convergence. At first, this factor is less than 1 and then increases step by step up to one after several updating operations. The initial value of this factor could be 0.05 and increases step by step by 0.05.

By applying this factor causes the gradual increase of mutual inductances in the system and prevents the R and L from being negative, and during the solution process, convergence happens. It should be noted that Eqs. (6.35a, 6.35b) and (6.36a, 6.36b) will be the same as (6.33a, 6.33b) and (6.34a, 6.34b), respectively, for $\alpha = 0$ which they are used for determining the initial values of parameters.

6.6.1 Case Study

As a case study for analyzing the proposed model, the winding of Fig. 6.4 is simulated. The winding is contained sixteen disk coils, and each coil contains sixteen turns [1].

A homogeneous cylindrical shape core is used inside the winding, and in the simulation, it is shown as a nonconductive material ($\mu_r = 1000$). Turn dimensions are $2 \times 5.5\, mm$, and turn insulation thickness is 0.5 mm. It should be noted that this is not an actual winding. The end of the winding is earthed in this simulation. The

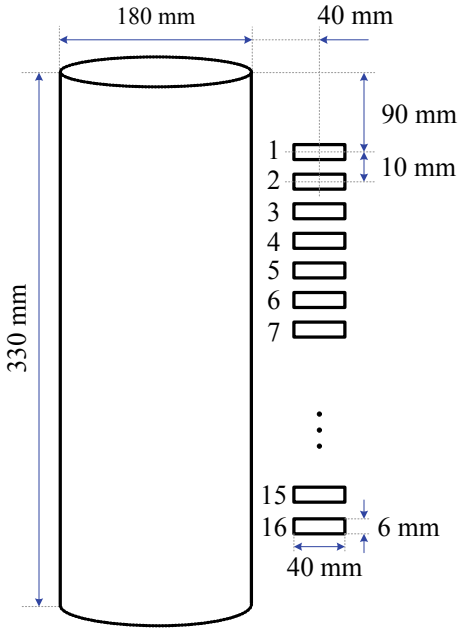

Fig. 6.4 Dimensions of simulated winding [1]

value of series capacitance of the first and last disks is 100 pF but for other disks is 180 pF. The value of capacitance to the ground of each disk is 10 nF divided into two 5 nF capacitance and located on both ends of the disk (in simulation).

The value of capacitance to ground is primarily chosen to keep the winding resonance frequency in the power transformers' resonance frequency range less than 1 MHz.

For finding an equivalent model, the matrix of the winding impedance was computed in the frequency range of 3 kHz to 1 MHz in several specification frequencies. (The linear and logarithmic interpolations were used to compute phase angle and magnitude respectively, concerning the logarithm of frequency for preparing enough data points in the frequency range of 1 kHz to 1 MHz). The geometry of winding, core and individual conductors are modeled in finite element method software (FEMM 4.2 [44]). In this simulation, copper conductivity is 58e6 S/m.

By applying currents to coils and computing the voltage drops, the value for self impedance and mutual impedance were extracted through a certain number of (2-D axisymmetric) FEM analyses.

In the next step, using the Vector Fitting matrix of system impedance (order $= 16 \times 16$) was fitted in rational functions. In this fitting, six stable poles are used, and the inverse of the square root of the matrix norm as the weighting applied to all matrix elements in each frequency. Finally, the equivalent model parameters were extracted using the equations mentioned earlier. The fitting results for the impedance matrix elements are shown in Fig. 6.5a and b. The RMS error of the process of fitting is 4.3e−3.

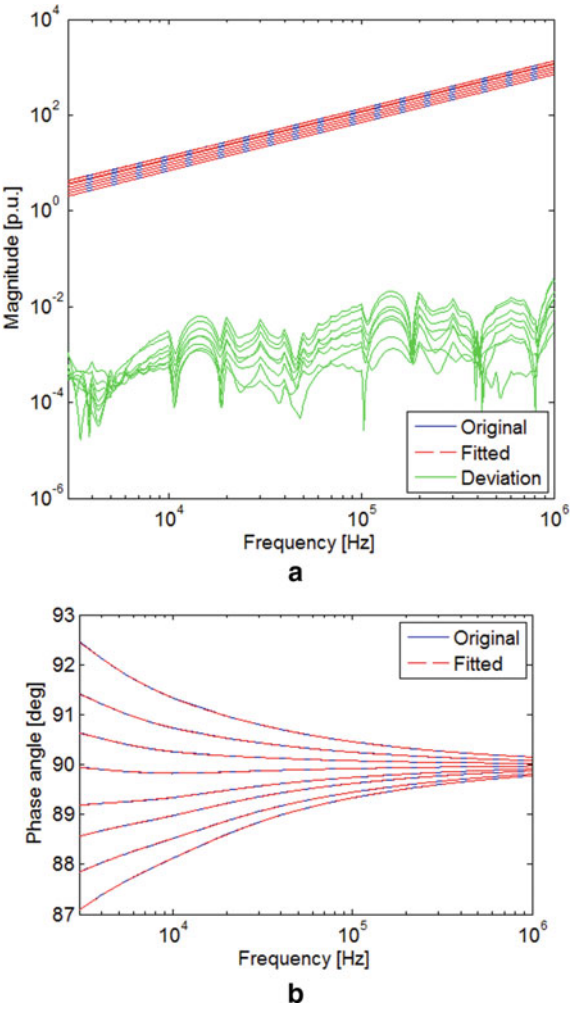

Fig. 6.5 **a** Fitting of impedance matrix by Vector Fitting (amplitude) with six stable poles for eight elements [1]. **b** Fitting of impedance matrix by Vector Fitting (phase) with six stable poles for eight elements [1]

The real and imaginary parts of Z_{11} and Z_{15}, calculated through FEM and obtained by equivalent circuit, are shown in Figs. 6.6a, b, 6.7a and b.

After obtaining the equivalent circuit, the frequency response of the voltage of all nodes of winding was calculated. For this proposal, the end of the winding was earthed, and voltage was applied to the beginning of the winding. The frequency responses of voltage for nodes 5 and 10 are shown in Fig. 6.8a and b,

In these figures, "calculated in frequency domain" means calculation by solving the equations of the detailed model with an impedance matrix that varies with frequency [45]. For clarity, polar curves are provided in Fig. 6.9a and b. In these figures, the high accuracy of the equivalent model is shown for the frequency response of voltages.

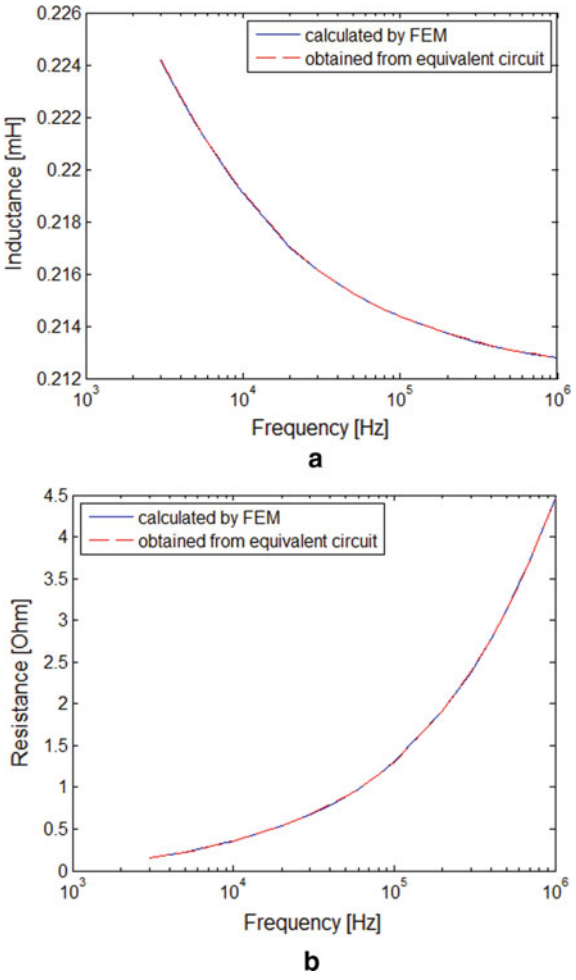

Fig. 6.6 **a** The real part of Z11 (L11) [1]. **b**. The imaginary part of Z11 (R11) [1]

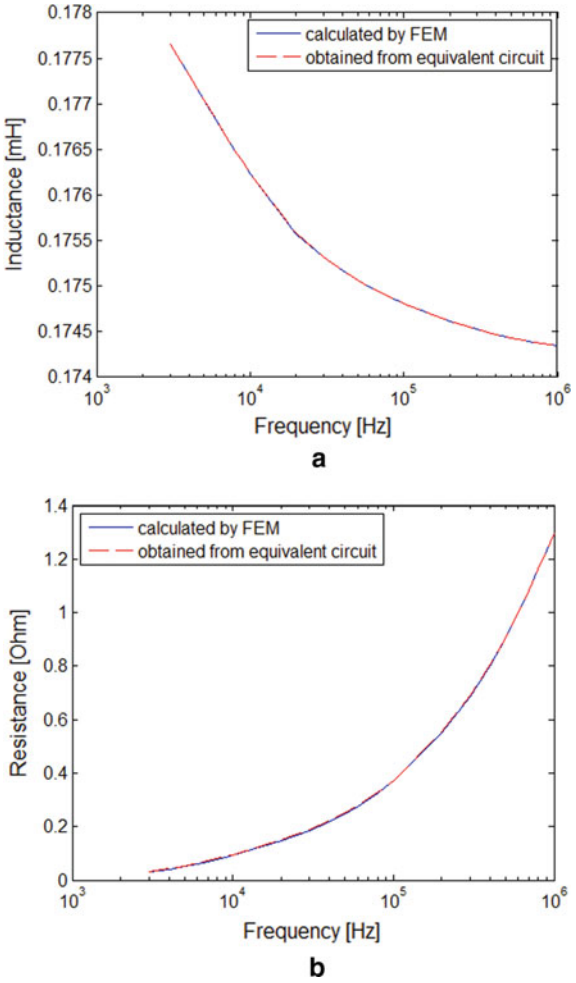

Fig. 6.7 **a** The real part of Z15 (L15) [1]. **b** The imaginary part of Z15 (R15) [1]

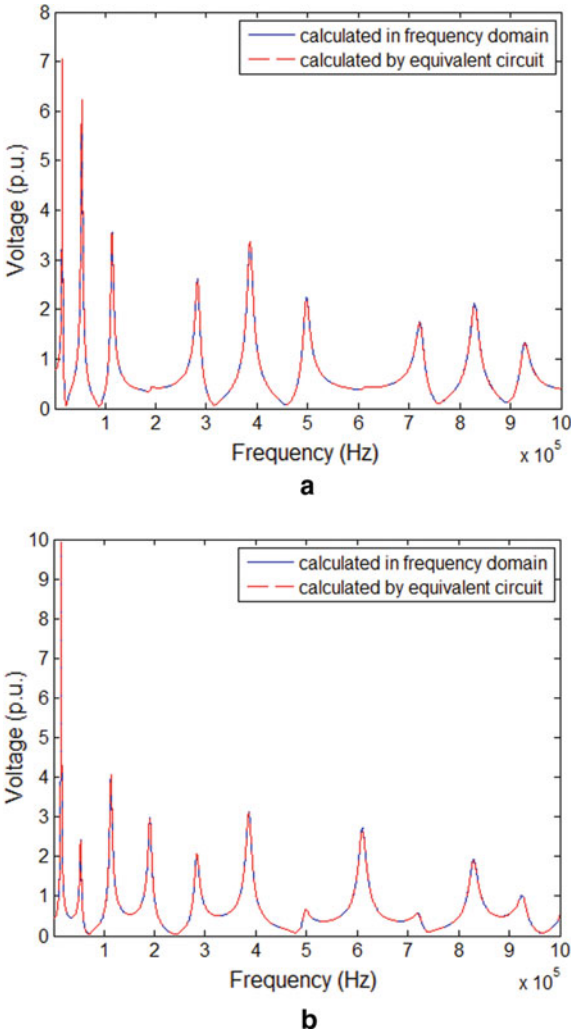

Fig. 6.8 **a** The frequency response of voltage for node 5 [1]. **b** The frequency response of voltage for node 10 [1]

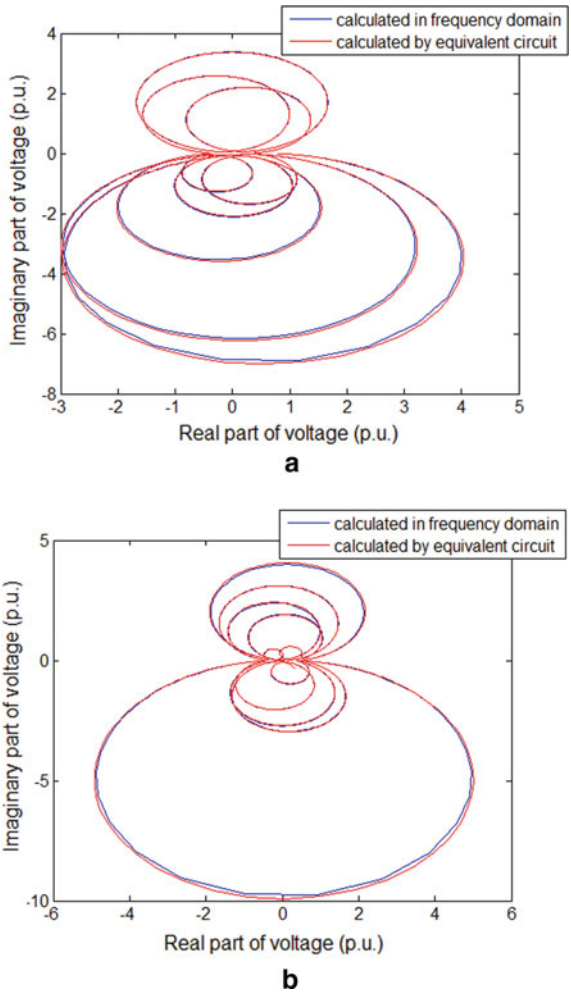

Fig. 6.9 **a** The polar frequency response of voltage for node 5 [1]. **b** The polar frequency response of voltage for node 10 [1]

References

1. M. Eslamian, An improvement in modeling of transformer winding for transients studies including eddy-current frequency-dependent losses, Ph.D. dissertation (Amirkabir University of Technology, Tehran, Iran, 2014)
2. P. Mishra, D.M. Vinod Kumar, R. Muthuraj, High frequency analysis of power transformer taking into account the frequency dependent losses. Int. J. Electr., Electron. Data Commun. **2**(7), 51–54 (2014)
3. A.J. McElroy, On the significance of recent EHV transformer failures involving winding resonance. IEEE Trans. PAS **94**(4), 1301–1307 (1975)
4. W.J. McNutt, T.J. Blalock, R.A. Hinton, Response of transformer windings to system voltages. IEEE Trans. PAS, 457–467 (1974)
5. P.A. Abetti, F.J. Maginniss, Natural frequencies of coils and windings determined by equivalent circuit. AIEE Trans., 495–503 (1953)

6. P.A. Abetti, G.E. Adams, F.J. Maginniss, Oscillations of coupled windings. AIEE Trans., 12–21 (1955)
7. E. Bjerkan, High frequency modeling of power transformers, Ph.D. thesis (Norwegian University of Science and Technology, 2005)
8. S. D. Cho, Parameter estimation for transformer modeling, Ph.D. thesis (Michigan Technological University, 2002)
9. K. Imdad, High frequency modeling of power transformers under transients, Ph.D. thesis (Universitat Politechnica De Catalunya (Barcelona Tech), 2017)
10. M. Eslamian, B. Vahidi, New equivalent circuit of transformer winding for the calculation of resonance transients considering frequency-dependent losses. IEEE Trans. Power Delivery **30**(4), 1743–1751 (2015)
11. X. Zhao et al., High frequency electric circuit modeling for transformer frequency response analysis studies. Electr. Power Energy Syst. **111**, 351–368 (2019)
12. E. Bjerlan, H. K. Hoidalen, High frequency FEM-based power transformer modeling: investigation of internal stresses due to network-initiated overvoltages, in *International Conference on Power Systems Transients (IPST'05)*, Paper No. IPST05-106 (Montreal, Canada, 2005)
13. K. Pedersen, et al, Detailed high frequency models of various winding types in power transformers, in *International Conference on Power Systems Transients (IPST'05)*, Paper No. IPST05-100 (Montreal, Canada, 2005)
14. H. Quaddi, et al., Determination of the high frequency parameters of the power transformer used in the railway substation, in *2010 IEEE Vehicle Power and Propulsion Conference* (Lille, France, 2010)
15. Kh. Elkamouny, et al., Sizing a single phase and high frequency transformer for a conversion string of photovoltaic energy, in *2ème Conférence Internationale des Energies Renouvelables CIER-2014* (Tunisia, 2014)
16. L. Brana, et al., Development of a power transformer model for high frequency phenomena, in *19th International Conference on Renewable Energies and Power Quality (ICREPQ'21)* (Spain, 2021)
17. M. Heindl et al, Transformer modeling based on standard frequency response measurements, in *XVII International Symposium on High Voltage Engineering* (Hannover, Germany, 2011)
18. A. Abu-Siada, Frequency response analysis using high frequency transformer model. Elixir Electr. Eng. **41**, 5827–5831 (2011)
19. Y. Yoon et al., High-frequency modeling of a three-winding power transformer using sweep frequency respose alalysis. Energies **14**, 1–10 (2021)
20. M. Hussain et al., High frequency modeling of transformer using black box frequency response analysis. Int. J. Eng. Work. **4**(10), 190–195 (2017)
21. N.A. Sabiha, M. Lehtonen, Lightning-induced overvoltages transmitted over distribution transformer with MV spark-gap operation—Part I: High-frequency transformer model. IEEE Trans. Power Delivery **25**(4), 2472–3248 (2010)
22. F. De León, A. Semlyen, Time domain modeling of eddy current effects for transformer transients. IEEE Trans. Power Del. **8**(1), 271–279 (1993)
23. E.E. Mombello, A novel method for the synthesis of magneticallycoupled networks considering the frequency-dependence of the impedances. IEEE Trans. Circuits Syst. I, Reg. Papers **52**(10), 2227–2233 (2005)
24. E. Mombello, Modeling of a coil system considering frequencydependent inductances and losses. Part I: Analysis of the impedance matrix characteristics. Elect. Eng. **84**(1), 3–10 (2002)
25. F. De León, A. Semlyen, Detailed modeling of eddy current effects for transformer transients. IEEE Trans. Power Del. **9**(2), 1143–1150 (1994)
26. E.E. Mombello, K. Möller, New power transformer model for the calculation of electromagnetic resonant transient phenomena including frequency-dependent losses. IEEE Trans. Power Del. **15**(1), 167–174 (2000)
27. E.E. Mombello, Modeling of a coil system considering frequency-dependent inductances and losses. Part II: Equivalent Circuit Synthesis. Elect. Eng. **84**(1), 11–19 (2002)

28. S. Mei, Y.I. Ismail, Modeling skin and proximity effects with reduced realizable RL circuits. IEEE Trans. Very Large Scale Integr. Syst. **12**(4), 437–447 (2004)
29. P. Holmberg, M. Leijon, T. Wass, A wideband lumped circuit model of eddy current losses in a coil with a coaxial insulation system and a stranded conductor. IEEE Trans. Power Del. **18**(1), 50–60 (2003)
30. E.J. Tarasiewicz, A.S. Morched, A. Narang, E.P. Dick, Frequency dependent eddy current models for nonlinear iron cores. IEEE Trans. Power Syst. **8**, 588–597 (1993)
31. J.H. Spreen, Electrical terminal representation of conductor loss in transformers. IEEE Trans. Power Electron. **5**(4) (1990)
32. B. Gustavsen, A. Semlyen, Rational approximation of frequency domain responses by Vector Fitting. IEEE Trans. Power Deliv. **14**(3), 1052–1061 (1999)
33. E.A. Guillemin, *Synthesis of Passive Networks* (John Wiley & Sons, New York, 1962)
34. O. Wing, *Classical Circuit Theory* (Springer Science, LLC, New York, 2008)
35. D. Deschrijver, M. Mrozowski, T. Dhaene, D. De Zutter, Macromodeling of multiport systems using a fast implementation of the vector fitting method. IEEE Microwave Wirel. Compon. Lett. **18**(6), 383–385 (2008)
36. B. Gustavsen, Improving the pole relocating properties of vector fitting. IEEE Trans. Power Deliv. **21**(3), 1587–1592 (2006)
37. A. Semlyen, B. Gustavsen, A half-size singularity test matrix for fast and reliable passivity assessment of rational models. IEEE Trans. Power Delivery **24**(1), 345–351 (2009)
38. B. Gustavsen, Fast passivity enforcement for pole-residue models by perturbation of residue matrix eigenvalues. IEEE Trans. Power Deliv. **23**(4), 2278–2285 (2008)
39. B. Gustavsen, A. Semlyen, Enforcing passivity for admittance matrices approximated by rational functions. IEEE Trans. Power Syst. **16**(1), 97–104 (2001)
40. B. Gustavsen, Wide band modeling of power transformers. IEEE Trans. Power Deliv. **19**(1), 414–422 (2004)
41. B. Gustavsen, Frequency dependent modeling of power transformers with ungrounded windings. IEEE Trans. Power Deliv. **19**(3), 1328–1334 (2004)
42. B. Gustavsen, A hybrid measurement approach for wideband characterization and modeling of power transformers. IEEE Trans. Power Deliv. **25**(3), 1932–1939 (2010)
43. B. Gustavsen, Computer code for rational approximation of frequency dependent admittance matrices. IEEE Trans. Power Deliv. **17**(4), 1093–1098 (2002)
44. D.C. Meeker, Finite element method magnetics (2013). http://www.femm.info
45. S.V. Kulkarni, S.A. Khaparde, *Transformer Engineering Design and Practice* (Marcel Dekker Inc., New York, 2004)

Index

B. Vahidi and R. A. Naghizadeh, *Principles and Modeling of the Power Transformers*, Energy Systems in Electrical Engineering,
https://doi.org/10.1007/978-981-99-5796-5